NASA Contractor Report 4143

Research Investigation of Helicopter Main Rotor/Tail Rotor Interaction Noise

J. Fitzgerald and F. Kohlhepp

CONTRACT NAS1-17126
MAY 1988

NASA Contractor Report 4143

Research Investigation of Helicopter Main Rotor/Tail Rotor Interaction Noise

J. Fitzgerald and F. Kohlhepp
United Technologies Corporation
Sikorsky Aircraft Division
Stratford, Connecticut

Prepared for
Langley Research Center
under Contract NAS1-17126

National Aeronautics
and Space Administration

**Scientific and Technical
Information Division**

1988

Abstract

Acoustic measurements were obtained in the NASA Langley 14 by 22 Foot Subsonic Wind Tunnel to study the aeroacoustic interaction of 1/5th-scale main rotor, tail rotor, and fuselage models which comprised a complete helicopter system (without engines). An extensive aeroacoustic data base was acquired for main rotor/tail rotor/fuselage aerodynamic interaction for moderate forward speed flight conditions (50 to 80 knots). The details of the rotor models, experimental design and procedure, aerodynamic and acoustic data acquisition, reduction, and results thereof are presented.

The model system was initially operated in "trim" (zero net yaw moment) for selected fuselage angle of attack, main rotor tip-path-plane angle, and main rotor thrust combinations. From these, the effects of repositioning the tail rotor with respect to the main rotor wake and the corresponding tail rotor countertorque requirements were determined. Each rotor was subsequently tested in isolation with the fuselage and operated at the thrust and angle of attack combinations selected for the trimmed system.

The acoustic data indicated that the helicopter system noise was primarily dominated by the main rotor, especially for moderate speed descent conditions where main rotor blade-vortex interaction occurs. The tail rotor noise increased when the main rotor was removed from the system indicating that tail rotor inflow was improved with the main rotor present. However, the influence of tail rotor position within the main rotor wake on tail rotor noise could not be definitively established from the data.

TABLE OF CONTENTS

TABLE OF CONTENTS (continued)

List of Tables

List of Figures

List of Figures (cont'd.)

List of Figures (cont'd.)

List of Figures (cont'd.)

Nomenclature

BLSPL	band-limited sound pressure level (500-3000 Hz), dB
BMTR	basic model test rig
BPF	blade-passing frequency
BVI	blade-vortex interaction
C_t	main rotor thrust coefficient
dBA	A-weighted sound pressure level
dBD	D-weighted sound pressure level
FFT	fast Fourier transform
GPIB	general purpose instrumentation bus
hp	horsepower
Hz	hertz (cycles per second)
lbs	pounds force
m	meter
m/s	meters/second
msec	milliseconds
MR	main rotor
MR/TR	main rotor/tail rotor
M_{rot}	rotor hover mach number
R	microphone radial distance from main rotor shaft centerline
RPM	revolutions per minute
TR	tail rotor
X	streamwise distance from microphone to main rotor shaft centerline
Y	lateral distance from microphone to main rotor shaft centerline
Z	vertical distance from microphone to main rotor shaft centerline

Greek Symbols

α_{sh}	main rotor shaft angle with respect to wind axis
α_{tpp}	main rotor tip-path-plane angle with respect to wind axis
χ	rotor downwash angle
λ	main rotor inflow ratio
ν	rotor induced velocity
μ	main rotor advance ratio
Ψ	angle in the main rotor plane commencing from the model tail position in the direction of main rotor rotation
Θ	angle below the wind axis commencing in the upstream direction

1.0 Introduction

1.1 Purpose

This report provides the documentation and results for an experimental program which studied the acoustic effects produced by the aerodynamic interaction of helicopter main and tail rotors at moderate forward flight speeds. In particular, main rotor/tail rotor (MR/TR) interaction noise was studied with and without the occurrence of main rotor (MR) blade vortex interaction (BVI).

1.2 Background

The Main Rotor/Tail Rotor Interaction Noise Test was the final part of a three-phase rotorcraft noise research program undertaken by the NASA Langley Research Center, the U.S. Army Aerostructures Directorate, and the Sikorsky Aircraft Company. The primary objectives of this three phase research effort have been to study the acoustic characteristics of: isolated main rotors having different blade and blade-tip geometries (Phase I); isolated tail rotors and tail rotor installation effects (Phase II); and the aerodynamic interaction of main and tail rotors (Phase III). The results from Phase I were reported by Martin and Connor [1 & 2], Shenoy [3], and Martin, Hoad, and Elliott [4]. The results from Phase II were reported by Jacobs [5] and by Jacobs, Fitzgerald, and Shenoy [6].

In addition, detailed study of blade-vortex interaction (BVI) noise and the development of an acoustic database for verification of BVI noise prediction methods were also important objectives of this program. Phases I and III were conducted in the NASA Langley 14 by 22 Foot Subsonic Tunnel while Phase II was conducted in the United Technologies Research Center - Acoustic Research Tunnel (UTRC-ART). The results from the isolated rotor test programs (Phases I and II) were utilized to formulate the test design and model rotor configurations utilized in Phase III.

2.0 Experimental Approach

2.1 14 by 22 Foot Subsonic Tunnel Facility

Phase III was conducted in the NASA Langley 14 by 22 Foot Subsonic Tunnel with the tunnel configured as an open-throat test chamber. The dimensions of the rectangular jet inlet to the test section are 4.42 m (14.5 ft) tall by 6.63 m (21.75 ft) wide. In the open-throat configuration, the ceiling was raised to approximately 7.5 m (24.6 ft) above the test chamber floor, the walls were removed, while the floor section remained in place as for the closed-throat configuration. A rectangular collector was installed at the outlet of the test section. The centerline of the model was positioned 5.33 m (17.5 ft) downstream of the inlet nozzle. Top and side views of the positioning of the model in the test section are shown in figures 1 and 2, respectively.

Acoustic treatment was applied to the walls, floor, and ceiling of the test section to reduce acoustic reflections. The treated areas are shown by the shaded areas in figures 1 and 2. The walls and floor of the test section area were covered with perforated sheet metal panels filled with 12.7 cm (5 in) thick fiberglass. The floor and ceiling areas adjacent to the test section were covered with 15.2 cm (6 in) open cell polyurethane foam.

The physical lay-out for tunnel control, model performance data acquisition, and acoustic data acquisition is shown in figure 3. The Army test conductor directed operation of the model, operation of the tunnel, model safety of flight monitoring, performance data acquisition, and acoustic data acquisition. Performance data were obtained using the tunnel's data acquisition system while acoustic data were simultaneously tape-recorded in a remote van positioned below the test section.

2.2 Test Apparatus and Model Performance Data Acquisition

2.2.1 Model and Rotor Drive Systems Description

Sikorsky Aircraft's Basic Model Test Rig number one (BMTR#1) was used for the Phase III test. The rotors and fuselage of BMTR#1 are a 1/5.727 scale representation of the UH-60 Black Hawk. Some of the significant model features and the resulting test configurations are described below.

The BMTR#1 was mounted atop an aerodynamic fairing in the tunnel test section as shown schematically in figure 4 and pictorially in figure 5. The

main rotor drive hardware and model instrumentation signals were routed through the fairing. The fairing was designed to minimize acoustic reflections produced by the rotor drive hardware and structural supports. The fairing was made using #22 gage 304 perforated stainless steel with 1.27 cm (0.5 in) diameter holes in 1.91 cm (0.75 in) in-line centers (yielding 35% open area) and a 2 in. thick acoustic foam lining was attached to the perforated steel.

Three balances were used to measure forces and moments on the BMTR#1 during the test; one for fuselage loads, one for the total tail load summing the contributions of both the pylon and the tail rotor, and a single main rotor balance (mounted in a gimbal support to reduce dynamic interactions) measured main rotor loads. The balance forces and moments were resolved to the center of the main rotor to simplify the determination of model trim conditions. The force and moment contributions produced by the fuselage and the tail pylon were not seperated from those produced by the tail rotor on-line during the test. Therefore, the test load conditions were based upon total force and moment measurements and not those for the tail rotor alone.

The BMTR#1 main rotor drive was fully articulated and featured both collective and cyclic control inputs. Blade flapping was monitored to resolve rotor tip-path-plane angle. This capability permitted independent variation of main rotor shaft angle and rotor tip-path plane angle for the test. The shaft angle was controlled with a hydraulic actuator which pivoted the complete model and support fairing assembly about a point along the centerline of the test section. The center of the rotor hub was positioned 17.8 cm (7 inches) above the tunnel centerline thus producing small changes in the streamwise rotor hub position with model rotation. Therefore, $\pm 10°$ pitch changes of the rotor shaft moved the hub 3.1 cm (1.22 inches) downstream or upstream and about 0.305 cm (0.12 inches) down. The main rotor was driven by a 90 hp variable speed motor provided by NASA Langley. Main rotor torque was measured by a load cell mounted between the shaft drive transmission and the transmission support frame. Main rotor speed was measured with an optical encoder. In model body coordinates, the main rotor centerline was positioned at 151.4 cm (59.61 in.) axial model station, 138.44 cm (54.5 in.) vertical model station, and laterally centered on the body.

The tail rotor drive system provided collective control but had no cyclic control input. The rotor blades were free to flap but were fixed in-plane. Blade flapping was monitored for safety of flight but was not resolved during the test. The tail rotor was driven by a 20 hp variable speed motor which

was supported by the vertical tail pylon with control hardware and safety of flight instrumentation. An aerodynamic fairing was streamlined around the tail rotor drive hardware where it extended beyond the model contours. Tail rotor shaft speed was measured with a magnetic pick-up. The tail rotor could be operated in either the pusher or tractor mode. The test position for the tail rotor model is shown in figure 6. The model scale position for the canted tail rotor of the UH-60 is also shown for reference. In model body coordinates, the tail rotor model centerline was postioned at 303.5 cm (127.63 in.) axial model station, 120.8 cm (47.05 in.) vertical model station, and 6.7 cm (2.63 in.) lateral model station. The tail rotor was uncanted for this test.

The main and tail rotor drive motors were started and controlled independently without any connecting gearing or linking speed control apparatus. Therefore, the speed ratio between the rotors could vary and as well as the relative position of the main and tail rotor blades.

2.2.2 Rotor Configurations

The model was operated in three basic configurations during the test; the first being the main rotor and tail rotor together (MR/TR), the main rotor alone (MR) and the tail rotor alone (TR). A single Black Hawk main rotor blade set, configured with the nonstandard large-swept-tapered tip and new airfoil, was tested. The tail rotor was operated as a tractor at the model location discussed in Section 2.2.1.

The spanwise twist and blade airfoil distribution for the main rotor blades are shown in figure 7 and and a detail of the large swept tapered tip geometry is shown in figure 8. The selection of these blades for testing was based upon the results of the Phase I test which showed that BVI noise generation was reduced with the high-twist UH-60 type blades having the advanced tips [1 & 3]. With the exception of the tips, the main rotor model blades were geometrically and dynamically similar to those of the full-scale Black Hawk. The main rotor blades were instrumented to measure flatwise, chordwise, and torsional strains.

Two sets of blades were used with the tractor tail rotor model. Both sets were -15° equivalent twist blades with rectangular planform. The first blade set utilized in the test was configured with SC1095RN airfoils. Acoustic data were obtained with these blades for the entire MR/TR interaction test matrix but the blades were damaged at the completion of the MR/TR runs and could

not be used for the TR alone test conditions. The TR alone test conditions were conducted using blades configured with SC1095 airfoils. The tail rotor blade sets were instrumented to measure flatwise, chordwise, and torsional strains. The planform and spanwise twist distribution for both blade sets are shown in figure 9.

Figure 10 illustrates the airfoil sections for the SC1095 and SC1095RN. The SC1095RN section incorporates a leading edge modification to the SC1095 designed for the reduction of impulsive noise during BVI. Its development utilized the ATRAN2 two-dimensional small disturbance code. Owen and Shenoy [7] have shown that ATRAN2 is an efficient tool for studying the effect of airfoil modifications on the unsteady pressures produced during BVI.

2.2.3 Model Performance Data Acquisition

The model rotor performance data were acquired using the tunnel data acquisition system. The main rotor balance, fuselage balance, tail balance, and transmission torque cell signals were conditioned and converted to engineering units. In addition, the main and tail rotor RPM indicators were conditioned on-line for setting rotational speed as required. The acoustic test conditions were set by adjusting the main rotor shaft angle (body angle of attack) α_{sh}, main rotor tip-path-plane angle α_{tpp}, main rotor thrust coefficient C_t, tunnel speed, total model torque, and total tail thrust. The blade strain gage signals and drive motor(s) bearing and winding temperatures were monitored on-line for safety of flight.

2.3 Acoustic Data Acquisition

Ten "in-flow" microphones were set up in the tunnel test section at the locations shown in figures 1 and 2. The microphone locations, with respect to the main rotor shaft centerline at 0° pitch, are listed in table 1. Microphones 5 to 9 were mounted to the traversing wing. The wing position was adjustable from 1.31 m (4.3 ft) to 4.88 m (16 ft) upstream of the main rotor shaft centerline. Most of the acoustic data were obtained with the wing at the 2.52 m (8.3 ft) position although additional data were obtained by incrementing the streamwise wing position in 0.61 m (2 ft) and 0.91 m (3 ft) increments for selected test conditions. This position was selected for a large portion of the rotor noise measurement conditions because it places the wing microphones 30° below and forward of the main rotor tip-path-plane (please refer to table 1); the peak BVI noise directivity region for both full-scale and

model-scale helicopters, as observed by Schmitz et al. [8]. Only data for the 2.52 m wing location will be presented in this report.

A schematic of the complete acoustic data acquisition system is shown in figure 11. The microphones were B&K Type 4134 1.27 cm (0.5 in.) pressure microphones. These were fitted with B&K UA 0386 nose cones. The microphones were calibrated at the beginning, during shift change, and at the end of each test day using a B&K 4220 pistonphone (the pistonphone level is 124 dB at 250 Hz re 20 μPa). The pistonphone signals were recorded on each tape used for data recording. B&K type 2619 preamplifiers and type 2426 amplifiers were employed for conditioning and amplification of the microphone signals which were sent through 30 meter cables to an instrumentation van located below the tunnel test section. Prior to tape recording, the microphone signals were high-pass filtered at 50 Hz using Ithaco No. 4113 filters. This filtering was required because of excessive low-frequency tunnel background noise. Further discussion of the background noise is provided in Section 3.4. The filtered microphone signals were recorded on a Honeywell 101 14-track tape recorder operating at 30 inches/second using Wideband I mode. In addition to the 10 microphone signals, the main and tail rotor RPM signals, IRIG A time code signal, and a FM synchronization signal were recorded simultaneously on tape.

For system response calibration, a random noise signal (white noise) was simultaneously inserted into each microphone channel of the measurement system and tape recorded. This technique provides documentation of the frequency response of each microphone system with the exception of the microphone diaphragms.

2.4 Test Design and Test Conditions

2.4.1 Test Design

As previously discussed, Phases I and II studied isolated configurations of main and tail rotor models respectively. An important objective of these studies was to determine the model configurations best suited for studying the interaction characteristics of the main and tail rotors in Phase III. The principle criteria for selecting each rotor configuration were the lowest isolated noise levels (based on flight scaled weighted metrics) and, for the tail rotor, selection of a configuration which was minimally sensitive to empennage effects.

The Phase I results [1 & 3] showed that the overall noise metrics for the higher-twist rotors (UH-60 model with various tips) were less sensitive to flight speed and blade-vortex interaction (BVI) than the lower-twist rotors (S-76 model with various tips). In addition, the noise of the high-twist rotors was strongly affected by tip design. The large swept tapered tip configured with SSCA07 airfoils generated the lowest BVI levels when tested on the high-twist rotor.

In the Phase II study [5], there was insufficient data to permit a reliable comparison of the pusher and tractor configurations, based on a review of overall acoustic metrics. However, the spectral characteristics were sufficiently different, especially in the mid-frequency region where BVI is normally evident. The tractor configurations exhibited less sensitivity in the mid-frequency range to empennage (vertical pylon and horizontal stabilizer) interactions than the pusher [6]. Two tractor tail rotors were tested in Phase II, one with -15° equivalent twist blades and a second with -23° twist blades. The effects of twist on the rotor noise were very small, especially with the pylon present. The full-scale UH-60 tail rotor is more closely approximated by the -15° twist blades than the -23° blades.

Based on these test results, the UH-60 main rotor model configured with large swept tapered tips and SSCA07 airfoils and the -15° equivalent twist tractor tail rotor were selected for studying the MR/TR acoustic interaction effects. Several key flight regimes were identified for the main rotor alone, tail rotor alone, and main rotor/tail rotor configurations. The primary objective was to observe the acoustic effects produced with the tail rotor positioned inside and then outside the main rotor wake. These effects were studied with and without main rotor BVI occurring. The MR tip-path-plane angle was controlled by longitudinal flapping of the rotor as the model pitch angle (MR shaft angle) was adjusted to change the relative TR position. Flapping limits of ±5° were imposed for safety-of-flight. The complete test matrix detailing the rotor operational parameters is discussed below in section 2.4.2.

2.4.2 Test Conditions

Table 2 lists the nominal model test conditions conducted during the test. The test conditions are grouped by the model operational parameters which were varied to set each condition. Comments are shown to illustrate the desired physical objective for each test condition; i.e., "maximum BVI" for the main rotor with the "TR low" inside the main rotor wake.

For the interaction test runs, the main and tail rotor rotational speeds were 1478 and 6800 RPM, respectively. These correspond to hover tip speeds of 725 ft/sec (M_{rot} = 0.643) for the main rotor and 685 ft/sec (M_{rot} = 0.607) for the tail rotor which are the same as the full scale UH-60. At these speeds, the blade passing frequency (BPF) of the MR model is 24.63 Hz and the BPF for the TR model is 113.33 Hz. Acoustic data were recorded at each test condition for the MR/TR, MR alone, and TR alone configurations. The MR/TR combination was the initial configuration tested. The main rotor trim settings and corresponding total tail thrust were determined for this configuration and used as test parameters for the isolated rotor configurations.

The main rotor flapping trends (runs 114 & 115) and the check of the main rotor Phase I trends (runs 112 & 113) were obtained with a main rotor hover tip speed of 756 ft/sec (M_{rot} = 0.669), which is 4.2% higher than the full-scale UH-60. The higher tip speed operation was unintentional and resulted from a software error in the data acquisition system during these measurements. The error should not have a significant effect on the conclusions drawn from these data since they were acquired for the basis of comparison at the same tip speed.

3.0 Facility Acoustic Measurement Results and Analysis

3.1 Acoustic Data Reduction

A large portion of the acoustic data presented in this report are in the form of, or derived from, 1/12th octave spectral analysis. This analysis format was selected for several reasons: 1) the 1/5.727 scale rotor models generate noise over a wide frequency range; 2) full-scaled flight metrics, in levels of dBA and dBD, may be easily calculated from 1/12th octave spectra; 3) the 1/12th octave constant percentage filters are sufficiently narrow to resolve the lower frequency main and tail rotor harmonic levels of the model while providing a convenient format for analysis of the mid and high frequency noise trends; 4) previous analyses performed on the data from Phases I and II [refs. 5 and 6] also utilized the 1/12th octave format.

The acoustic data analysis is not limited to the 1/12th octave format. Since the rotor noise signals are inherently deterministic, narrow-band analyses (constant bandwidth in the frequency domain) are very useful for resolution of the discrete frequency signal components over limited frequency ranges. Intermodulation tones produced by the interaction of the main and tail rotors may be easily identified with narrow-band analysis, while 1/12th octave analysis is unable to resolve modulation components. For selected conditions, both narrow-band frequency domain and time domain analysis are presented to enhance the causal relationships for the observed phenomena. Time histories are particularly useful for identifying important aerodynamic events contained in the acoustic signature.

The acoustic data reduction instrumentation system used for the various analyses formats is shown schematically in figure 12. The analog tape recordings of the acoustic data (copies provided by NASA Langley) were played back on a Thorn/EMI SE 9000 recorder. Each tape record was accessed using the time code data recorded during the test. The time code signal was resolved by a Datum 9210 time code translator. The analog tape signals were input to either a B&K 2131 digital frequency analyzer or a HP 3562A signal analyzer, depending on the desired analysis format. The B&K analyzer generates 1/12th octave digital filters as a result of control statements from the HP 9836 computer and samples the input signal for level in each 1/12th octave band (168 total filter bands). The total data sampling time was set to 64 seconds. The computer controls the analyzer over the GPIB instrumentation bus. Data storage is via floppy disk. In addition, background noise may be subtracted, on a mean-squared basis,

from the model acoustic data in 1/12th octave format as a function of tunnel speed and wing position. Hard copy output of the spectral data and overall metrics are available using a HP 7475 plotter or HP 2623A printer.

The HP analyzer was used either as a storage oscilloscope (time domain analysis) or narrow band spectrum analyzer (frequency domain analysis). The HP analyzer digitally samples the input signal 2048 times per measurement. For time domain analyses, sampling was triggered by the 1p signal from the main rotor. An ensemble of 25 measurements were obtained from which synchronously averaged time histories were computed. Frequency domain measurements were obtained via a 2048-point fast Fourier transform for which a power spectrum was computed. Averaged power spectra were computed from an ensemble of 25 spectra.

Flight scaled acoustic metrics (dBD and dBA) may be calculated from the 1/12th octave model data. The metrics are calculated by scaling the appropriate weighting (A-weighting or D-weighting) as a function of frequency for each 1/12th octave band to correspond with the 1/5.727 scale models. The resulting scaled spectra are then integrated to obtain the equivalent full-scale weighted metrics. Integrated BPF harmonic levels were also calculated from the 1/12th octave spectra for each rotor. The integrated levels consisted of the BPF and its first nine harmonics in 1/12th octave spectral bands.

3.2 Acoustic Measurement Instrumentation Frequency Response

Narrow-band analysis of the random noise calibration recording was performed to check the frequency response characteristics and identify any channel-to-channel anomalies with the acoustic measurement system. A typical noise spectrum is shown in figure 13(a). This is a power spectrum measurement obtained by averaging an ensemble of 200 spectra. The spectrum has 50 Hz resolution over the range of 0 to 25.6 kHz and is shown with an expanded amplitude scale of 2 dB/division. The response is very uniform measuring within ±1 dB from 50 to 20 kHz. The response variation below 50 Hz is a result of the 50 Hz high-pass filters employed (please see Background Noise Results, Section 3.4) and the roll-off in response above 20 kHz is characteristic of frequency-modulated wideband recordings made at 30 inches/second tape speed.

The variations between channels were very small as shown by the frequency response function measurement in figure 13(b). The frequency response was

calculated by dividing the random noise response recording of microphone channel 4 by that of microphone 2. The very small variations in magnitude and phase response apparent between these channels were also observed for the other channels in the system, with the exception of stationary phase shifts produced by the physical displacement of the tape recording and playback heads for different channels along the tape path. The results indicate that the channels were electrically well matched.

3.3 Acoustic Reflections

Acoustic reflection measurements were obtained for all the microphones with the model installed without blades. These data were acquired by igniting small explosive charges, positioned at either the main rotor or tail rotor hub, and recording the decay of the impulsive sound field. Reflection data were also recorded with the tunnel operating at 80 knots to observe the effects of flow.

The traversing microphone wing was positioned 4.87 m (16.0 ft) forward of the main rotor shaft for most of the reflection measurements. The resulting microphone locations, with respect to the main rotor hub, are listed in table 3. This positioning was chosen so that the radial distance from the charge locations to the microphones would be at the maximum available, which should minimize the amplitude of the direct acoustic field in relation to the reflected field. Also, this positions the wing mounted microphones closer to the inlet nozzle and closer to the side walls of the test section (figure 1).

The reflection data were analyzed in the time domain to determine the relative contribution of tunnel echoes to the integrated acoustic results and, where possible, determine the source(s) of reflections. Microphone signals were captured by triggering the HP 3562A signal analyzer on the incident arrival pulse produced by the charge. The analyzer stored the succeeding sound field for 70 milliseconds. A typical set of measurements is shown in figure 14 for microphone 9. The data are shown as pascals vs. time and have been inverted to correct for microphone output polarity [9]. Fourier analysis of the impulsive signals showed that the charge energy was concentrated in the 0 to 1800 Hz frequency range.

In general, most of the reflections resulting from the wind tunnel surfaces were less than 30% in amplitude of the incident sound. However, relatively large short-term reflections (1-3 msec) were apparent for all the microphones. These are attributed to the model fuselage and hardware

surfaces. Table 4 lists the delay times, the normalized amplitudes of the reflected to direct sound, and the most probable reflecting surfaces for the principle reflections observed at microphones 1, 4, 5, 9, and 10.

Figure 14 illustrates the reflection characteristics measured at microphone 9 with the charge positioned at the main rotor hub, at the main rotor hub with 80 knots wind, and at the tail rotor hub. The direct and reflected signals are marked in this figure. At microphone 9, both charge position and wind had very little effect on the reflection characteristics. The other microphones exhibited similar characteristics, with the exception of microphones 2 and 5, for which there was no direct line-of-sight between the tail rotor charge position and these microphones. This effect of charge position is illustrated in figure 15 for microphone 5. The multiple short-term reflections present for the tail rotor charge, as compared with the main rotor position, indicate that the sound field contains multiple reflections from the model fuselage.

Although several anomalies have been identified concerning the free-field "high fidelity" of the open test section configured with the UH-60 model fuselage, the amplitude of reflections from the test section surfaces were well below the direct sound in the measurement space. Reflections from the test hardware are unavoidable in any circumstance. The reflected signals from the test section surfaces should be at least 10 dB below ($\leq$30%) the direct rotor signal and as such, should not contribute to the measured sound field. Therefore, the rotor acoustic results shall not be corrected for reflections.

3.4 Background Noise

Background noise measurements were obtained for all the microphones with the model installed and the main and tail rotor drives spinning (without blades). Data were acquired at speeds of 50 to 80 knots, in 10 knot increments, with the microphone wing positioned 2.52 m (8.3 ft) forward of the model, at 80 knots as a function of main rotor shaft pitch from -9 to +9 degrees, and at 80 knots as a function of wing position from 1.3 to 4.85 m (4.3 to 16 ft) forward of the model.

The initial background noise measurements revealed the presence of excessive low frequency noise in the tunnel and excessive low frequency vibration of the traversing microphone wing. To improve the signal to noise ratio of the rotor signal to background noise for tape recording, 50 Hz high-pass filters were employed to reduce the low frequency noise signals. Although the filters inherently introduce signal phase distortion, their use

could not be avoided. The white noise response of the high-pass filters was recorded for documentation of their frequency response. These results are presented in section 3.5 and shall be used for correction of the rotor acoustic signals for time domain analysis.

During the initial "wind-on" testing the traversing microphone wing exhibited high vibration. Wire cables measuring 0.635 cm (0.25 in) diameter were attached to the lower surface of the wing and fixed to the wing support base. These were tensioned with turn buckles to increase the wing's transverse bending stiffness which substantially reduced the vibration. Masking tape was attached to the downstream end of the cables for streamlining to reduce the propensity for vortex shedding noise.

3.4.1 Tunnel Velocity Effects

A series of background noise spectra are shown in figure 16 for microphone 5. These data were obtained with the traversing microphone wing positioned 2.52 m (8.3 ft) forward of the main rotor shaft and incrementing the tunnel velocity in 10 kt (5.2 m/s) steps from 50 kts (25.8 m/s) to 80 kts (41.2 m/s). The spectra are overlayed to illustrate the trend of increasing noise with velocity, which was typical for all the microphones. The mid-frequency "hump" apparent from 1 kHz to about 1.5 kHz, was generated by vortex shedding of the flow off the wing stiffening cables. The same characteristic was observed for microphones 6, 7, 8, and 9, which were also mounted to the wing, but was not present at the stationary microphones. The upward shifts in the center frequencies of this noise, apparent with increasing tunnel speed, are directly related to the Strouhal number for periodic vortex formation behind a cylinder [10].

An interesting characteristic was observed in the background noise data, particularly for microphones 1 and 10. This is shown by the velocity sweep for microphone 10 in figure 17. At 70 and 80 knots, high frequency peaks were apparent above 10 kHz. Narrowband analysis of this data showed that the noise consisted of discrete tones. The tonal frequencies did not exhibit any known relationships with the rotor drive apparatus or tunnel machinery. The tones were not present during rotor operational conditions, as shown by figure 18. Figure 18 overlays the background noise spectrum and main rotor alone noise spectrum at microphone 1 for a test point considered a minimum main rotor noise condition at 80 kts. Note the high level background noise above 10 kHz. The presence of the high frequency background noise is believed to have been singular to these background noise measurements and

unrelated to any rotor drive or tunnel noise present during model testing.

The background noise data presented in figures 16 through 18 were acquired with the traversing microphone wing positioned 8.3 ft. upstream of the main rotor shaft with the main rotor shaft angle (α_{sh}) set to 0°.

3.4.2 Wing Position Effects

Background noise data were also obtained for various wing positions to determine these effects on the noise. Wing position effects were measured at 80 knots tunnel speed by incrementing the wing position forward of the main rotor shaft from 1.31 m (4.3 ft) to 4.87 m (16.0 ft) in approximately 0.91 m (3 ft) steps. The angle α_{sh} was set to 0° during these measurements.

Wing position affected the background noise for most of the microphones. For the wing mounted microphones (5 to 9), the overall noise levels increased with increasing upstream wing pisition. The frequencies of the vortex shedding noise tones, which were discussed in Section 3.4.1, also shifted upward in frequency as the wing moved upstream. These characteristics indicate that the free stream velocity at the height of the wing increased as the wing moved forward in the test section. The background data for microphones 1, 2, and 3 were also affected by wing position. As the wing moved forward, the broadband noise below 1.5 kHz increased by at least 10 dB, which indicates that the wing wake area increases sufficiently to engulf these microphones. It should be noted that the wake may also affect the rotor in-flow.

3.4.3 Main Rotor Shaft Angle Effects

Lastly, background noise data were acquired as a function of the main rotor shaft angle (α_{sh}). The main rotor shaft angle was varied from -9° to +9° in 3° steps with the tunnel operating at 80 kts and the wing positioned 8.3 ft forward of the main rotor shaft. The effects of shaft angle on the background noise were insignificant at all the microphones. In general, the variations in 1/12th octave band levels were less than 2 dB over the full shaft angle range at each microphone. The only exceptions to this trend were noted at microphones 1 and 3, which were mounted to the model support fairing, where variations of up to 4 dB were exhibited in some of the 1/12th octave bands above 12 kHz.

3.5 Filter Phase Characteristics

As discussed in section 3.4, 50 Hz high-pass filters were employed in the microphone instrumentation circuit to improve the rotor noise to background noise signal ratio for tape recording. To measure the frequency response of the filters, unfiltered and filtered white noise signals were simultaneously recorded.

The instrumentation used to measure the filter response is shown in figure 19. The unfiltered and filtered white noise signals were simultaneously played back into the HP dual-channel spectral analyzer and the frequency response was calculated by dividing the filtered signal by the unfiltered signal (a transfer function measurement). The resulting measurement is shown in figure 20 which illustrates the filter's amplitude and phase response vs. frequency. The 3 dB down point, which identifies the filter cut-off frequency, occurrs at 50 Hz at which point the phase shift is 180°. Above 50 Hz, the filter gain rapidly approaches unity (0 dB) while the phase shift gradually approaches 0°. The phase shift is the item of primary concern with the rotor data. The main rotor and tail rotor blade passing frequency (BPF) harmonics are indentified in figure 20 with the filter response. It is obvious that the phase of the lower main rotor BPF harmonics will be substantially shifted by the filters. These phase shifts will be manifested by the appearance of the rotor acoustic time histories because they alter the phase relationships of the Fourier components which comprise the rotor signature. Power spectral data are unaffected by phase shift because they represent the squared Fourier amplitude coefficients.

Correction for filter phase shift in the acoustic time histories may be accomplished by Fourier transformation of the time averaged signals and subtraction of the phase shift in the frequency domain. The resulting spectrum may then be inverse transformed to the time domain. The major assumption concerning the filter characteristics on actual data is that their frequency response is stationary and ergodic.

The effects of filter phase distortion were investigated by selecting MR alone noise data which were dominated by the low-frequency MR BPF harmonics. Figure 21 illustrates the effect of the filter phase shift on the in-plane MR noise (microphone 10) for a level flight condition where BVI noise should be minimal. Microphone 10 is shown because rotor thickness noise dominates the in-plane acoustics and is characterized in the time domain by a sharp negative pulse for each blade passage, as shown by Schmitz and Yu [11] and

Dahan and Gratieux [12]. In the frequency domain, these pulses are comprised of the BPF and its harmonics and the phase of these frequency components (98.5 Hz and multiples thereof) should be substantially shifted by the high-pass filters used in the tape recording circuit. Figure 21(a) illustrates the averaged acoustic time history for microphone 10 and figure 21(b) illustrates the time history corrected for the filter phase response. The uncorrected data fail to exhibit the large negative pressure peaks associated with thickness noise whereas the corrected time history restores the negative peak typical of in-plane noise.

3.6 Corrections to Acoustic Measurements

The 1/12th octave results presented in Section 4.0 are corrected for tunnel background noise as a function of free stream velocity in the test section. Corrections of the data for body shaft angle effects on background noise, measurement system frequency response, and wall reflections are unnecessary based upon the small signal effects observed for these parameters.

Acoustic time histories are corrected only for the phase shift introduced by the high-pass filters. The filter phase correction is applied using the approach described in Section 3.5. Only phase corrections are applied because the filter amplitude response does not affect the frequency range of interest for the rotor data, which is greater than 90 Hz. Also, synchronous averaging of the acoustic time histories tends to remove the random background noise from the rotor signature.

4.0 Measurement Results and Analysis

4.1 Phase I Repeatability - Main Rotor BVI Acoustic Trends

One of the principal trends observed in Phase I of the program was that at constant thrust coefficient (C_t) and advance ratio (μ), the model rotors exhibited a peaking of noise level as a function of tip-path-plane angle due to the onset of BVI [1 & 3]. The tip-path-plane angle (α_{tpp}) corresponding to maximum BVI noise levels decreased with increasing μ. The sensitivity of BVI noise to descent rate (or angle), advance ratio, and thrust has been reported previously by many investigators [13 & 14]. The Phase I trend may be explained qualitatively in the manner given by Boxwell and Schmitz [14]: "...as the [rotor] descent rate is increased, a rotor blade is more likely to interact with other tip vortices." This trend is only qualitative, however, and will tend to reverse as the rate of descent becomes so large as to force these older tip vortices above the interacting blade.

From the data acquired in the Phase I program, it was shown that an effective metric for quantifying BVI noise strength from model-scale data in the frequency domain was the Band Limited Sound Pressure Level (BLSPL) from 500 to 3000 Hz [1 & 3]. For models of this scale, BVI impulses manifest themselves over this frequency range, which corresponds to the 5th through 30th BPF harmonics. This characteristic is illustrated by the 1/12th octave spectra shown in figure 22 which compare the MR noise with and without strong BVI occurring (α_{tpp}=-2° and +4° respectively) for μ=0.134 at microphone 7. Both the low frequency BPF harmonics and the midfrequency rotor noise levels increase by as much as 10 dB when strong BVI occurs.

To verify the acoustic trends observed in Phase I, the rotor tip-path-plane angle was swept from negative to positive attitude while holding C_t constant at 0.007. Two sweeps were conducted at μ of 0.134 and 0.178. Each sweep was performed by tilting the rotor shaft angle and trimming the model to 0° longitudinal flapping. The resulting trends are shown in figure 23 for microphones 1, 7, and 9. The BLSPL is very sensitive to rotor tip-path-plane angle and peaks at a given angle as a function of μ. This is the same trend as that observed in Phase I. The effect of μ is very important because for a fixed thrust and tip speed, the rotor's inflow parameter (or inflow ratio) is controlled by the tip-path-plane angle. Thus varying μ under these conditions varies the vertical seperation between the rotor and its downwash. For a given tip-path-plane, increasing μ reduces the vertical seperation between the rotor and its downwash and increases the potential

for BVI. Conversely, for a given μ, increasing α_{tpp} (from negative to positive angles) reduces the seperation distance between the rotor and its trailing wake and again, increases the potential for BVI.

Rotor/wake interaction is not the distinguishing feature which raises the BLSPL as a function of α_{tpp} and μ, it is the BVI produced from tip vortices contained in the downwash. This factor accounts for the peaking in level of BLSPL with α_{tpp} and μ and is best illustrated by the acoustic time histories shown in figure 24 for microphone 7. The amplitudes of the BVI pulses reach a maximum and then reduce as α_{tpp} is increased sufficiently to alter the tip vortex trajectory away from the plane of the rotor disk. This trend is very similar to the one described by Boxwell and Schmitz [14] and quoted above.

4.2 Effect of Longitudinal Flapping on the MR Acoustics

By design, the test matrix followed for the MR/TR interaction conditions necessitated adjustment of the MR control axis to maintain constant longitudinal tip-path-plane angle for various shaft angles. The ability to adjust the MR shaft (or fuselage) angle of attack with respect to the MR tip-path-plane was required to reposition the TR with respect to the MR and its wake. The effects of longitudinal flapping on the MR acoustics were measured for the MR alone configuration to isolate the control input effect on the noise. In this discussion, longitudinal flapping refers to flapping motion with respect to the MR shaft axis, designated as a_{1s} by Gessow and Meyers [15].

Acoustic time histories are very useful for illustrating the flapping effects. Figure 25(a) illustrates synchronously averaged time histories measured at microphone 7 for a condition of minimum flapping and figure 25(b) shows one where $a_{1s} = -3.5°$. The strong impulsive characteristics are indicative of BVI and are typical for this model at a tip-path-plane angle of +5.1° and μ of 0.112, as discussed in Section 4.1. Although "blade-to-blade" variations are evident for both conditions, the variations between blades are affected by flapping. At these conditions, flapping appears only as a blade-to-blade modulation of the impulse amplitudes. Overlaying these time histories shows that the phases of the BVI impulses are basically unchanged by flapping.

In the frequency domain, blade-to-blade variations are manifested by frequencies corresponding to the rotor speed (1p = 25.67 Hz for these data). Integer multiples of the rotor speed frequency are referred to as rotor shaft

harmonics. Those integers based on the order of 4 are BPF harmonics since the rotor has 4 blades (i. e., 4p = BPF, 8p = 2xBPF). Sofrin [16] has shown that blade-to-blade differences cause the amplitude of intermediate shaft-ordered harmonics to increase relative to the BPF harmonics as order, or frequency, increases.

Figure 26 illustrates the effects of flapping on the rotor acoustic spectra for the same test conditions shown in figure 25. The lower frequency rotor shaft harmonics and BPF harmonics are identified to illustrate the spectral effects of flapping. The amplitudes of the shaft-ordered and BPF harmonics are strongly affected by flapping.

At 0° α_{tpp}, the effects of flapping are more pronounced, as shown by the acoustic time histories in figure 27. Again these are strongly impulsive conditions, indicative of BVI, for minimum flapping and where a_{1s} = -3.5°. For these conditions, flapping modifies and increases the blade-to-blade variations as well as increasing the overall noise by 1.5 dB, although the BVI impulses remain aligned in time with respect to the rotor 1p signal.

In summary, longitudinal flapping affects the MR acoustics in varying degrees. The variations between blades, which are apparent in every acoustic time signature, are increased by flapping, especially at 0° α_{tpp}. Since the phase of the BVI impulses in the acoustic time histories are unaffected by flapping, the basic rotor/wake azimuthal and radial geometry remains constant with α_{tpp}. However, the significant changes in BVI impulse amplitude and blade-to-blade variations apparent with flapping clearly indicate that smaller scale, local flow effects are produced by flapping. It is believed that the acoustic sensitivity to flapping is produced by the potential field of the fuselage, which assumes a different angle of attack as a function of α_{sh}. The fuselage influences the rotor inflow and local wake characteristics sufficiently to alter the rotor noise. The sensitivity of the noise to flapping appears greatest when the fuselage effect is pronounced, such as for the 0° α_{tpp} conditions discussed above.

4.3 MR/TR Test Results

4.3.1 A Review of Model Operation

As discussed in section 2.4.2, the sequence followed for the testing was to operate the MR/TR combination over the entire test matrix and determine the corresponding control and thrust settings for each rotor from the trimmed (zero net model torque) combination. The isolated rotors were subsequently tested at the same thrust conditions. MR longitudinal flapping was adjusted to the given test condition and MR lateral flapping was trimmed to produce zero net rolling moment.

4.3.2 Main Rotor and Tail Rotor Performance

4.3.2.1 MR Performance: MR/TR and MR Alone

The performance of the MR was reviewed to determine the effects produced by the TR. Figure 28 illustrates MR thrust vs. collective for the MR/TR and MR alone configurations. The data reflect that the test matrix included a limited range of thrust coefficients (C_t=0.007-0.0085) at constant rotational tip speed (220 m/s). The broad distribution of collective angle for these nominally equivalent thrust conditions is produced by the variations in MR α_{tpp}, where the rotor is partially windmilled by the tunnel free stream for positive α_{tpp}.

Figure 29 illustrates the MR horsepower vs collective pitch as linear trends which were calculated from the data for each configuration. The correlation of these trends were 0.97 for the MR/TR configuration and 0.99 for the MR alone. The trends show that the MR performance for the two configurations was very nearly the same such that the standard error in the fitted data is greater than the MR performance difference between configurations.

These consistent MR performance results provide a good basis for comparing the MR/TR and MR alone acoustics. Also, since the MR/TR conditions represent a fully trimmed model configuration, the gross MR wake effects on the TR noise should be representative of a full-scale helicopter.

4.3.2.2 TR Performance: MR/TR and TR Alone

The analysis of the TR performance results was complicated by the fact that the model tail balance was not configured to measure tail rotor loads only; it

measured total tail loads which included tail rotor loads, vertical pylon loads, and motor fairing loads. Figure 4 illustrates the location of the tail balance within the model fuselage. The loads measured by the tail force balance were resolved to the TR centerline and the side force was assumed to be TR thrust. As a result, the TR thrust measurements included the side force generated by the vertical pylon and the motor fairing. If the pylon and motor fairing load tares were affected by the MR wake and MR operational parameters, the indicated tail thrust would not represent comparable TR thrust levels for the MR/TR and TR alone configurations.

Indeed these load tares were significant with respect to the total tail thrust, as shown in figure 30. Figure 30 illustrates the total tail side force as a function of the tail rotor collective pitch angle for the MR/TR and TR alone configurations. A significant reduction in tail rotor performance is apparent for the isolated TR configuration. For the isolated TR to generate the same total tail side force as the MRTR system, a much higher collective pitch setting is required. Also note that the tail rotor thrust is more strongly correlated to collective angle for the rotor alone than with the MR present. Thus, for equivalent total tail side force conditions, the TR thrust generated was substantially different for the MRTR and TR alone configurations. Therefore, it is necessary to account for the pylon and fairing load tares from the tail side force measurements to study and compare the MR/TR interaction effects on TR performance.

Figure 31 illustrates the effects of main rotor shaft angle (or fuselage angle of attack) on the total tail side force for the main rotor only and no rotor configurations. With no main rotor installed, the total tail side force is very small and unaffected by shaft angle. With the MR wake present, the tail side force is strongly affected by shaft angle. Interaction of the MR wake with the tail pylon produces the weakly correlated trend shown. The scatter present in the side force loads for given MR shaft angles is produced by the variations in MR α_{tpp}, MR thrust, and free stream velocity contained in the test matrix. These affect the position and intensity of the MR wake with respect to the tail pylon. The effects of MR α_{tpp} are shown in figure 32, again for the entire test matrix which also produces considerable data scatter. Of the parameters varied in the test matrix, MR α_{tpp} exhibited the strongest correlation to total tail side force.

Utilizing the simple least squares curve fit shown in figure 32, the total side force data from the MR/TR test configuration were corrected for the MR wake effects as a function of MR α_{tpp}. Figure 33 illustrates these results. As

discussed above, the data for the TR alone correlate very strongly to rotor collective angle. The corrected TR thrust from the MR/TR data show the scatter typical of all these side force measurements; however the level of thrust correlates better to absolute collective angle and more closely matches the isolated rotor results. The data for the uncorrected MR/TR tail side force measurements are shown for comparison.

The corrected MR/TR and TR alone tail force data were sorted for each free stream velocity on the basis of TR Thrust, MR α_{tpp} (not applicable to TR alone) and MR α_{sh} to determine comparable TR test conditions for these configurations. The sort produced a reasonable number of comparable test points at the low speed test conditions (25.8 and 30.9 m/s) but only a few at the higher speed conditions (36.1 and 41.2 m/s). The sorted data are listed in table 5 and the points judged comparable are grouped in boxes. The MR/TR interaction acoustic results will be shown for both the original and corrected TR thrust conditions.

4.3.3 Discussion of MR Wake/TR Interaction

References made to MR/TR interaction actually imply MR wake/TR interaction where the TR ingests components of the MR wake. One of the original objectives of the test program was to measure the MR downwash angle in the plane of the TR, just behind the model fuselage, and correlate the wake position with the TR noise for the various test conditions. Unfortunately, the wake measurement technique was unable to resolve the details required to "map out" the MR downwash. Nevertheless, a simple analytical wake model may be utilized which illustrates the intersection of the TR and the MR wake. Levine [17] applied this approach in an analytical study of tail rotor noise reduction concepts. A simple overview of the model is presented below.

On the basis of momentum theory, Gessow and Meyers [15] show that the induced velocity for a uniformly loaded rotor in forward flight is:

$$\text{induced velocity:} \quad v = \frac{\frac{1}{2} C_t \, \Omega R}{\sqrt{\lambda^2 + \mu^2}},$$

$$\text{where advance ratio:} \quad \mu = \frac{V \cos\alpha}{\Omega R} \quad \text{, and inflow ratio:} \quad \lambda = \frac{(V \sin\alpha - v)}{\Omega R}.$$

The test parameters equating to the terms shown above are free stream velocity (V), MR α_{tpp} (α), MR hover tip speed (ΩR), and MR thrust coefficient (C_t).

Since ν and λ are mutually dependent, the solution must be iterated until the momentum induced velocity converges. The advance ratio and the inflow ratio are the dimensionless paramters which define the velocity components parallel to the rotor disk (μ) and normal to the rotor disk (λ). The simple wake can be treated as a cylinder of vorticity which is skewed at:

$$\text{rotor downwash angle:} \quad \chi=\tan^{-1}\left(\frac{\mu}{\lambda}\right).$$

Using the simple wake results, the intersection of the MR wake and the TR can be illustrated for the various test conditions. Some typical results are shown in figure 34 for two MR/TR interaction test conditions at 41.2 m/s (80 kts) where the MR advance ratio is 0.186. The intersection of the MR wake with the TR changes as a function of MR α_{tpp} and α_{sh} and occurs on the advancing, retreating, or both sides of the TR disk. In fact, this analysis shows that for every condition in the test matrix, some portion of the TR disk was imbedded in the MR wake. The MR longitudinal flapping limits and the inability to test alternate TR positions prevented total isolation of the TR from the MR wake.

4.3.4 Main Rotor and Tail Rotor Acoustics

4.3.4.1 TR Acoustics: MR/TR and TR Alone

The MR/TR interaction acoustic data exhibited an unexpected trend when compared with data for the TR alone. For the majority of test conditions and microphones, the TR noise levels were unchanged or were decreased by the MR presence. Figure 35 illustrates a comparison of spectral results at microphone 4 for a level flight condition at 41.2 m/s (80 kts). The increase in noise level above 2 kHz for the TR alone configuration was typical for many of the test conditions. TR rotational harmonics (multiples of 113.3 Hz) and BPF harmonics (multiples of 453.3 Hz) were also reduced by the MR presence. Microphones positioned below (1 and 3) and forward (10) of the model, where the TR noise was also strongly evident, exhibited this trend as well.

It was shown in Section 4.3.2.2 that the indicated TR thrust for the MR/TR configuration was distorted by side force tares produced by MR wake impingement on the model fuselage. Corrections developed for TR thrust produced the "comparable" test conditions listed in table 5. The comparable MR/TR and TR alone acoustic data exhibit the same trend as observed for the original data; the TR noise levels were reduced in the presence of the MR. These results are typified by the spectral data shown in figure 36 for microphone 4, where TR noise largely contributes to the sound. The results imply that, from an overall noise standpoint, the main rotor wake improves the TR inflow in forward flight over that produced by turbulence from the model fuselage even for conditions of nearly equivalent thrust. However, it must be recognized that excessive scatter exists in the tail side force data and the comparison of these results may be invalid. These observations are provided because the TR noise was consistently lower with the MR present.

An interesting characteristic was observed in the TR noise which may be related to the changes in TR performance for the MR/TR and TR alone configurations discussed above. Narrow band power spectral analyses of the TR alone data exhibited a sinousoidally modulated broadband noise floor which was aligned with the rotor BPF harmonics, as shown in the typical baseband and zoom spectra in figure 37 for microphone 1. This characteristic was also observed, although to a lesser degree, for the TR in some of the MR/TR interaction conditions but was far more evident for the TR alone. Synchronously averaging the data with the TR 1p signal had no effect on the noise floor characteristic. This implies that this noise was produced by and remains stationary with the TR. Several possible mechanisms may account for this feature in the noise; turbulence injestion from the fuselage, blade stall effects, vortex shedding from the blades, or rotor wake/pylon interaction.

The effects of the fuselage wake on the TR noise were strongly apparent at microphones 2 and 4. Figure 38 illustrates acoustic spectra from microphone 2 with a free stream velocity of 25.6 m/s (50 kts) for α_{sh} of -6° and +1°, and at approximately 18 lbs TR thrust. As the TR position is lowered into the fuselage wake (α_{sh} becoming positive), the rotor noise increases across its entire spectrum. However, as the rotor is lowered further, by further increasing α_{sh}, the noise is not significantly changed except at the TR BPF, as shown by the spectra in figure 39 from microphone 4 for α_{sh} of +5.8° and +10°, and at approximately 12 lbs thrust. This basic trend was observed for all the microphones.

Additional discussion of the TR noise characteristics is presented in the following section from data for the MR/TR system.

4.3.4.2 Relative Importance and Directivity of MR and TR

For the purposes of general helicopter noise prediction, in-flight noise abatement procedures, and the application of noise reduction concepts, knowledge of the acoustic directivity of the helicopter noise sources is required. The MR/TR interaction test data base provides the in-flight directivity trends over a broad low-speed forward flight regime. The spatial distribution of the microphones in the test section, shown in figures 1 and 2, provides data in the directions considered important to both civil certification and military acoustic requirements. These may be summarized as follows:

-In MR Plane & Forward:	Microphone 10
-Below MR Plane:	Wing Mounted Microphones 5-9
-Directly Below MR Plane:	Microphones 1&3 (suspect to near-field effects)
-Sideline:	Microphones 2&4

The results presented herein are limited to data with the traversing microphone wing positioned 2.52 m (8.3 ft) forward of the model centerline. The contribution of each rotor at the various microphones will be shown by comparing the noise for the MR/TR and MR alone configurations at the matching test conditions listed in table 2.

Tables 5 and 6 list the overall noise levels and flight-scaled dBA levels, respectively, for the MR/TR and MR alone configurations at microphones 1, 4, 5, 9, and 10. The tables include data from the entire interaction test matrix for the nominally equivalent test conditions. The statistics given at the bottom of these tables are included to illustrate some basic characteristics of the noise.

The average overall levels for the microphones listed in table 6 show that the noise increases for the MR/TR configuration above that for the MR alone, but in varying degrees. Based on the differences in average level between the two configurations, the MR is significantly louder than the TR at microphones 5, 9 and 10 (by at least 10 dB), the MR is about 6 dB louder at microphone 1, and the contributions from each rotor are nearly equal at microphone 4.

Because of the similarity in weighted frequency response between perceived noise level (PNL) and A-weighting, dBA is a good metric for studying the relative contribution of the MR and TR to PNL. The flight-scaled dBA levels listed in table 7 illustrate the importance of TR noise to full-scale aircraft PNL. The TR contribution is most significant at microphone 4 where an increase of nearly 10 dBA occurs when the TR is added to the system. Large TR contributions to dBA are also apparent at microphones 1 and 10. However, at microphones 5 and 9, the TR contribution is less significant to dBA. These results form a basis from which to study directivity.

The contributions to the overall noise from each rotor at a given measurement position are highly dependent on the operating conditions of the rotors. In-plane and forward of the model at at microphone 10, the MR is particularly dominant at higher speeds and during MR BVI. The TR contribution is greater at lower speeds and increases as its position is raised within the MR wake and the model assumes a forward flight attitude. Figures 40 and 41 illustrate 1/12th octave spectra for the MR/TR and MR alone configurations (microphone 10) for a forward speed of 41.2 m/s (80 kts). Figure 40 is a strong MR BVI condition (α_{tpp}=2°) where the TR is in a relatively low position in the MR wake (α_{sh}=6°). Figure 41 illustrates the effect of raising the TR (α_{sh}=-6°) further into the MR wake as the MR assumes a forward flight attitude (α_{tpp}=-2°). The increased contribution from the TR above 1 kHz is clearly apparent. The corresponding MR/TR wake intersection figures for these conditions are shown in figure 34 and shows the MR wake impinging on a larger portion of the TR disk for the α_{tpp}=-2° condition.

The wing mounted microphones exhibit very similar trends with respect to the contributions from each rotor. These were all strongly dominated by MR noise over the entire test matrix. In the case of microphone 7, rarely is any evidence of TR noise apparent, as shown by figure 42 for a MR BVI condition (α_{tpp}=5°) at 25.8 m/s (50 kts). This may be due to partial blockage of the in-plane TR noise due to the acoustically treated model support fairing. It should be noted that the wing microphones were deliberately positioned in the areas known to be sensitive to MR BVI noise. Since the test matrix primarily addressed the moderate speed low-power MR conditions (typical for aircraft approach), the masking of TR noise by more dominant MR shaft and BPF harmonic noise, caused by BVI, would be expected at these locations. This is the same result as that presented by Sofrin [16] where it was also shown that the TR contribution increases at higher speeds typical of forward

flight cruise.

As shown by the overall metric results, the relative TR noise contribution is more significant below than forward of the model. This was especially true for level flight and minimum MR BVI conditions. During MR BVI, the MR noise contribution is significantly greater at microphone 1 than at microphone 3. These results are illustrated by the 1/12th octave spectra in Figures 43 and 44 which compare the MR/TR and MR alone configurations for microphones 1 and 3 respectively. These are MR BVI conditions (α_{tpp}=5°) at 25.8 m/s (50 kts). For microphone 1, the MR BVI, which is manifested over the 500 to 3000 Hz frequency range, masks the TR noise except at very high frequencies where the TR produces a "humping" characteristic centered near 10 kHz. At microphone 3, the TR noise components are clearly apparent in the acoustic spectrum and there is much less evidence of MR BVI.

A possible explanation for this effect lies with the microphone locations and their position with respect to the MR. Both microphones 1 and 3 were positioned in very close proximity to the MR (R/D≈0.409) and were effectively isolated from the noise generated on opposite sides of the rotor disk. The isolation was produced by the acoustic fairing positioned over the model support structure. Since strong BVI is a local, or compact phenomenon on the rotor disk usually occurring in the first quadrant of the advancing side of the rotor it went undetected at microphone 3 because of the acoustic fairing. Since this general result occurred for most of the test matrix at microphones 1 and 3, it implies that observers positioned in the areas where MR BVI noise radiation is greatest, will find that noise to be dominant even in the presence of a TR.

Behind the model, at microphones 2 and 4, is where the TR contribution is greatest to the overall noise. Although the overall noise is not fully controlled by the TR, the significance of the TR to aircraft flyover events is strongly manifested at these locations because of the weighting characteristics of PNL calculations. Consider that microphone 4 was nearly the same radial distance from the model centerline as the wing mounted microphones and study the average dBA results in table 7. With the exception of microphone 1, which was positioned less than one-half the radial distance at overhead, the average dBA level at microphone 4 for the MR/TR configuration is the highest in the table. During MR BVI at the lower advance ratios (0.116 and 0.14), the TR noise was clearly apparent in the acoustic spectra, as shown in figure 45 at microphone 4, but did not change significantly with position inside the MR wake, except at BPF, as shown by

the spectra in figure 46 for MR α_{sh}=9° and 1° at 25.8 m/s (50 kts) forward speed. During MR BVI at the higher advance ratios, the noise was increasingly MR dominant, as shown by the spectra in figure 47 for MR α_{tpp}=2°, 41.2 m/s (80 kts) forward speed, at microphone 2. In the absence of MR BVI during level flight conditions, the importance of the TR is shown in figure 48 for MR α_{tpp}=-2.5° and 36.1 m/s (70 kts) forward speed, again at microphone 4.

In summary, the overall noise was primarily MR dominated, particularly during MR BVI and for the microphones forward and below the model on the traversing wing. The TR noise contribution was greatest during level flight conditions below and behind the model.

4.3.4.3 MR Wake Effects On TR Noise

Since the MR/TR configuration was operated in a "trimmed" mode, the acoustic results from the test matrix should be representative of normal helicopter flight conditions. The effects of MR wake and TR position therein can be studied from the available data. However, two additional factors must be considered. First, it was already shown in Section 4.3.2.2 that MR α_{tpp} had a significant effect on the side force tares generated by the model fuselage and vertical pylon, therefore the TR thrust level required to trim the model varied for different test conditions. Secondly, when the MR assumed a positive tip-path-plane attitude, the resulting windmill effect reduced the MR torque requirements, thus reducing the countertorque requirements from the TR. These factors, which alter TR thrust requirements for different flight conditions, may mask or offset the effects of the MR wake on the TR noise.

Table 7 was constructed to study the effects of the independent test parameters on the TR thrust and noise. Table 7 lists the TR thrust levels for the MR/TR test matrix which are corrected for tail side force tares using the technique described in section 4.3.2.2. Also, the integrated sound pressure level of the first 10 TR BPF harmonics are listed for each test condition for microphones 3, 4 and 10. The TR thrust level varies substantially over the test matrix because of the varying MR countertorque requirements and the side force tares generated by the pylon. These effects complicate the interpretation of the true MR wake effect on the TR noise.

In the discussion on rotor noise directivity in Section 4.3.4.2, TR noise was shown to strongly contribute to the sound at microphones 1, 2, 3, 4 and 10. The MR wake effects were difficult to assess because of masking of the TR

noise by MR BVI noise. For example, in figure 47 the effect of TR position on the noise at microphone 4 is shown during MR BVI for α_{sh} of 9° and 1°. With the exception of the TR BPF, the spectra are very similar over the frequency range where the TR dominates the noise in spite of the large apparent shift in TR position with respect to the MR wake. Figure 49 illustrates the MR wake/TR intersection for these test conditions. The shift in TR position with respect to the MR wake is clearly apparent, however, note that the advancing side of the TR remains fully imbedded in the wake for both test conditions. The advancing side of the rotor is considered the most acoustically significant because it is the region of highest unsteady lift. That being the case, the net effect of moving the TR within the MR wake may be small if the advancing area always remains in the wake, and this is indicated by the acoustic data.

Figure 50 further illustrates the apparent insensitivity of the TR noise to changes in the basic test parameters MR α_{tpp} and α_{sh}. These data are for microphone 10 with α_{tpp}=2°, α_{sh}= -2° and 6°, and free-stream velocity of 41.2 m/s. Small changes in level of the TR BPF and BPF harmonics are evident but the integrated harmonics levels are within about 1 dB for each condition (table 8). Although the overall wake effects appeared small, there were some conditions where the TR noise was affected by changes in location. Shown in figure 51 are acoustic spectra for microphone 2 at MR α_{tpp}=-2° and 41.2 m/s free stream velocity. The TR noise increases substantially as the rotor position is raised within the MR wake.

The acoustic data given in table 8 provides a spatial distribution of the TR harmonic noise at the locations which were shown to be sensitive to TR noise. Correlation matrices were computed for the TR harmonic levels using the data listed in table 8 to determine which test parameters affect the TR noise. The matrices are listed in table 9 and contain correlation coefficients between the test variables and the harmonic noise. The correlation coefficients are a measure of how well each of the variables accounts for the variability in the other variables. Values of ±1 imply perfect correlation while 0 implies no correlation. Values greater than ±0.8 imply that some correlation exists between variables. MR α_{sh} shows a reasonably strong negative correlation (R of -0.823) with the TR harmonic levels at microphone 3 which implies that the TR noise increases as its position is raised with respect to the MR. A similar, but much weaker trend is evident for microphones 4 and 10. The remaining test parameters only weakly affect the TR noise. It may only be surmised from the data that the TR noise increases with free-stream velocity, increases as the TR is raised within the MR wake, increases as the MR operation changes from descent to a forward flight attitude, and increases

with MR and TR thrust.

The entire data base reflects the trends described above. Most of the TR noise data fail to exhibit any strong sensitivity to the operational parameters which affect MR wake intersection. This result is best illustrated by the correlation matrices listed in table 9. In general, only weak correlation exists between TR noise and free-stream velocity, MR thrust, α_{tpp}, α_{sh}, and TR thrust. It is believed that the variable, potentially offsetting effects of relative MR wake position, fuselage wake effects and net TR thrust mask these results. A larger data base is required to definitively establish the MR wake influence on the TR noise.

5.0 Conclusions

The experiment documented herein concludes the final part of a three-phase research program jointly undertaken by the NASA Langley Research Center, the U.S. Army Aerostructures Directorate, and Sikorsky Aircraft. An extensive acoustic data base was acquired for main rotor/tail rotor/fuselage aerodynamic interaction for moderate forward speed flight conditions. The details of the rotor models, experimental design and procedure, aerodynamic and acoustic data acquisition, and data reduction are presented.

Based on the results and the discussion presented, the following conclusions are drawn from this experiment:

1) Longitudinal flapping of the main rotor (MR) tip-path-plane altered the variations observed between blades in the acoustic time histories as well as the overall amplitude of the rotor noise. In the frequency domain, longitudinal flapping principally affects the amplitudes of the rotor shaft-ordered harmonics. The influence of flapping on the rotor noise was attributed to modification of the main rotor inflow by the model fuselage, which assumed a different angle of attack as the rotor was flapped.

2) The MR exhibited consistent performance with and without the tail rotor (TR) present.

3) The total tail side force, which was used to determine TR thrust with the model trimmed, was strongly affected by MR wake impingement on the model fuselage and tail pylon. The countertorque forces produced by MR wake impingement were in some cases large with respect to the TR thrust, thus altering the TR operating conditions between the main rotor/tail rotor and tail rotor alone configurations. A correction scheme was developed to account for the fuselage tare forces and estimate correct TR thrust but large data scatter limited the confidence in its application.

4) MR wake/TR intersection was studied using a simple wake model. It was shown analytically that MR wake/TR intersection probably occurred for every condition in the test matrix.

5) The TR noise was generally greater in isolation than with the MR present. This result was attributed to an improvement in TR inflow (based on noise) with the MR present as compared with the inflow when only the fuselage was present. Comparisons of these data may be invalid because

of fuselage tare effects on estimated TR thrust.

6) The overall model noise levels and spectra were primarily dominated by the MR, particularly during MR BVI. By comparison, the TR noise was low below and upstream of the model, low but more strongly evident in-plane and upstream, strongly evident below, and about equal to the MR to the model sideline. TR noise was shown to be significant to flight-scaled dBA sound level.

7) It was very difficult to discern the influence of the MR wake on TR noise. Only very weak correlations were evident between the primary test parameters and the TR noise level and spectra. This result is attributed to the variable and potentially offsetting effects of MR wake/TR interaction, model fuselage wake injestion, and net TR thrust on the TR noise. Within the limitations posed by the data base, it may be surmised that the TR noise increases as the TR is raised within the MR wake, increases as the MR assumes a forward flight attitude, and increases with MR and TR thrust.

6.0 Recommendations

Since the main rotor/tail rotor (MR/TR) experimental program described herein is a novel one on the basis of helicopter system interaction noise, additional study of this acoustic data base should be conducted. In particular, in-flight noise abatement procedures should be studied for the descent flight regime comprised in the data base. Additional analyses should be performed to determine the effects of the tail rotor (TR) and fuselage on the main rotor (MR) noise.

The following recommendations are offered for future experimental studies on MR/TR interaction noise:

1) Since it has been shown that MR BVI noise dominates the helicopter noise for moderate speed/low MR power conditions, future tests should explore higher speed flight regimes to determine the conditions of TR noise dominance.

2) Future MR/TR interaction tests should measure TR thrust independently so that the aerodynamic and acoustic effects of fuselage wake and MR wake may be isolated from TR thrust.

3) Future MR/TR interaction tests should incorporate additional methods to adjust the TR position with respect to the MR since MR flapping places limits on the available TR locations.

4) A detailed MR wake survey is required to determine the location and the composition of the wake near the TR. A test should be conducted which singly addresses this issue.

7.0 Acknowledgement

As with any major experimental program, the support and dedication provided by a great many professionals were instrumental in the conduct of this test. The authors greatly appreciate the contributions of Sikorsky Aircraft's Experimental Aerodynamics group. Danny R. Hoad and Joe W. Elliott of the Army Aerostructures Directorate were very helpful with the test conduct, supplying the rotor performance data and technical assistance with its analysis. And the support and technical advice received from personnel at the NASA Langley Research Center are greatly appreciated. Ruth M. Martin was instrumental with the test planning, execution and extremely helpful with technical documentation and insight following its completion. The opportunity to have a professional association with these people has been greatly valuable and rewarding.

8.0 References

1. Martin, R.M., and Connor, A.B., "Wind-Tunnel Acoustic Results of Two Rotor Models With Several Tip Designs," NASA TM-87698, July 1986.

2. Connor, A.B., and Martin, R.M., "Correlation of Helicopter Impulsive Noise From Blade-Vortex Interaction With Rotor Mean Inflow," NASA TP-2650, March 1987.

3. Shenoy, R.K., "1/5-Scale Model Helicopter Rotor Blade Vortex Interaction Noise Trends at Low to Moderate Advance Ratios," Sikorsky Engineering Report No. SER-510225, July 1986.

4. Martin, R.M., Elliott, J.W., and Hoad, D.R., "Experimental and Analytical Predictions of Rotor Blade Vortex Interaction," Journal of the American Helicopter Society, Volume 36, No. 4, October 1986.

5. Jacobs, E.W., "An Investigation of Tail Rotor - Empennage Acoustic Characteristics in Forward Flight," Sikorsky Engineering Report No. SER-510231, April 1986.

6. Jacobs, E.W., Fitzgerald, J.M., and Shenoy, R.K., "Acoustic Characteristics of Tail Rotor and the Effects of Empennage Interactions," Presented at the 43rd Annual Forum and Technology Display of the American Helicopter Society, St. Louis, Missouri, May 1986.

7. Owen, S.J. and Shenoy, R,K., "Numerical Investigation of Two-Dimensional Blade-Vortex Interaction," NASA CR−178326, September 1987.

8. Schmitz, F.H., Boxwell, D.A., Lewy, S., and Dahan, C., "Model- to Full-Scale Comparisons of Blade-Vortex Interaction Noise," Journal of the American Helicopter Society, Volume 29, No. 2, May 1984.

9. Condenser Microphones and Microphone Preamplifiers- Data Handbook, published by Bruel & Kjaer Instruments Inc., September 1982.

10. Roberson, J.A. and Crowe, C.T., Engineering Fluid Mechanics, Houghton Mifflin Company, Boston, MA, 1975.

11. Schmitz, F.H., and Yu, Y.H., "Theoretical Modeling of High-Speed Helicopter Impulsive Noise," Paper No. 54 presented at the Third European Rotocraft and Powered Lift Aircraft Forum, Aix-En-Provence, France, September 1977.

12. Dahan, C., and Gratieux, E., "Helicopter Rotor Thickness Noise," Journal of Aircraft, Vol. 18, No. 6, June 1981.

13. Hoad, D.R., "Helicopter Model Scale Results of Blade-Vortex Interaction Impulsive Noise As Affected By Tip Modification," Presented at the 36th Annual Forum of the American Helicopter Society, May 1980, pp. 80-62-1 – 80-62-13.

14. Boxwell, D.A., and Schmitz, F.H., "Full-Scale Measurements of Blade-Vortex Interaction Noise," Journal of the American Helicopter Society, Volume 27, No. 2, October 1982.

15. Gessow, A., and Myers, G.C., Aerodynamics of the Helicopter, College Park Press, Eighth Printing, 1985.

16. Sofrin, T.G., "Acoustic Characteristics of the S-76," Presented at the 1983 Proceedings of the Helicopter Noise Reduction Program, Hampton, Virginia, November 1983, NASA Conference Publication 2308.

17. Levine, L.S., "An Analytic Investigation of Techniques to Reduce Tail Rotor Noise," NASA CR-145014, July 1976.

Tables and Figures

Table 1.

Microphone Positions With Respect To The Main Rotor Shaft Centerline

(Traversing Wing Positioned at 2.52m)

Microphone	X (m)	Y (m)	Z (m)	R (m)	Ψ (°)	Θ(°)
1	0	-0.37	-1.02	1.09	90.04	43.04
2	-1.47	1.82	-1.06	2.57	309.1	22.4
3	0.04	0.37	-1.03	1.12	264.3	43.1
4	-1.76	-1.9	-1.04	2.79	47.3	20.5
5	2.52	0.86	-1.72	3.24	198.3	28
6	2.52	0.3	-1.72	3.14	186.6	28.7
7	2.52	-0.25	-1.72	3.13	174.4	28.8
8	2.52	-0.87	-1.72	3.24	161.6	27.9
9	2.52	-1.37	-1.72	3.41	152.3	26.8
10	3.15	-2.84	-0.01	4.24	138	0.1

Table 2.

Nominal Test Conditions For The Main Rotor/Tail Rotor Interaction Test

Config/Run #			Velocity	α sh	α tpp	MR Thrust	Tail SF*	Wing	Comments
MR/TR	MR	TR	(kts)	Angle, °	Angle, °	Coef, Ct	(lbs)	Pos, ft	
MR/TR Interaction Conditions:									
162.3	169.2	181.2	50	9.0	5.0	0.007	23.1	8.3	Max BVI, TR low
162.4	169.3	181.3	50	1.0	4.9	0.007	18.4	8.3	Max BVI, TR high
162.14	169.13	181.7	50	2.0	-2.1	0.007	27,1	8.3	Min BVI, TR low
162.15	169.14	181.8	50	-6.0	-2.0	0.007	25.3	8.3	Min BVI, TR high
163.1	170.1	182.4	60	2.0	5.7	0.007	13.5	8.3	Max BVI, TR high
163.4	170.3	182.2	60	10.0	6.1	0.007	14.6	8.3	Max BVI, TR low
163.7	171.2	183.3	60	2.0	-1.8	0.007	23.9	8.3	Min BVI, TR low
163.8	171.3	183.5	60	-6.0	-1.9	0.007	24.1	8.3	Min BVI, TR high
166.2	172.2	184.2	70	0	4.0	0.007	15.2	8.3	Max BVI, TR high
166.5	172.4	184.4	70	2.0	-1.9	0.007	24.6	8.3	Min BVI, TR low
166.6	172.1	184.1	70	-6.0	-2.0	0.007	23.0	8.3	Min BVI, TR high
167.1	173.7	185.4	80	-2.0	2.1	0.007	17.2	8.3	Max BVI, TR high
168.3	173.2	185.1	80	6.0	2.0	0.007	16.9	8.3	Max BVI, TR low
168.4	173.3	185.2	80	2.0	-2.0	0.007	22.0	8.3	Min BVI, TR low
168.7	173.9	185.5	80	-6.0	-2.0	0.007	27.6	8.3	Min BVI, TR high
Higher MR Thrust Conditions:									
162.5	169.4	181.4	50	1.0	4.9	0.0085	27.2	8.3	Max BVI, TR low
162.16	169.15	181.9	50	-6.0	-2.1	0.0085	34.7	8.3	Min BVI, TR high
Level Flight Conditions:									
162.7	169.6	181.5	50	0.4	-2.0	0.0075	28.8	8.3	Level Flight
163.5	170.6	183.4	60	0.5	2.8	0.00735	20.9	8.3	
166.8	172.3	184.3	70	0.9	-2.5	0.0071	21.9	8.3	
168.5	173.4	185.3	80	1.1	-3.0	0.0074	26.0	8.3	
Advance Ratio Trend:									
162.9	169.8	181.14	50	5.7	4.1	0.0072	20.2	11.61	Max BVI, TR low
163.6	170.4	182.3	60	5.8	4.1	0.0073	17.3	8.3	"
166.9	172.5	184.5	70	6.2	3.6	0.00723	15.2	8.3	"
*As measured using total tail side force for the MR/TR configuration.									
MR Flapping vs. No Flapping (MR alone):									
	114.1		50	4.5	5.1	0.007		8.3	Minimum Flap
	114.2		50	8.6	5.1	0.007		8.3	Negative Flap
	114.3		50	0	4.6	0.007		8.3	Positive Flap
	115.2		50	-0.5	0	0.007		15.7	Minimum Flap
	115.3		50	-0.4	0	0.007		12.3	Minimum Flap
	115.4		50	-0.4	0	0.007		8.3	Minimum Flap
	115.5		50	-3.8	0	0.007		8.3	Positive Flap
	115.6		50	3.1	0.1	0.007		8.3	Negative Flap
Check of MR Phase I Trends (MR alone):									
	112.1		80	-2	-2		0.007	8.3	Min BVI
	112.2		80	0	0	0.007		8.3	
	112.3		80	2	2	0.007		8.3	
	112.4		80	4	4	0.007		8.3	Max BVI

Table 2. (Continued)
Nominal Test Conditions For The Main Rotor/Tail Rotor Interaction Test

Config/Run # MR/TR	MR	TR	Velocity (kts)	α sh Angle, °	α tpp Angle, °	MR Thrust Coef, Ct	Wing Pos, ft	Comments
	112.5		80	6	6	0.007	8.3	
	112.6		80	8	8	0.007	8.3	
	112.7		80	10	10	0.007	8.3	
	113.2		60	-4	-4	0.007	8.3	Min BVI
	113.3		60	-6	-6	0.007	8.3	
	113.4		60	-8	-8	0.007	8.3	
	113.5		60	-10	-10	0.007	8.3	
	113.6		60	-2	-2	0.007	8.3	
	113.7		60	0	0	0.007	8.3	
	113.8		60	3	3	0.007	8.3	
	113.9		60	4	4	0.007	8.3	Max BVI
	113.10		60	6	6	0.007	8.3	
Background Noise Measurements (Rotor Drives w/o Blades):								
840.2 - 840.7			50 - 80				8.3	Bkgd. noise w/ Tunnel Velocity Sweep
841.1 - 841.7			80	-9 to +9 (3° increments)			8.3	Bkgd. noise w/ Shaft Angle
843.2 - 843.7			80				4.3 - 15.7	Bkgd. noise w/ wing pos.
Tunnel Relection Measurements (no blades present):								
801			0	0			15.7	Charge @MR Hub
802, 803			80	0			15.7	Effects of Flow
805			0	0			4.3	Wing Pos. Effects
805			0	0			15.7	Charge @TR Hub

Table 3.

Microphone Positions With Respect To The Main Rotor Shaft Centerline (Tunnel Reflection Data)

(Traversing Wing Positioned at 4.85m)

Microphone	X (m)	Y (m)	Z (m)	R (m)	Ψ (°)	Θ(°)
1	0	-0.37	-1.02	1.09	90	43
2	-1.47	1.82	-1.06	2.57	309.1	22.4
3	0.04	0.37	-1.03	1.12	264.3	43.1
4	-1.76	-1.9	-1.04	2.79	47.3	20.5
5	4.85	0.86	-1.72	5.21	190.1	18.2
6	4.85	0.3	-1.72	5.15	183.6	18.4
7	4.85	-0.25	-1.72	5.15	177	18.5
8	4.85	-0.87	-1.72	5.21	169.9	18.2
9	4.85	-1.37	-1.72	5.33	164.2	17.9
10	3.15	-2.84	-0.01	4.24	138	0.1

Table 4.

The Delay Times and Amplitudes of Principle Refelections Observed From Recorded Impulse Data

Microphone	Charge Location	Reflection Times	Relative Amplitude (ref/dir)	Expected Surface
1	MR Hub*	1.404 ms	16.7%	Model Fuselage
		3.152 ms	37.5%	Floor
		7.5 ms	35.5%	Unknown
		27-40 ms	16.7%	Walls and Ceiling

Note: Mic 1 was positioned in the shadow of the fuselage for the various charge locations measured. At Mic 1, the phase of the incident pulse was inverted relative to the other microphones. It is believed that the shadowing produced this effect by shielding the microphone from the compressive component of the impulse.

4	MR Hub*	1.41 ms	62.5%	Model Fuselage
		5.3-6.24 ms	30%	Floor
		23-40 ms	20%	Walls and Ceiling
5	MR Hub w/ and w/o airflow	1.44 ms	30%	Floor
		12.2 ms	25%	FLoor
		22-40 ms	18.8%	Walls and Ceiling
	TR Hub (multiple reflections)	0-6 ms	up to 75%	Random, Unknown
		23-40 ms	30%	Walls and Ceiling
9	MR Hub*	1.56 ms	32.5%	Model Fuselage
		17.4 ms	30%	Floor
		20-30 ms	15%	Walls and Ceiling
10	MR Hub*	1.406 ms	18.8%	Model Fuselage
		17.5-26 ms	25%	Walls and Ceiling

*The reflection characteristics were essentially unchanged in the presence of flow or with the charges moved to the tail rotor hub location.

Table 5.
MR/TR and TR Alone Data Sorted For Comparison

Config.	Run#	Pt#	Vel (kt)	α_{tpp} (°)	α_{sh} (°)	TR Thr. (lbs)
TR	181	3	50.0		1.0	12.9
MR/TR	162	4	49.7	5.0	1.1	13.6
TR	181	14	50.0		5.7	13.6
TR	181	13	50.0		5.7	13.6
TR	181	2	50.0		8.8	13.7
MR/TR	162	12	50.1	4.2	5.7	13.8
TR	181	12	50.0		5.7	13.8
TR	181	15	50.0		5.7	13.9
MR/TR	162	8	50.4	4.2	5.7	14.1
TR	181	6	50.0		5.7	14.5
MR/TR	162	10	50.1	4.2	5.7	14.6
TR	181	11	50.0		5.7	14.9
MR/TR	162	11	50.1	4.2	5.7	14.9
MR/TR	162	9	50.4	4.2	5.7	15.1
MR/TR	162	3	50.5	5.1	9.0	15.6
MR/TR	162	15	50.4	-2.0	-6.0	17.6
TR	181	8	50.0		-6.1	18.2
MR/TR	162	2	50.8	5.1	9.0	18.4
TR	181	4	50.0		1.0	18.4
MR/TR	162	13	50.4	-2.0	2.0	18.9
MR/TR	162	14	50.1	-2.2	2.0	19.4
TR	181	7	50.0		2.1	20.2
TR	181	5	50.0		0.4	20.5
TR	181	10	50.0		2.0	21.3
MR/TR	162	5	50.2	5.1	1.1	22.5
TR	181	9	50.0		-6.0	26.1
MR/TR	162	16	49.5	-2.0	-6.0	27.1
MR/TR	163	1	60.5	5.4	2.0	8.9
TR	183	2	60.0		2.0	9.9
MR/TR	163	4	60.8	6.1	10.1	10.3
TR	182	4	60.0		2.0	10.9
TR	182	2	60.0		10.0	11.6
TR	182	3	60.0		5.8	12.0
MR/TR	163	6	60.8	4.1	5.8	12.1
MR/TR	163	3	60.7	6.0	2.0	15.8
TR	183	4	60.0		0.5	15.9

Table 5.(continued)

MR/TR and TR Alone Data Sorted For Comparison

Config.	Run#	Pt#	Vel (kt)	α_{tpp} (°)	α_{sh} (°)	TR Thr. (lbs)
MR/TR	163	7	61.0	-2.2	2.0	16.2
MR/TR	163	8	61.1	-1.9	-6.1	16.5
MR/TR	163	2	60.9	6.1	2.0	16.5
TR	183	3	60.0		2.0	17.5
TR	183	5	60.0		-6.0	19.0
MR/TR	163	9	60.9	-2.1	-6.1	24.6
MR/TR	166	9	70.4	3.6	6.2	9.8
TR	184	5	70.0		6.2	11.0
TR	184	2	70.0		0.0	11.2
MR/TR	166	4	70.9	4.0	8.1	11.2
MR/TR	166	8	70.3	-2.5	0.9	14.1
MR/TR	166	6	70.0	-1.9	-6.1	15.4
TR	184	3	70.0		0.9	16.4
MR/TR	166	5	70.3	-1.8	2.0	17.1
TR	184	1	70.0		-6.0	17.3
TR	184	4	70.0		2.0	19.2
MR/TR	166	7	71.0	-2.1	-6.0	22.0
MR/TR	164	6	70.5	-2.1	-6.0	22.7
MR/TR	167	3	80.8	2.0	6.1	6.4
MR/TR	168	6	80.4	3.1	6.4	7.1
MR/TR	167	9	80.8	3.6	6.5	10.5
MR/TR	168	3	80.5	2.1	6.0	10.9
MR/TR	167	4	80.7	-1.9	2.0	11.1
TR	185	1	80.0		6.0	11.2
MR/TR	167	1	80.7	2.1	-2.1	11.2
MR/TR	167	8	80.1	3.2	6.4	11.3
TR	185	4	80.0		-2.0	14.2
MR/TR	168	4	80.7	-2.0	2.0	14.4
MR/TR	165	6	80.3	-2.0	-6.1	14.6
MR/TR	167	5	80.7	-2.1	-6.1	15.1
MR/TR	167	7	80.6	-3.0	1.1	15.5
TR	185	2	80.0		2.0	15.8
MR/TR	168	5	80.7	-3.0	1.1	18.0
MR/TR	167	2	80.1	2.0	-2.1	18.0
MR/TR	168	7	80.3	-2.1	-6.0	19.9
TR	185	3	80.0		1.1	21.0
MR/TR	167	6	80.1	-2.0	-6.1	21.8

Table 6.

Overall Sound Levels for the MR/TR and MR Alone Test Matrix

Vel. (m/s)	αsh (°)	αtpp (°)	MR Ct	TR Thr (lbs)	Mic 1		Mic 4		Mic 5		Mic 9		Mic 10	
					MR/TR	MR	MR/TR	MR	MR/TR	MR	MR/TR	MR	MR/TR	MR
25.8	9	5	0.007	15.6	117.4	117	112.2	110.5	106.7	107.1	110.6	110.5	107.8	107.4
25.8	1	4.9	0.007	13.6	116.8	115.2	111.3	109	105.7	105	110	109.1	106.1	105.4
25.8	2	-2.1	0.007	19.4	114.3	113.4	114	112.1	107.2	107	110.7	110.1	106.6	105.7
25.8	-6	-2	0.007	17.6	113.2	111.1	112.4	110.7	108.6	108.8	110	110.2	107.1	106
30.9	2	5.7	0.007	8.9	117.7	117.5	110.7	107.6	105.3	105.9	110.4	110.5	107.9	108.2
30.9	10	6.1	0.007	10.3	118	117.9	112.2	110.9	107.5	108	111.5	111.4	109.7	109.5
30.9	2	-1.8	0.007	16.2	114.9	113.3	113.6	109.9	105.2	103.4	110	109	106.8	105.5
30.9	-6	-1.9	0.007	16.5	114.4	113.5	111.6	107.8	107.1	106.3	108.3	109.2	106.4	105.1
36.1	0	4	0.007	10	119.1	119.3	111.1	109.6	108.4	107.2	112.5	112.8	109.4	110
36.1	2	-1.9	0.007	17.1	115.4	114.7	112.2	109.5	109.5	107	110.8	110.6	107	107
36.1	-6	-2	0.007	15.4	115.3	114.6	112.7	108.9	105.5	105.6	109.5	110.5	105.8	106.3
41.2	-2	2.1	0.007	11.2	120.2	119.8	111.8	109.8	109.5	109	113.5	113.1	109.2	110.7
41.2	6	2	0.007	10.9	120.2	119.3	113	111.6	108.9	108.2	113.6	113.2	110.2	110.5
41.2	2	-2	0.007	14.4	117.8	117.2	112.2	109.7	108.3	107.8	112.3	112.6	108.2	108.3
41.2	-6	-2	0.007	20	116.3	115.7	113.1	106.7	107.4	107.8	110.8	111	107.3	107.6
25.8	1	4.9	0.0085	22.5	117.6	116.3	113	111	109.3	110.3	113.2	112.7	108.8	107
25.8	-6	-2.1	0.0085	27.1	112.7	109.8	113.7	112.5	111.4	112.1	112.4	112.2	108.5	107.7
25.8	0.4	-2	0.0075	21.2	115.2	113.8	114.1	111.9	108.4	108	111.6	110.4	106.8	105.3
30.9	0.5	2.8	0.00735	14.9	116	114.7	111.5	108.8	106	105.4	109.3	108.5	105.6	104.7
36.1	0.9	-2.5	0.0071	14.1	115.4	113.6	112.1	110	104.3	105.4	110.5	110.2	106.6	106.2
41.2	1.1	-3	0.0074	18	116.7	114.4	113.4	108.9	107.2	106.8	111.8	111.6	108.1	107.8
25.8	5.7	4.1	0.0072	15.1	116.8	117.3	112.9	109.2	106.5	107	109.7	110.2	105.9	105.7
30.9	5.8	4.1	0.0073	12.1	117.4	117.5	111.4	109.3	105.2	105.1	110.2	110.2	108.3	108.8
36.1	6.2	3.6	0.00723	9.8	119.3	119.3	111.7	110	108.4	108.2	112.9	112.7	109.6	109.8
			Average Value		116.6	115.7	112.4	109.8	107.4	107.2	111.1	110.9	107.7	107.3
			Std. Dev.		2.0	2.6	0.9	1.4	1.7	1.9	1.4	1.4	1.4	1.8
			Max. Value		120.2	119.8	114.1	112.5	111.4	112.1	113.6	113.2	110.2	110.7
			Min. Value		112.7	109.8	110.7	106.7	104.3	103.4	108.3	108.5	105.6	104.7

Table 7.

Flight-Scaled dBA Sound Levels for the MR/TR and MR Alone Test Matrix

Vel. (m/s)	αsh (°)	αtpp (°)	MR Ct	TR Thr (lbs)	Mic 1 MR/TR	Mic 1 MR	Mic 4 MR/TR	Mic 4 MR	Mic 5 MR/TR	Mic 5 MR	Mic 9 MR/TR	Mic 9 MR	Mic 10 MR/TR	Mic 10 MR
25.8	9	5	0.007	15.6	107.2	103.9	104.5	94.6	96.4	96.3	100.1	99.3	99	94.4
25.8	1	4.9	0.007	13.6	108.3	100.2	103.7	92.1	96.2	93.9	100.2	97.3	96.4	93.3
25.8	2	-2.1	0.007	19.4	107.3	101.5	105.6	93.1	96.1	95	101.1	98.1	97.6	93.5
25.8	-6	-2	0.007	17.6	106.2	102.6	103.3	93.2	98.1	98.2	102.6	103.2	98.7	95.9
30.9	2	5.7	0.007	8.9	109.4	104.8	104.2	95.1	95.5	95.5	102.2	101.3	97.2	95.7
30.9	10	6.1	0.007	10.3	108.2	105.4	103.7	99.1	95.9	95	101.9	101.8	98.5	96.8
30.9	2	-1.8	0.007	16.2	109.3	101.4	105.6	93.3	95.4	94.9	101	98.9	98.3	94
30.9	-6	-1.9	0.007	16.5	109.6	102.5	105.8	93.1	98.7	96.3	101.8	101	98.8	95.4
36.1	0	4	0.007	10	110.7	105.6	105	98.6	97.5	96.5	104	102.3	98.5	97.3
36.1	2	-1.9	0.007	17.1	108.0	102.6	104.7	94.3	96.7	97.9	101.4	100.6	97.5	95.1
36.1	-6	-2	0.007	15.4	111.9	101.9	105.4	93.7	97.9	97	103.4	100.3	98.8	95.3
41.2	-2	2.1	0.007	11.2	112.1	106.4	105.8	98.4	100.6	98.7	106.5	104	99.4	98
41.2	6	2	0.007	10.9	110.8	108.1	104.6	100.5	97.9	96.3	104.2	104	100.3	98.2
41.2	2	-2	0.007	14.4	109.7	105.8	104	96.5	99.4	97.5	103.1	103.4	99.1	97
41.2	-6	-2	0.007	20	112.9	104.1	106.9	95	99.8	98.9	104.1	103.1	100.6	96.6
25.8	1	4.9	0.0085	22.5	109.1	103.4	104.6	93.2	99.9	98.6	96.1	93.9	100	97.3
25.8	-6	-2.1	0.0085	27.1	106.7	101.8	105.2	94	99.1	97.6	92.5	91.2	99.5	96
25.8	0.4	-2	0.0075	21.2	108.8	101.1	106.06	93.38	107.9	95.4	103.4	98.8	98.6	94.1
30.9	0.5	2.8	0.00735	14.9	109.2	101.4	104.9	93.6	96.3	95.2	101.5	99.1	96.6	94
36.1	0.9	-2.5	0.0071	14.1	109.1	102.1	105.2	94.4	95.8	96.6	101.6	99.9	98.4	95.2
41.2	1.1	-3	0.0074	18	110.9	104.1	105.3	96.2	98.7	97.6	101.9	101.4	100.2	96.9
25.8	5.7	4.1	0.0072	15.1	106.7	102.4	104.8	93.4	95.7	96.9	99.7	99.1	96.5	94.3
30.9	5.8	4.1	0.0073	12.1	109.0	104.9	104.3	96.6	95.4	95.1	101.8	101.3	98.4	95.2
36.1	6.2	3.6	0.00723	9.8	109.0	106.7	104.3	98.7	97.4	97.1	103.4	103.2	99.3	97.5
			Average Value		109.2	103.5	104.9	95.2	97.8	96.6	101.6	100.3	98.6	95.7
			Std. Dev.		1.7	2.1	0.8	2.3	2.7	1.4	2.8	3.1	1.2	1.5
			Max. Value		112.9	108.1	106.9	100.5	107.9	98.9	106.5	104.0	100.6	98.2
			Min. Value		106.2	100.2	103.3	92.1	95.4	93.9	92.5	91.2	96.4	93.3

Table 8.

Test Matrix With Corrected TR Thrust and TR BPF Harmonic Levels

Vel. (m/s)	α_{sh} (°)	α_{tpp} (°)	MR C_t	TR Thr. (lbs)	TR BPF Harmonic Level Mic3 (dB)	Mic4 (dB)	Mic10 (dB)
25.8	9	5	0.007	15.6	103	101.9	97.6
25.8	1	4.9	0.007	13.6	106.8	102.3	96.5
25.8	2	-2.1	0.007	19.4	104.6	103.6	96.1
25.8	-6	-2	0.007	17.6	107.6	101.4	100
30.9	2	5.7	0.007	8.9	105.7	103.3	97.8
30.9	10	6.1	0.007	10.3	102.8	104.3	100.5
30.9	2	-1.8	0.007	16.2	104.5	103.1	97.5
30.9	-6	-1.9	0.007	16.5	107.3	103.8	100
36.1	0	4	0.007	10	105.9	104.7	98.9
36.1	2	-1.9	0.007	17.1	104.8	103.4	98.3
36.1	-6	-2	0.007	15.4	106.8	106	98.8
41.2	-2	2.1	0.007	11.2	106.6	104.9	100
41.2	6	2	0.007	10.9	105	104.8	101.1
41.2	2	-2	0.007	14.4	106.2	104.1	99.9
41.2	-6	-2	0.007	20	106.4	106.1	100.5
25.8	1	4.9	0.0085	22.5	108.1	104.1	99.4
25.8	-6	-2.1	0.0085	27.1	108.6	104.3	101.1
25.8	0.4	-2	0.0075	21.2	107	105.1	98
30.9	0.5	2.8	0.00735	14.9	105.6	104	95.2
36.1	0.9	-2.5	0.0071	14.1	105.3	103.5	98.1
41.2	1.1	-3	0.0074	18	107.3	104.6	100.7
25.8	5.7	4.1	0.0072	15.1	104.4	104.4	96.2
30.9	5.8	4.1	0.0073	12.1	103.6	102.6	98.3
36.1	6.2	3.6	0.00723	9.8	104.1	103.7	100.6
				Avg.	105.8	103.9	98.8
				Std. Dev.	1.6	1.2	1.7
				Max.	108.6	106.1	101.1
				Min.	102.8	101.4	95.2

Table 9.

Correlation Matrix of Primary Test Parameters With Tail Rotor Harmonic Noise at Microphones 3, 4, and 10

	Velocity (m/s)	α_{sh} (°)	α_{tpp} (°)	MR C_t	TR Thrust (lbs.)
Velocity (m/s)	1.0				
α_{sh} (°)	-0.75	1.0			
α_{tpp} (°)	-0.253	0.613	1.0		
MR C_t	-0.357	-0.169	0.016	1.0	
TR Thrust (lbs)	-0.379	-0.493	-0.549	0.665	1.0
Mic3 Har* (dB)	-0.01	-0.823	-0.431	0.497	0.568
Mic4 Har* (dB)	0.515	-0.275	-0.229	0.121	0.118
Mic10 Har* (dB)	0.496	-0.209	-0.206	0.188	0.059

*Integrated sound pressure level of the first 10 TR BPF harmonics.

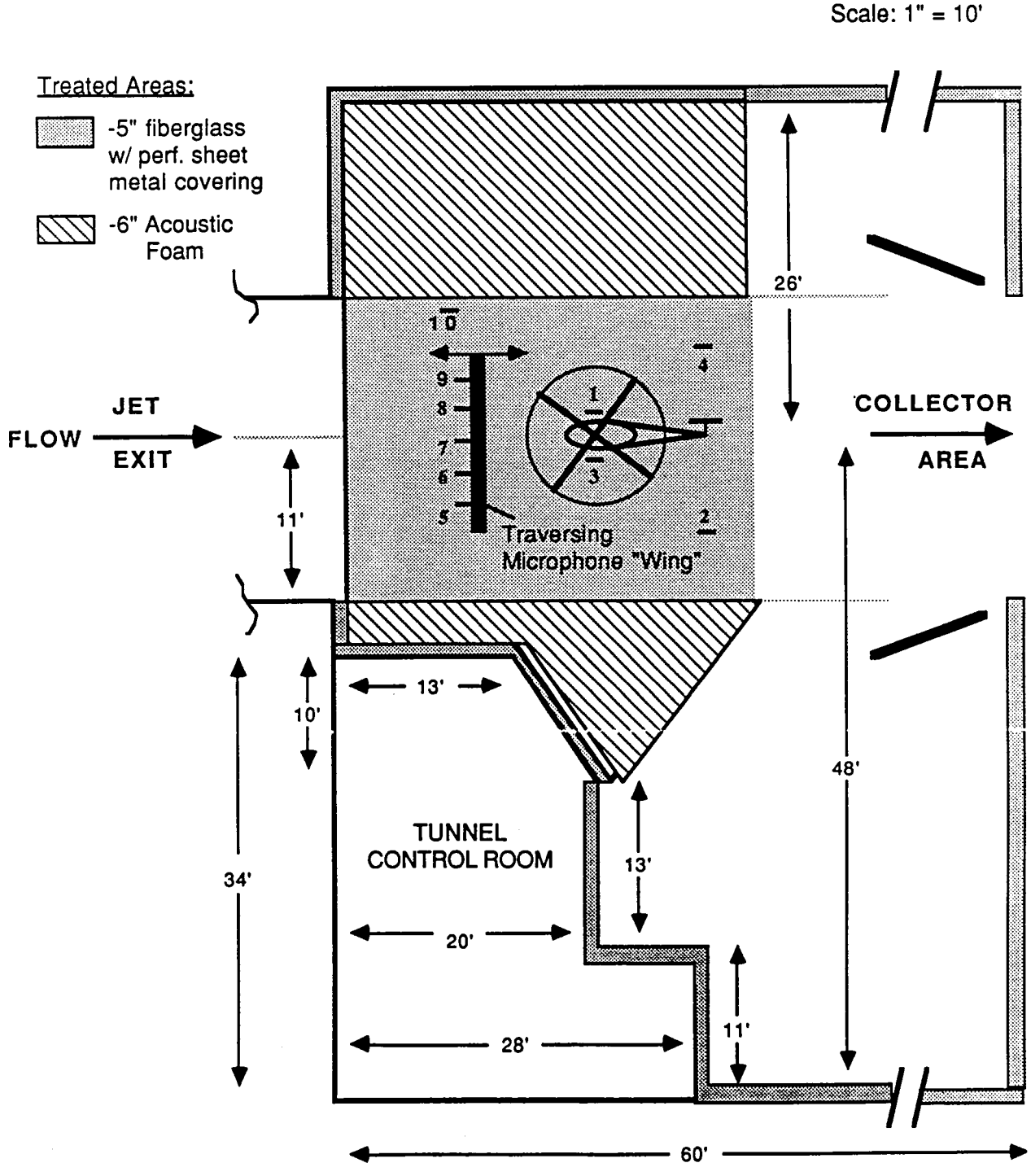

Figure 1. Top View of the model installation and the microphone locations in the 14 by 22 ft. subsonic wind tunnel test section.

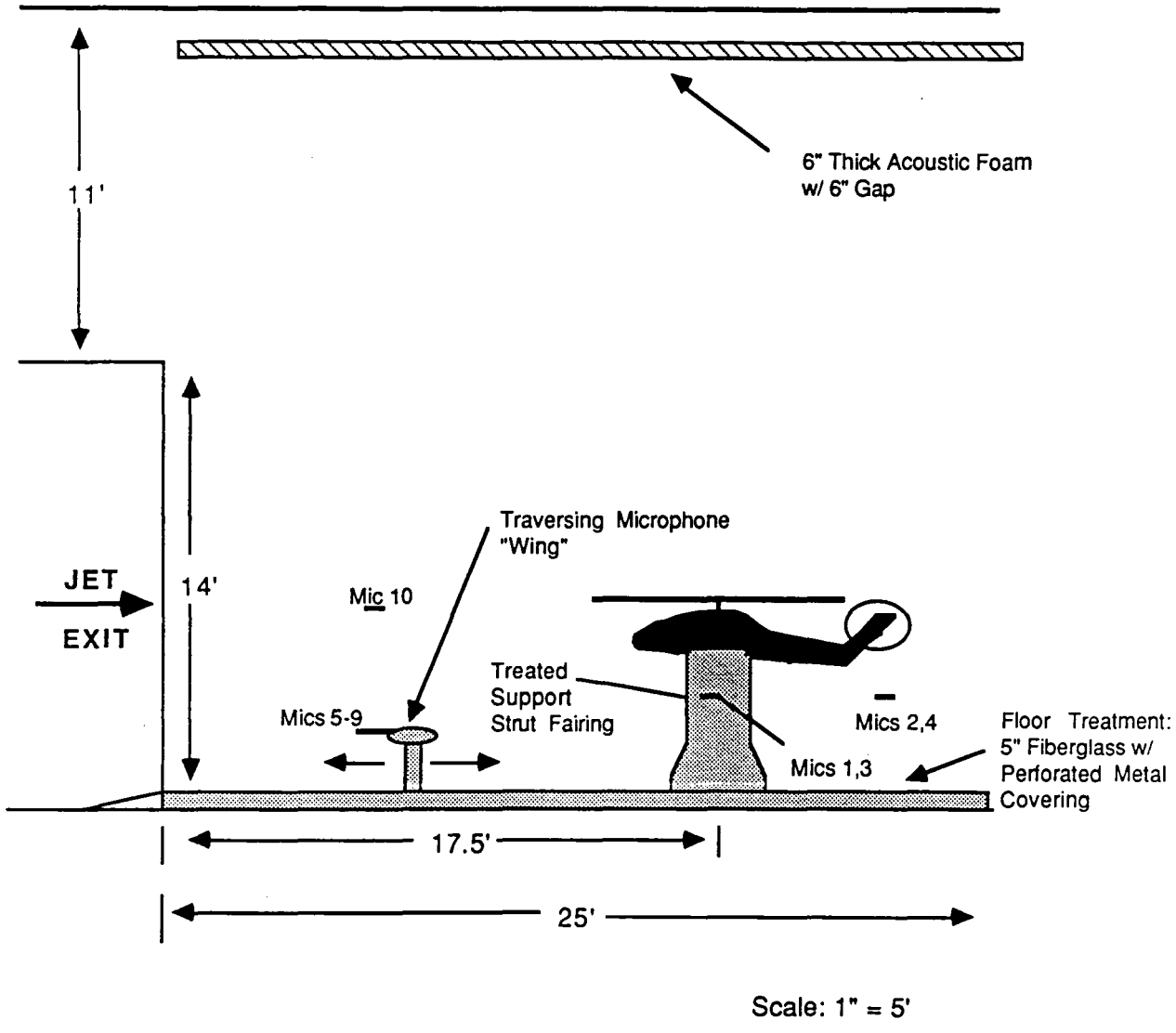

Figure 2. Side View of the Model Installation and the Microphone Locations in the 14 by 22 Ft. Subsonic Wind Tunnel Test Section.

Figure 3. Layout of the 14 by 22 Ft. Subsonic Wind Tunnel Control Areas.

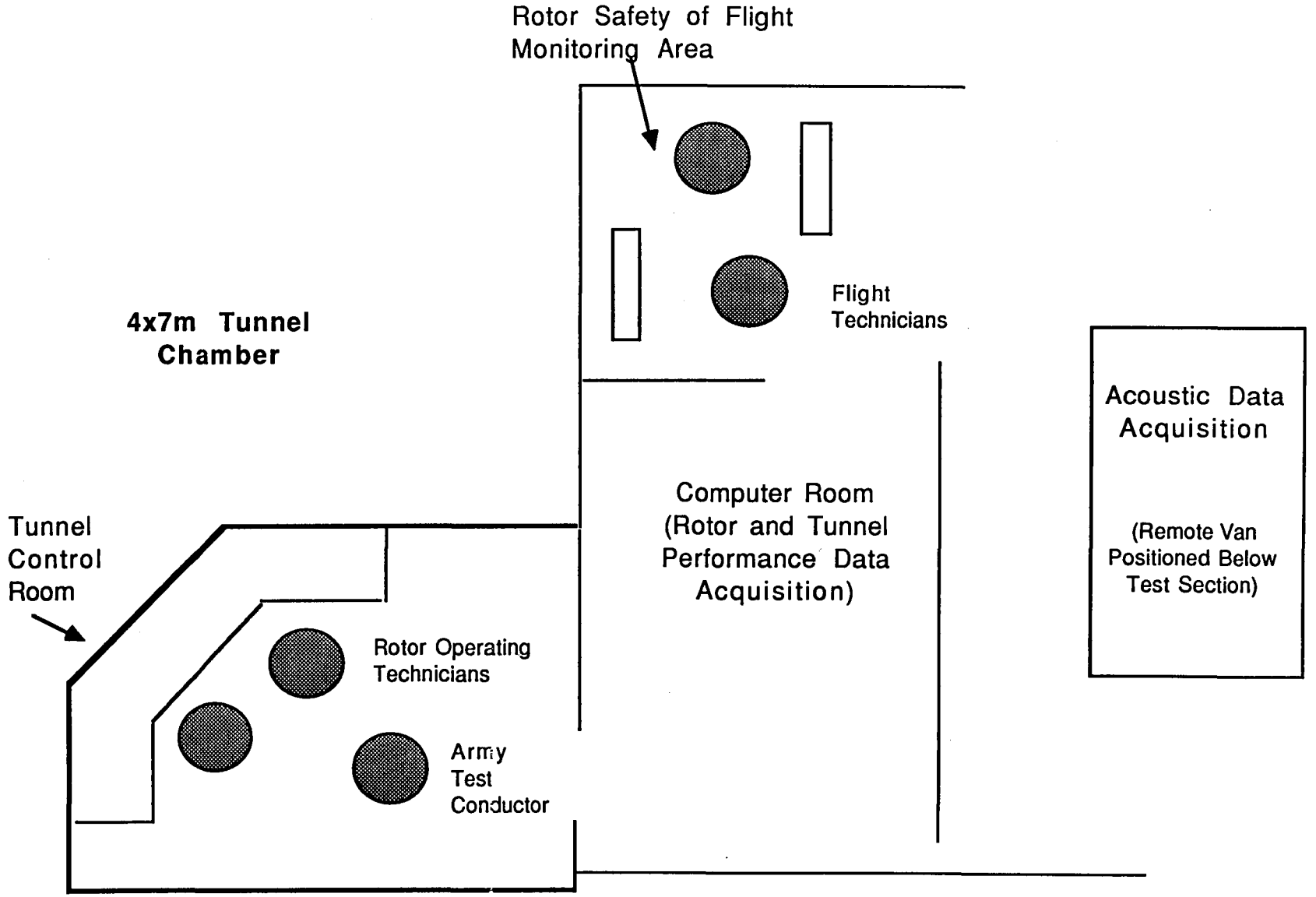

FIGURE 4. SCHEMATIC OF BMTR#1, 1/5.727 SCALE BLACK HAWK MODEL MOUNTED ATOP ACOUSTIC FAIRING IN THE LANGLEY 14'X22' WIND TUNNEL.

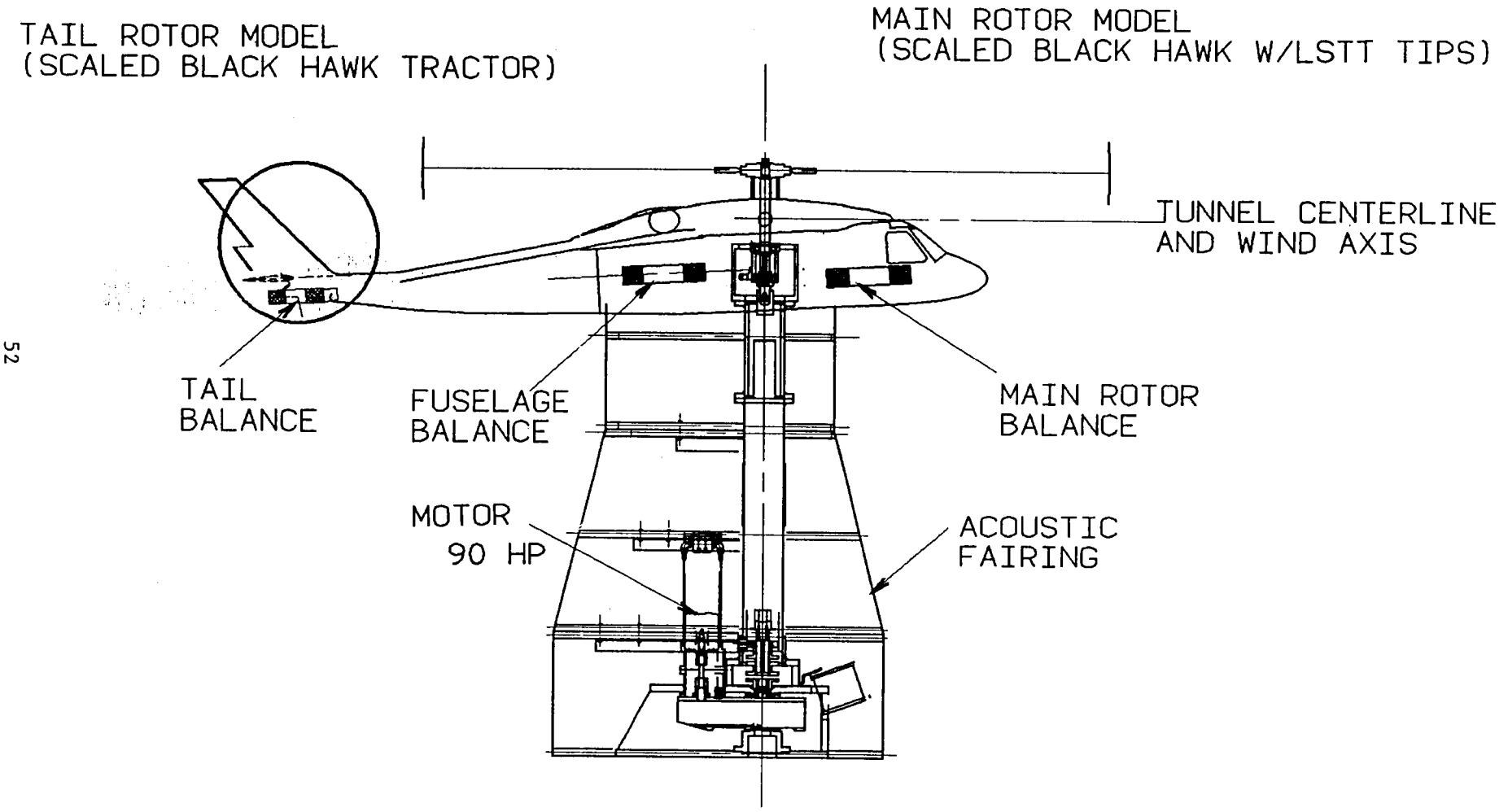

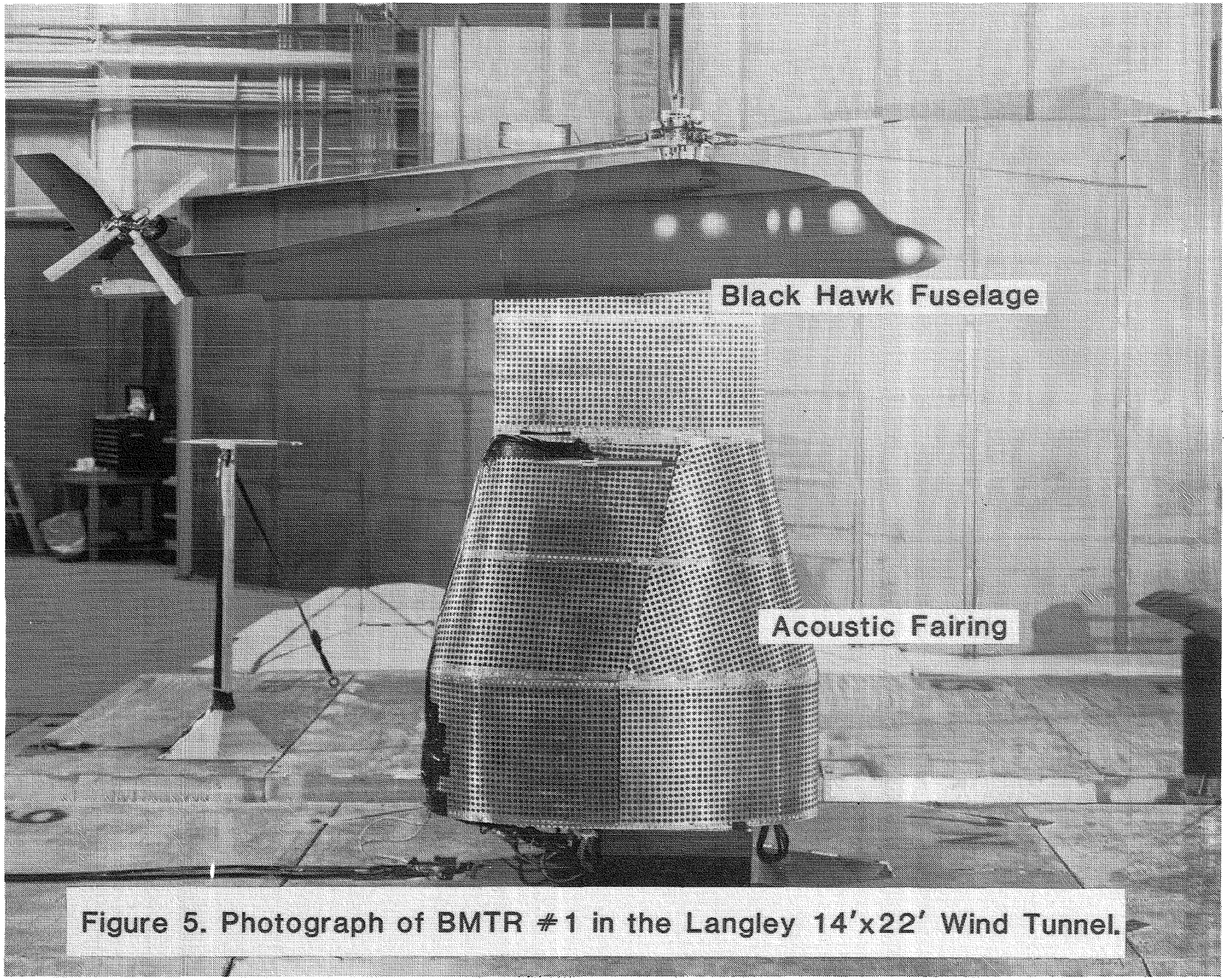

Figure 5. Photograph of BMTR #1 in the Langley 14'x22' Wind Tunnel.

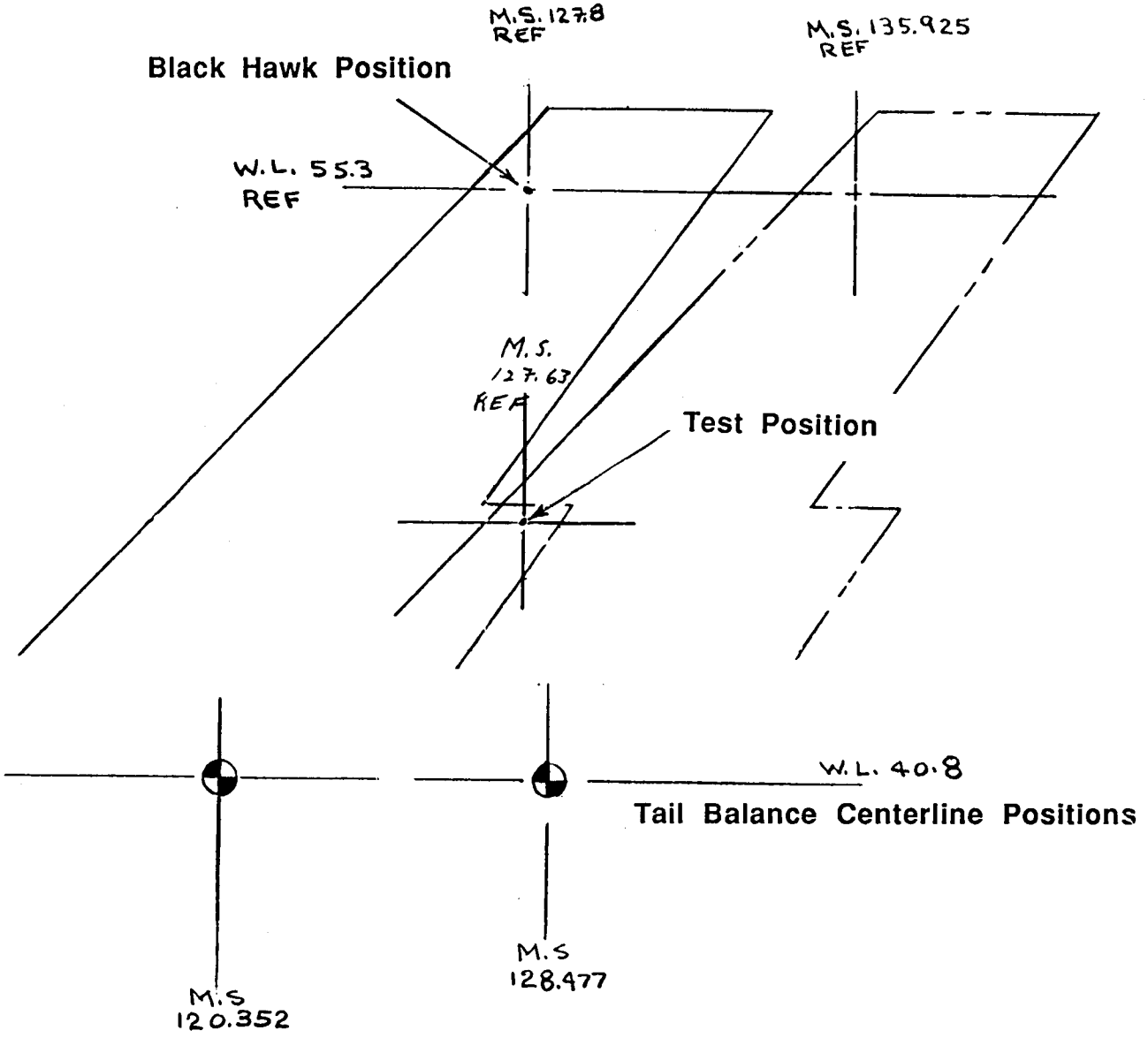

Figure 6. BMTR #1 available tail rotor centerline positions.

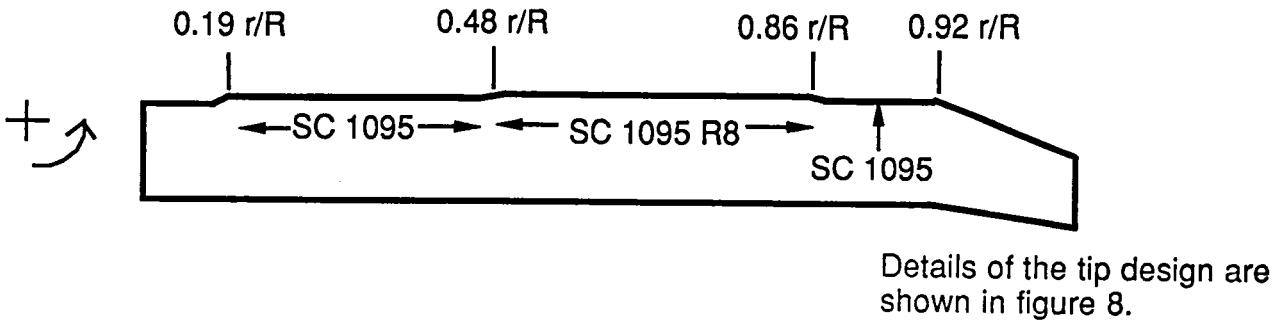

a) Main rotor blade planform.

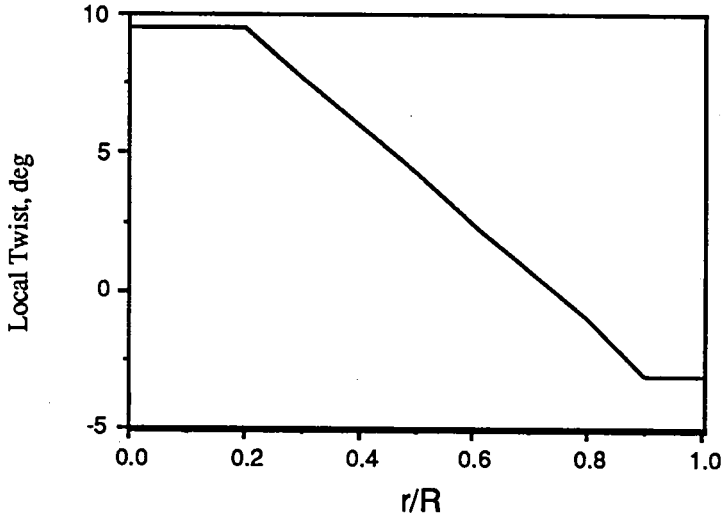

b) Main rotor blade twist distribution.

Figure 7. Model main rotor blade geometry.

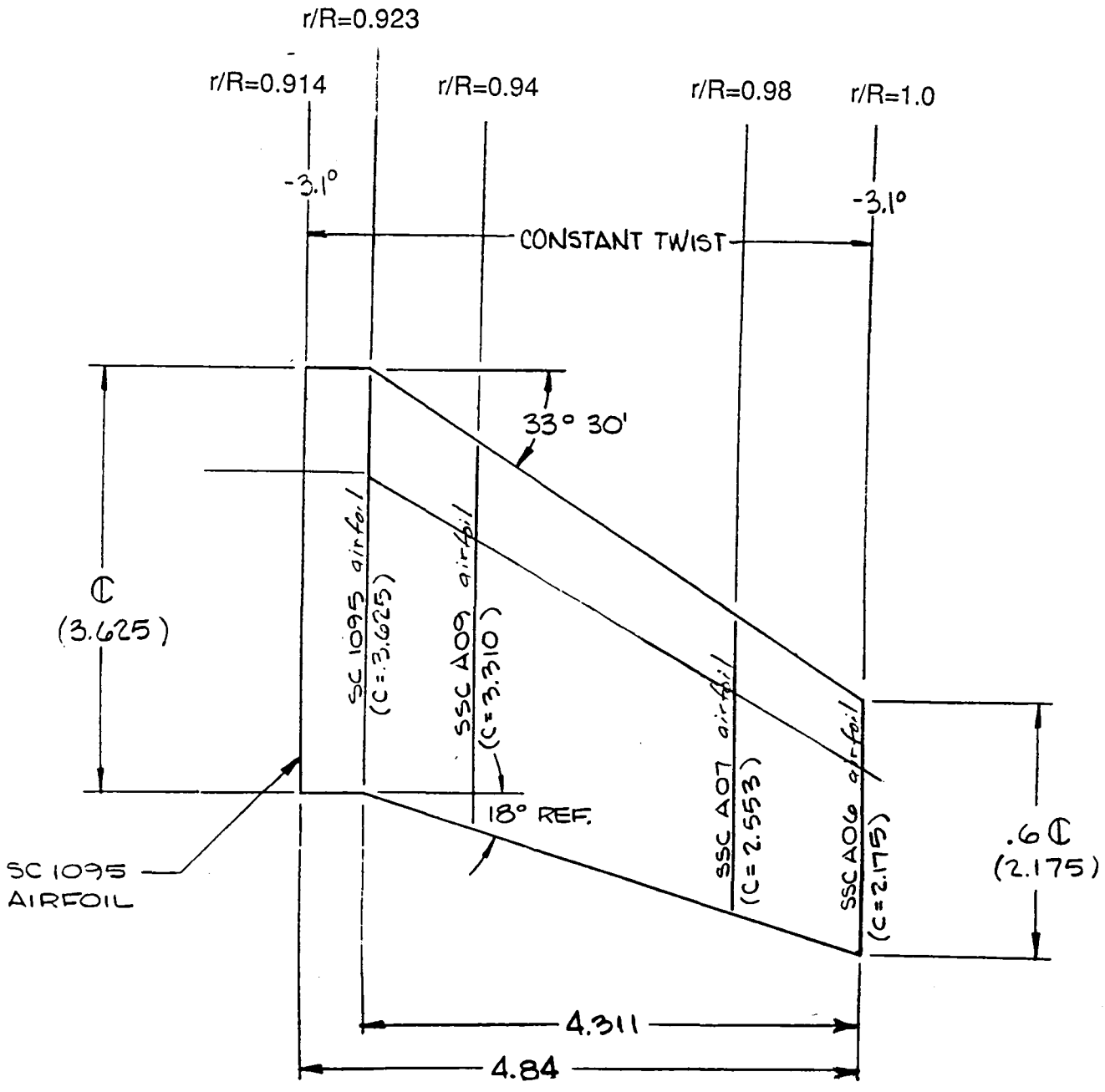

Figure 8. Model main rotor large swept tapered tip planform and airfoils (dimensions in inches).

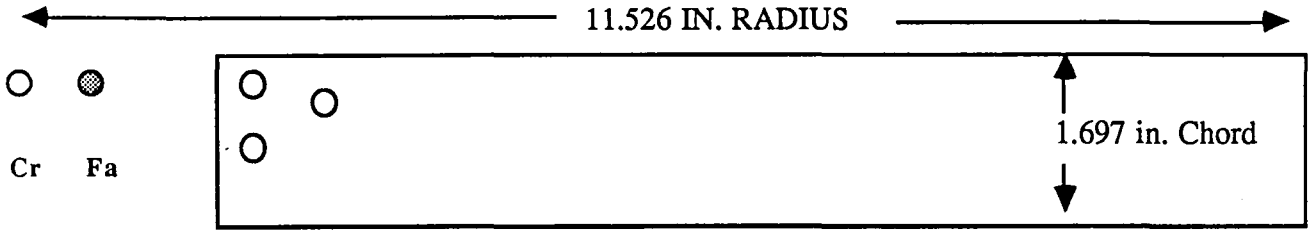

i) Tail rotor blades used for TR alone testing.

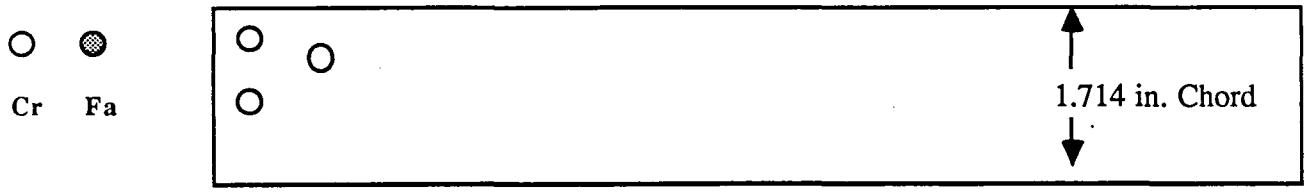

ii) Tail rotor blades used for MR/TR testing.

a) Tail rotor blade planforms.

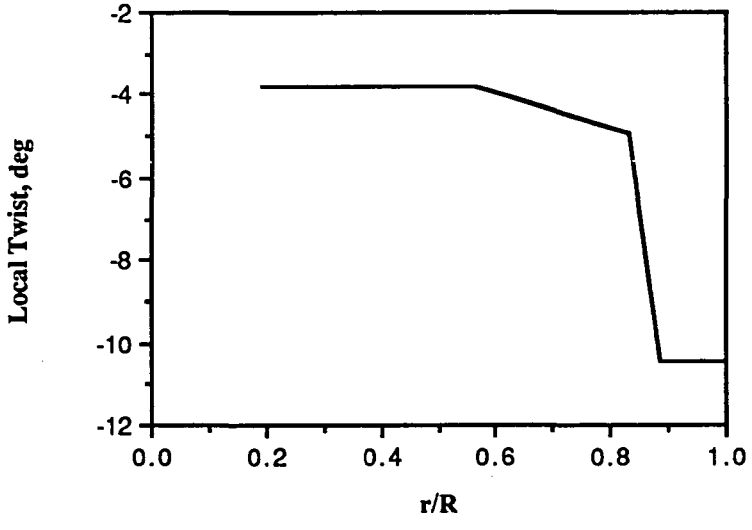

b) Tail rotor blade twist distribution.

Figure 9. Model tail rotor blade geometry.

Figure 10. SC1095 and SC1095RN airfoil sections utilized on the tail rotor models.

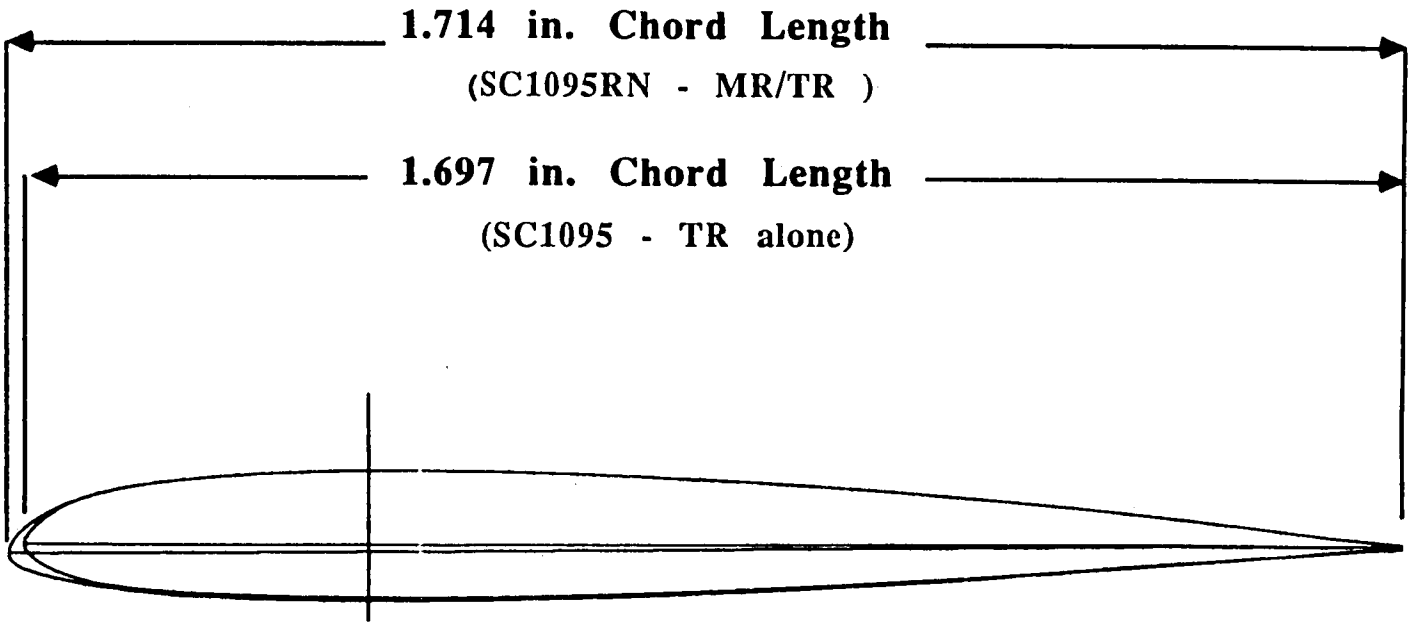

Figure 11. Acoustic data acquisition system schematic.

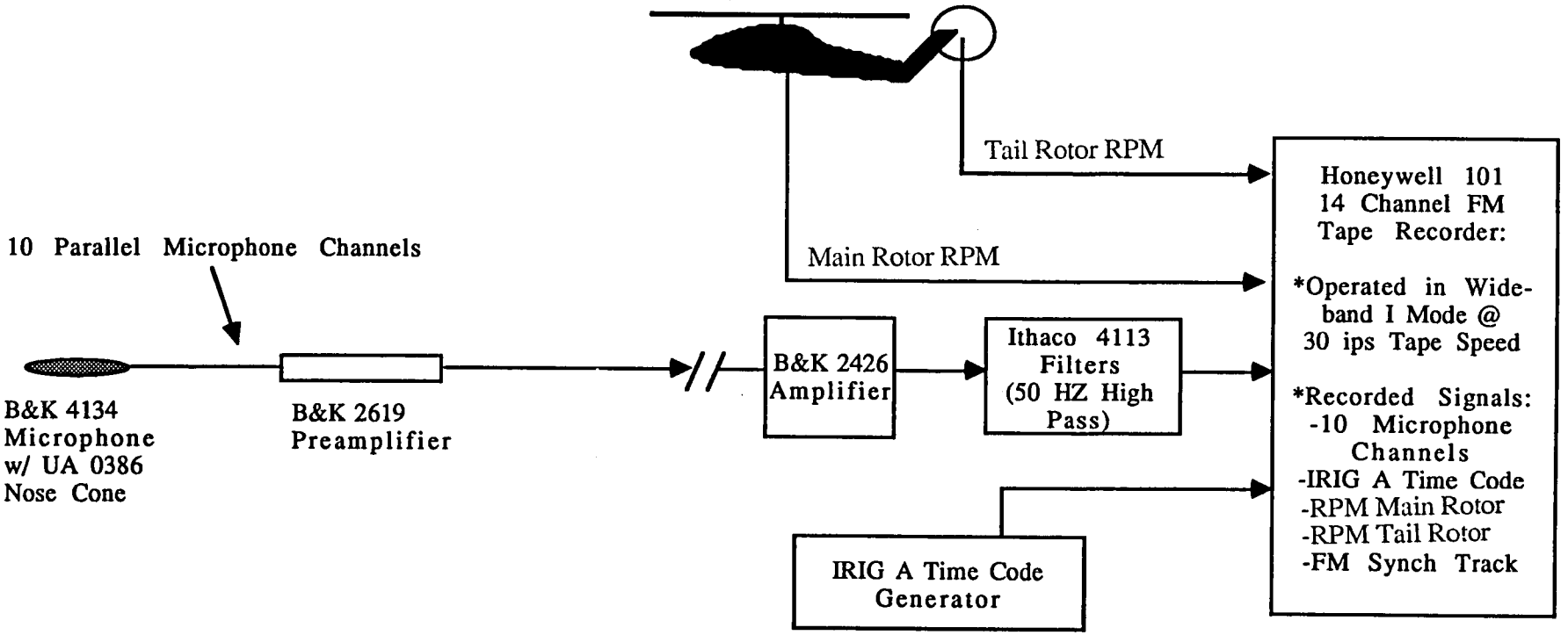

Figure 12. Acoustic Data Reduction Schematic.

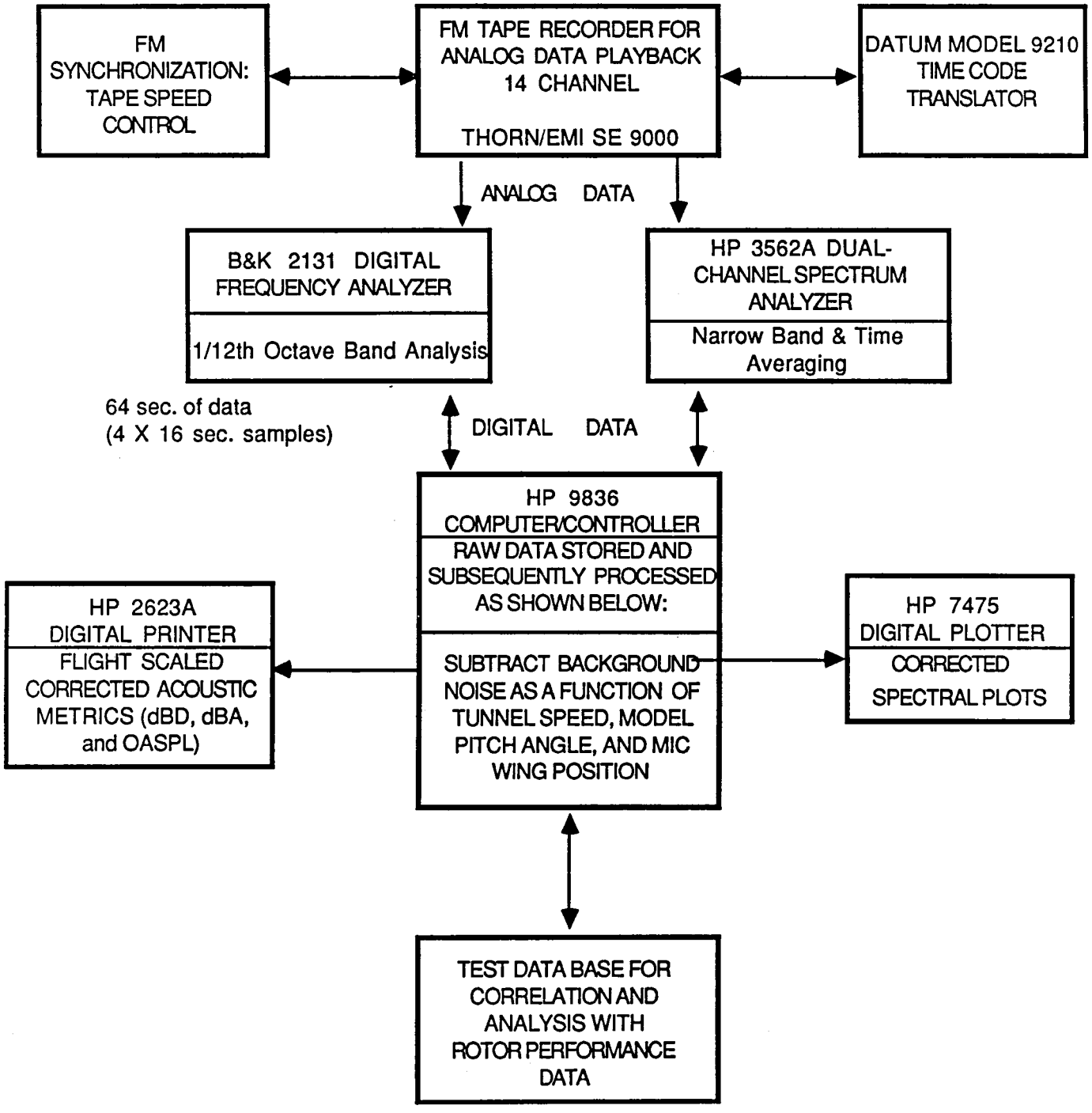

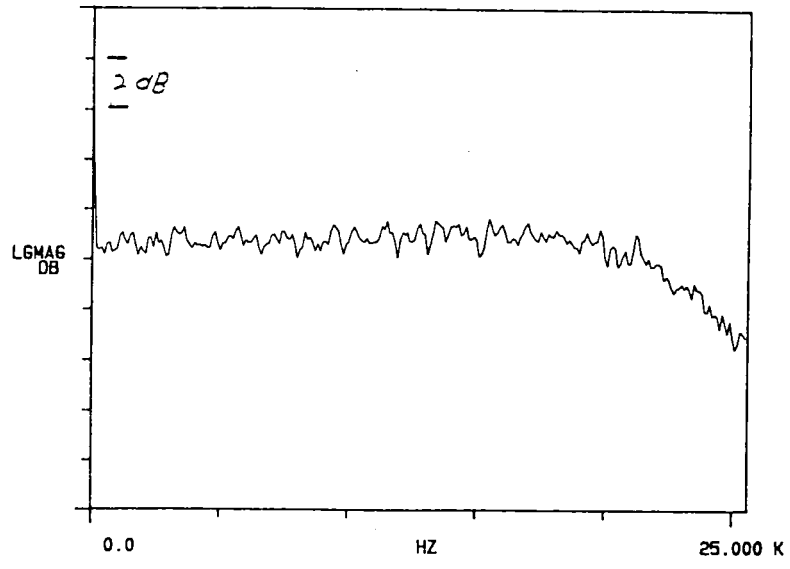

a) Typical random noise power spectrum, microphone channel #4 shown.

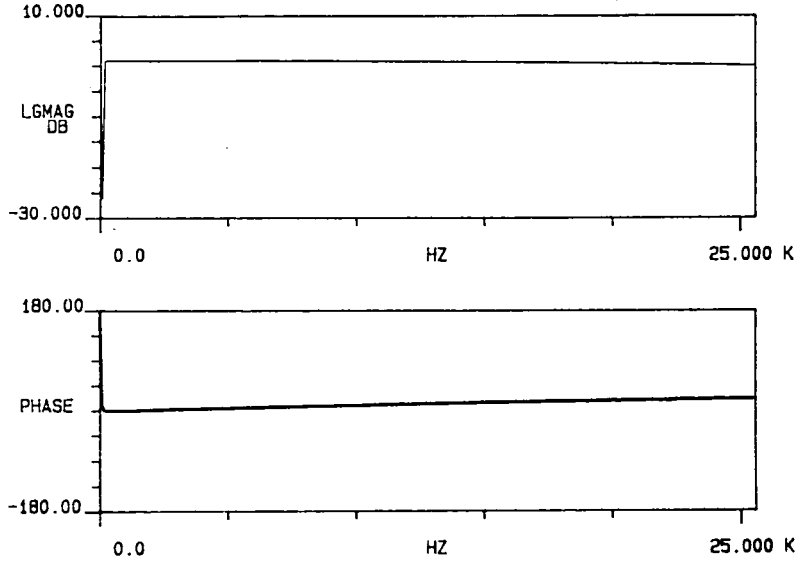

b) Typical channel-to-channel frequency response function, channel #4 with respect to channel #2 shown.

Figure 13. Measurement system random noise response characteristics (200 averages, 50 Hz resolution).

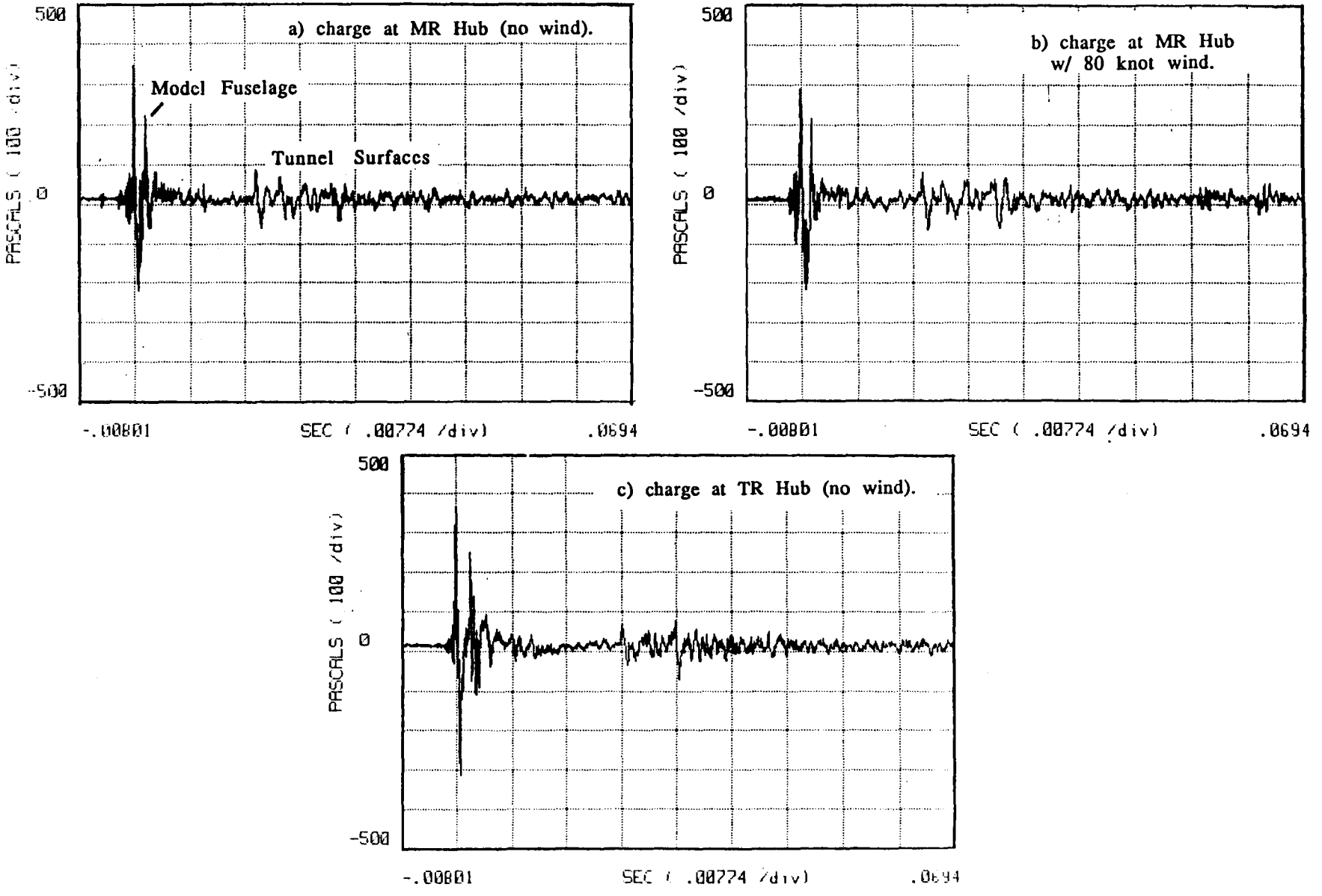

Figure 14. Impulsive source calibration data for microphone 9.

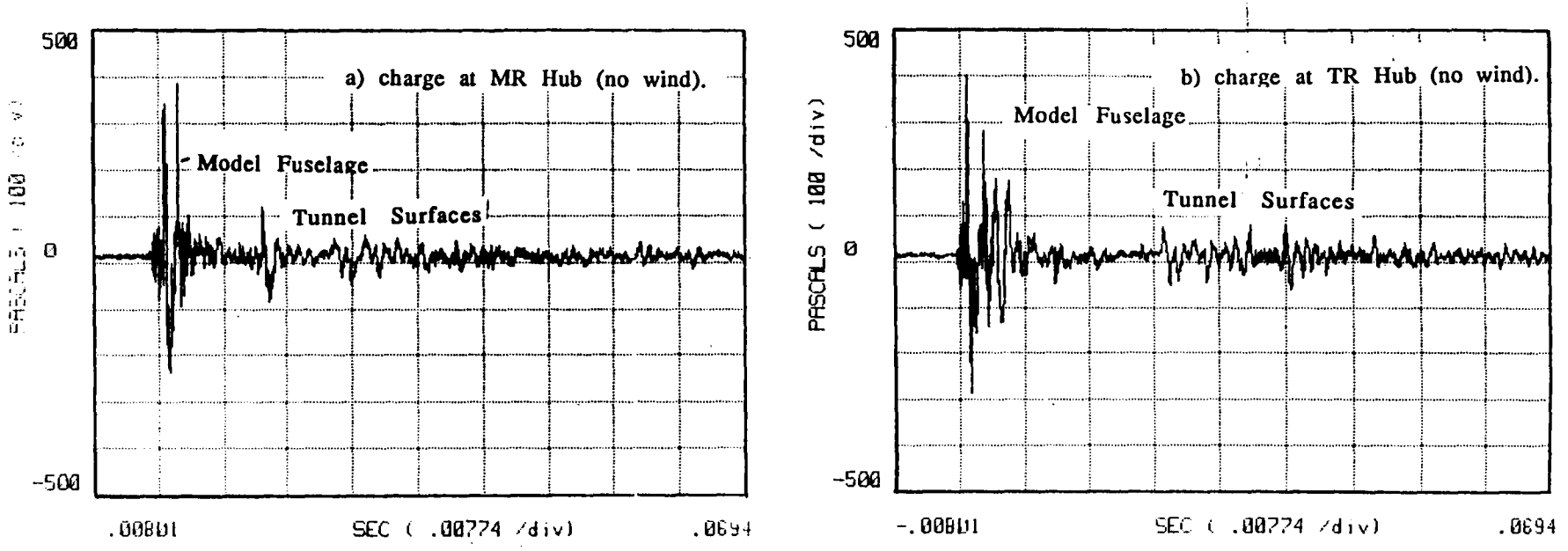

Figure 15. Impulsive source calibration data for microphone 5.

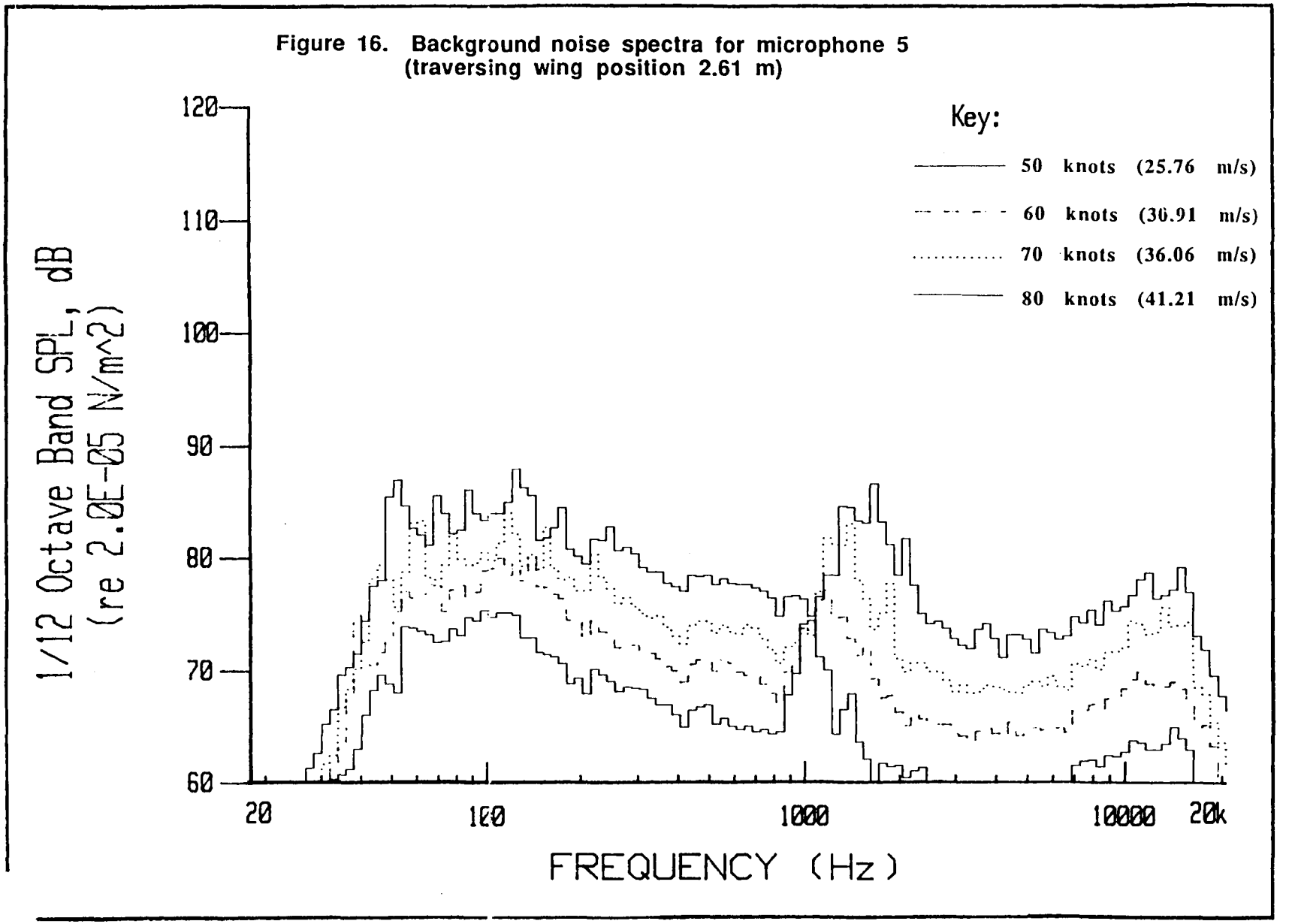

Figure 16. Background noise spectra for microphone 5 (traversing wing position 2.61 m)

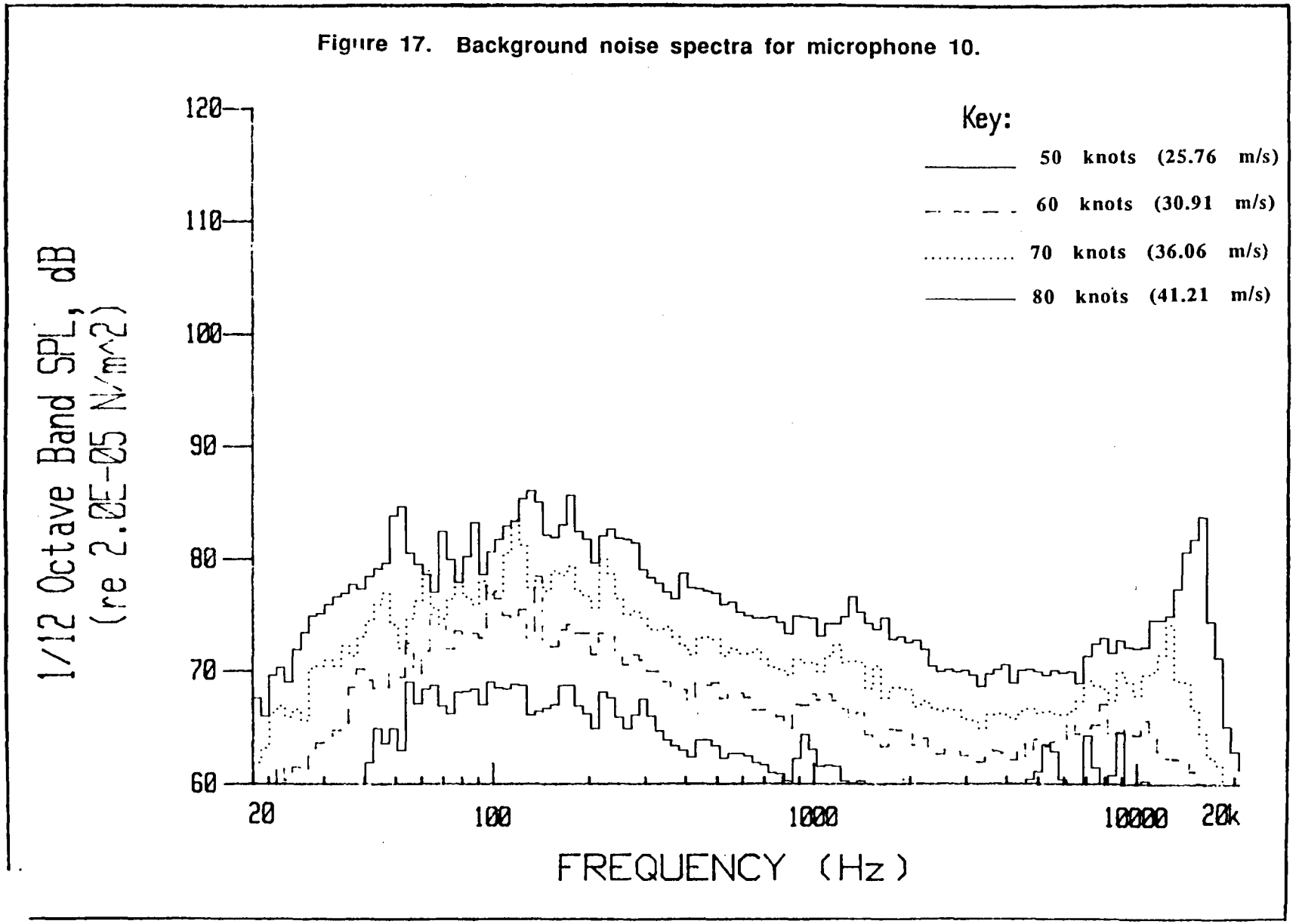

Figure 17. Background noise spectra for microphone 10.

Figure 18. Comparison of MR noise and background noise for microphone 1, 41.2 m/s, α_{tpp}=-2°, C_t=0.007.

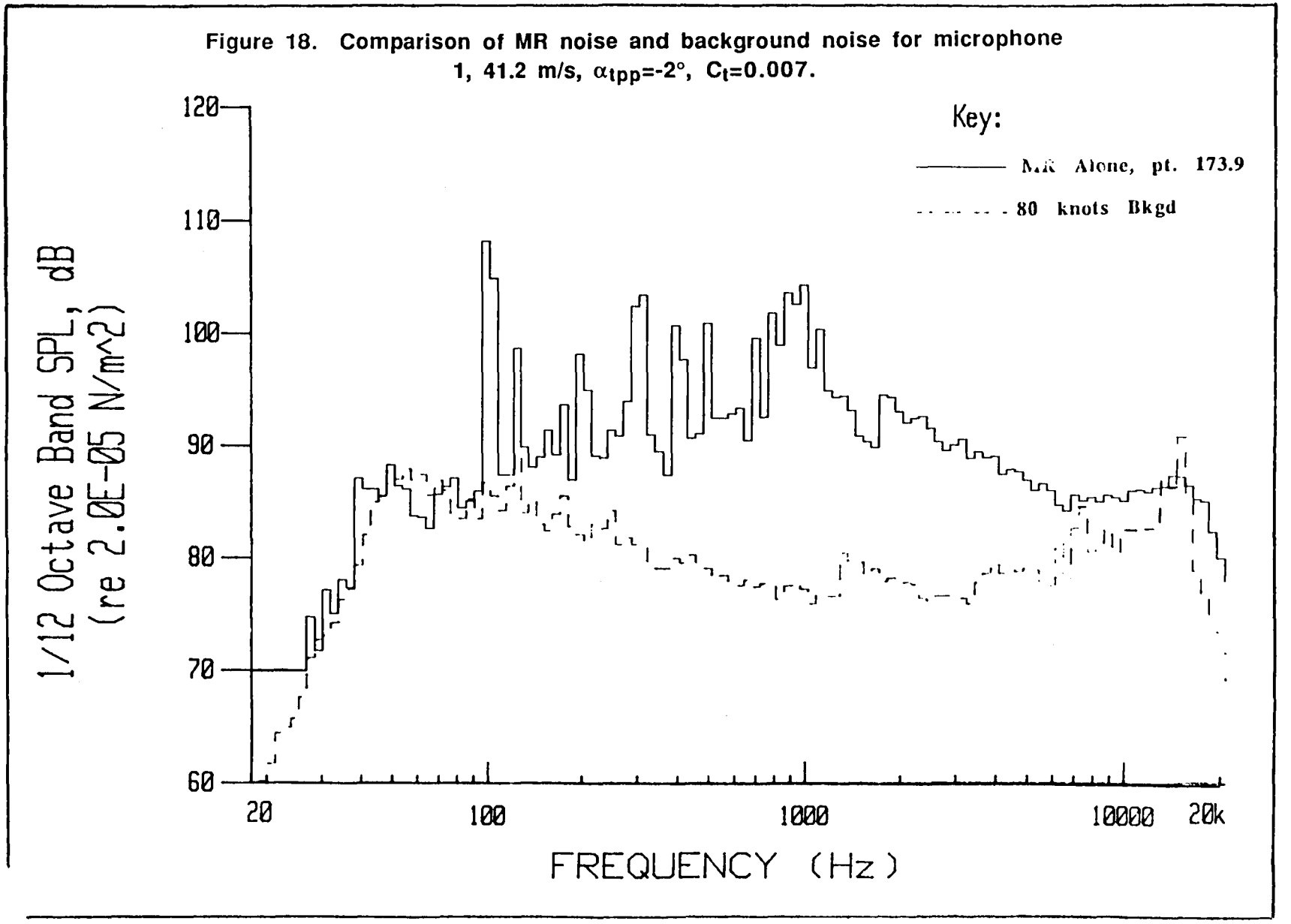

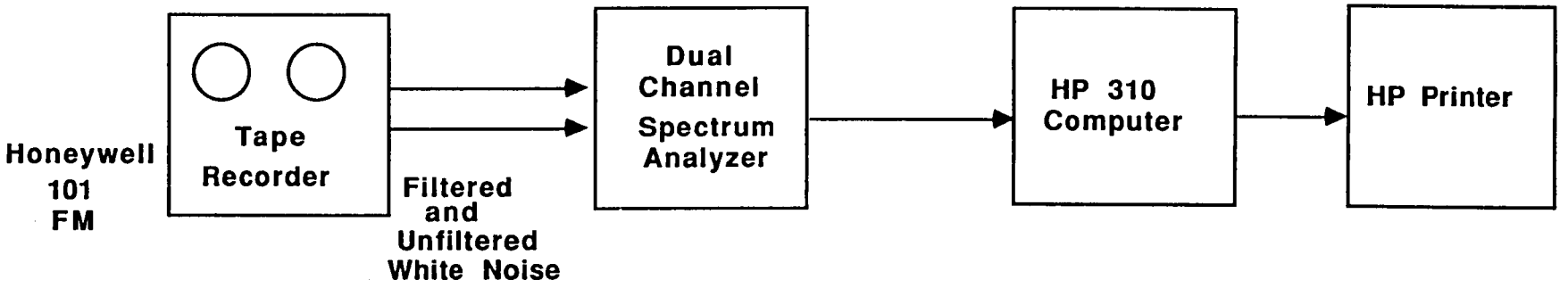

Figure 19. Instrumentation for high pass filter frequency response measurement.

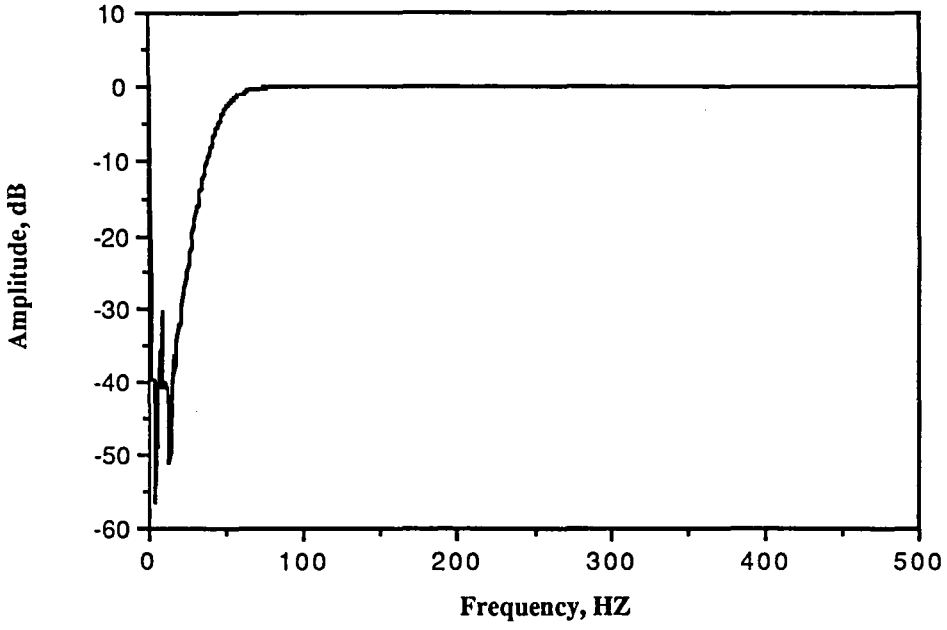

a) 50 Hz high pass filter amplitude response.

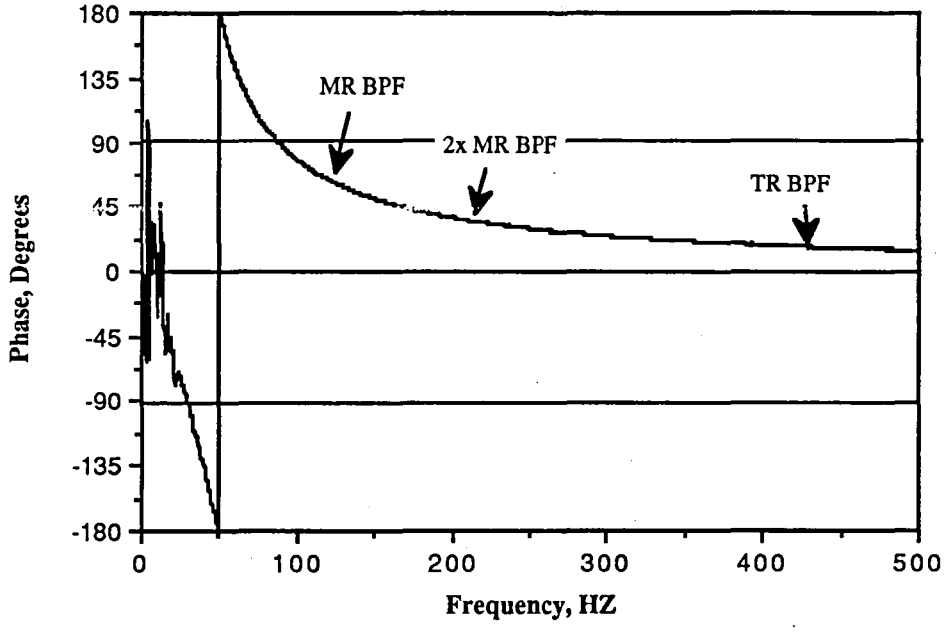

b) 50 Hz high pass filter phase response.

Figure 20. Amplitude and phase response of the high pass filters.

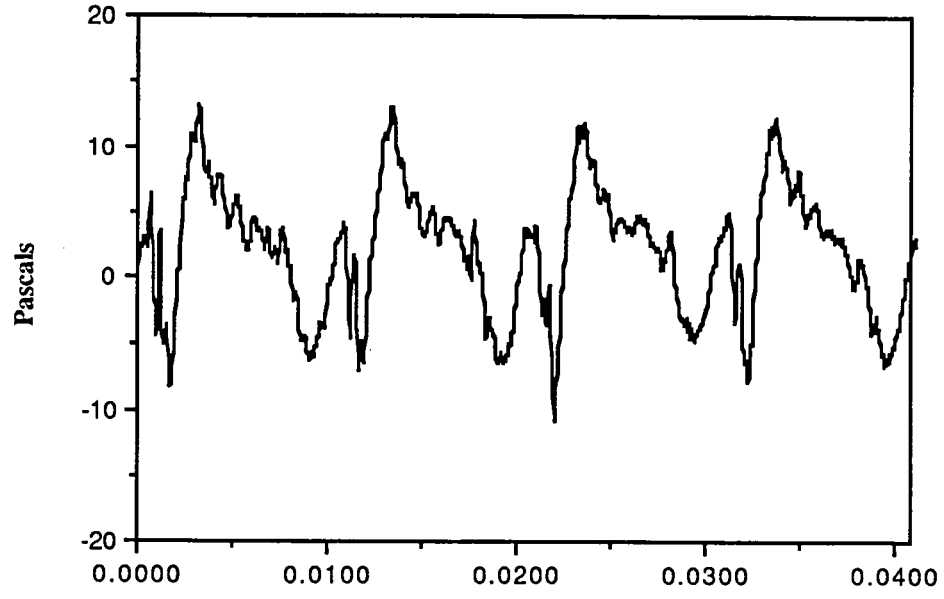

a) Uncorrected synchronously averaged pressure time history for microphone 10.

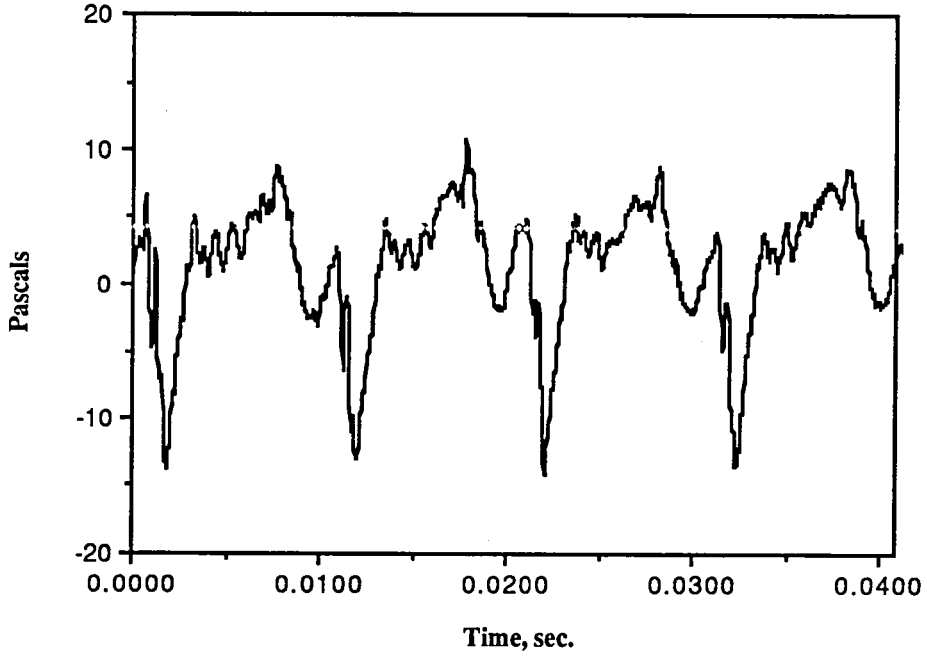

b) As above but corrected for filter phase response.

Figure 21. Filter phase response effects shown for microphone 10, μ=0.186, α_{tpp}=-3°, C_t=0.0074.

Figure 22. The effects of MR BVI on the acoustic spectra at microphone 7, μ=0.134, C_t=0.007.

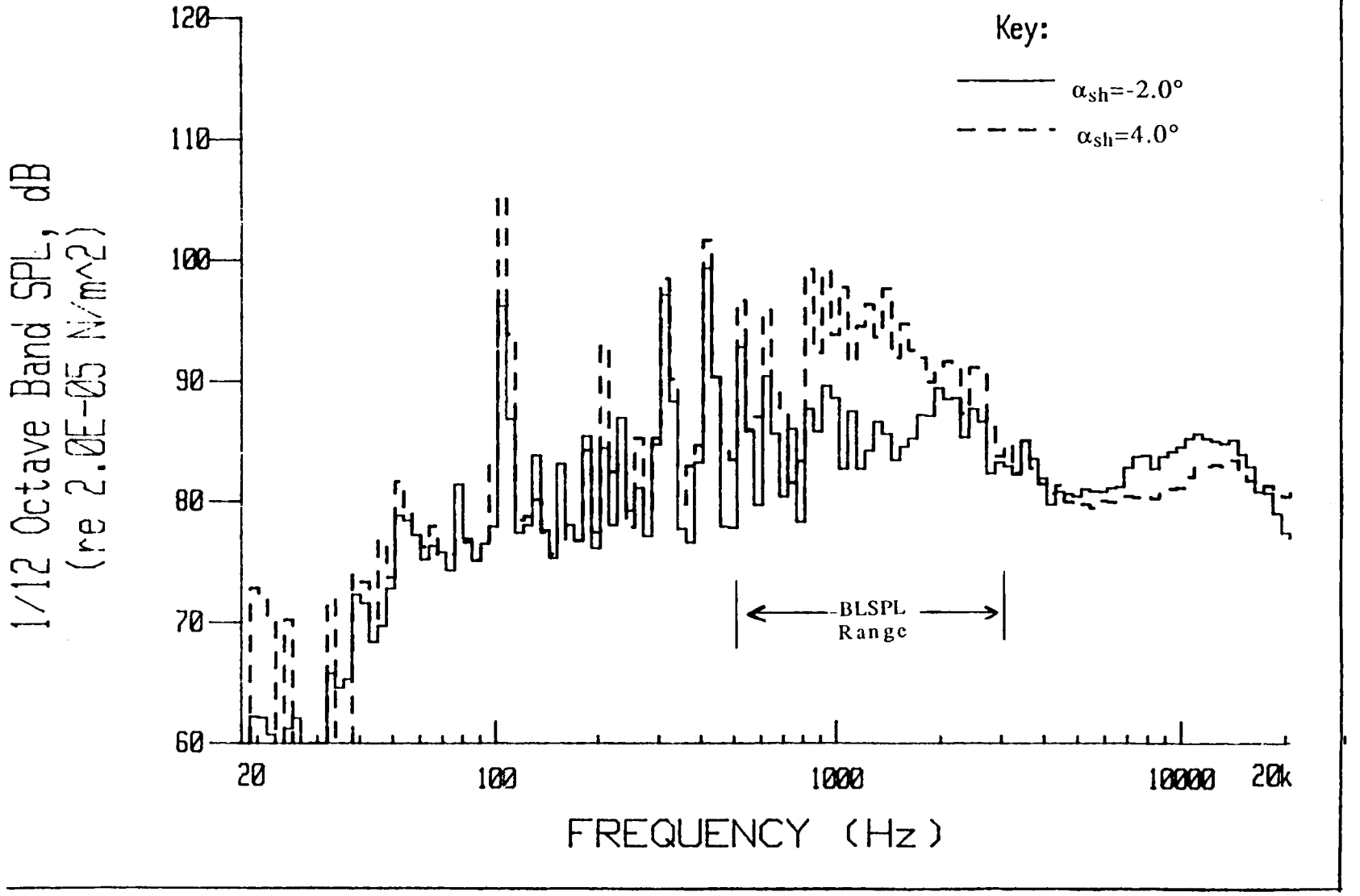

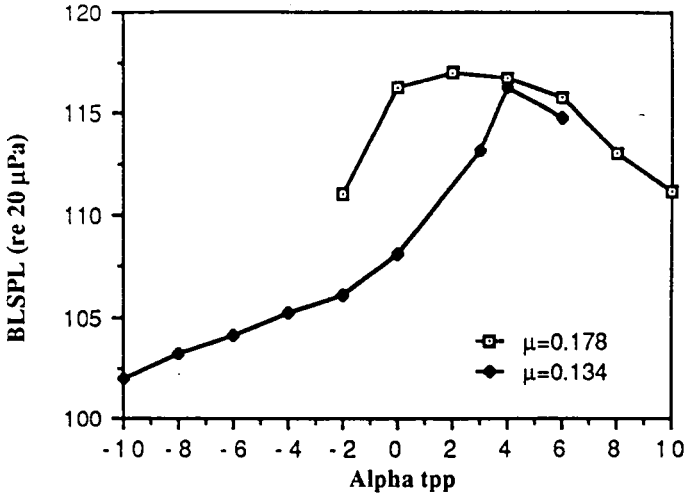

a) Microphone 1,

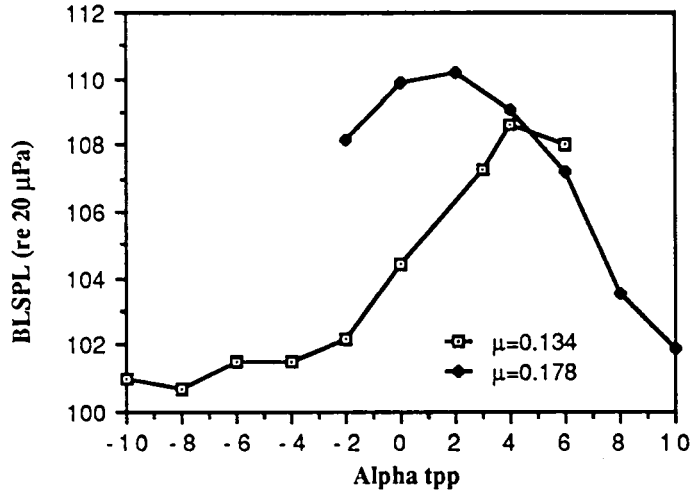

b) Microphone 7.

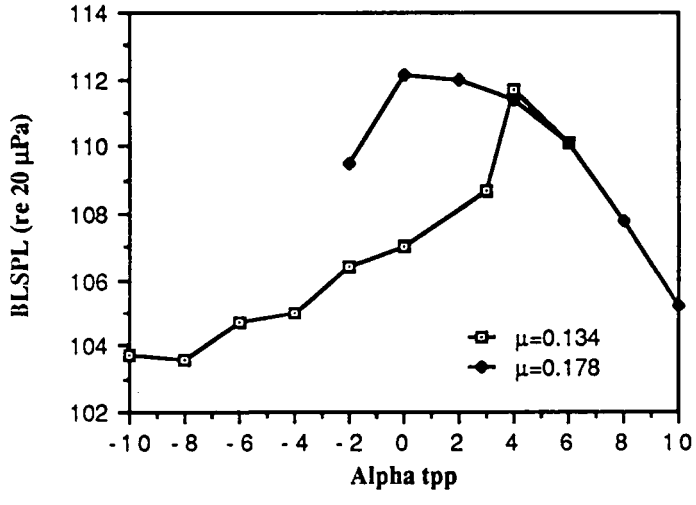

c) Microphone 9.

Figure 23. The effects of MR α_{tpp} on the BLSPL for μ=0.134 and 0.178.

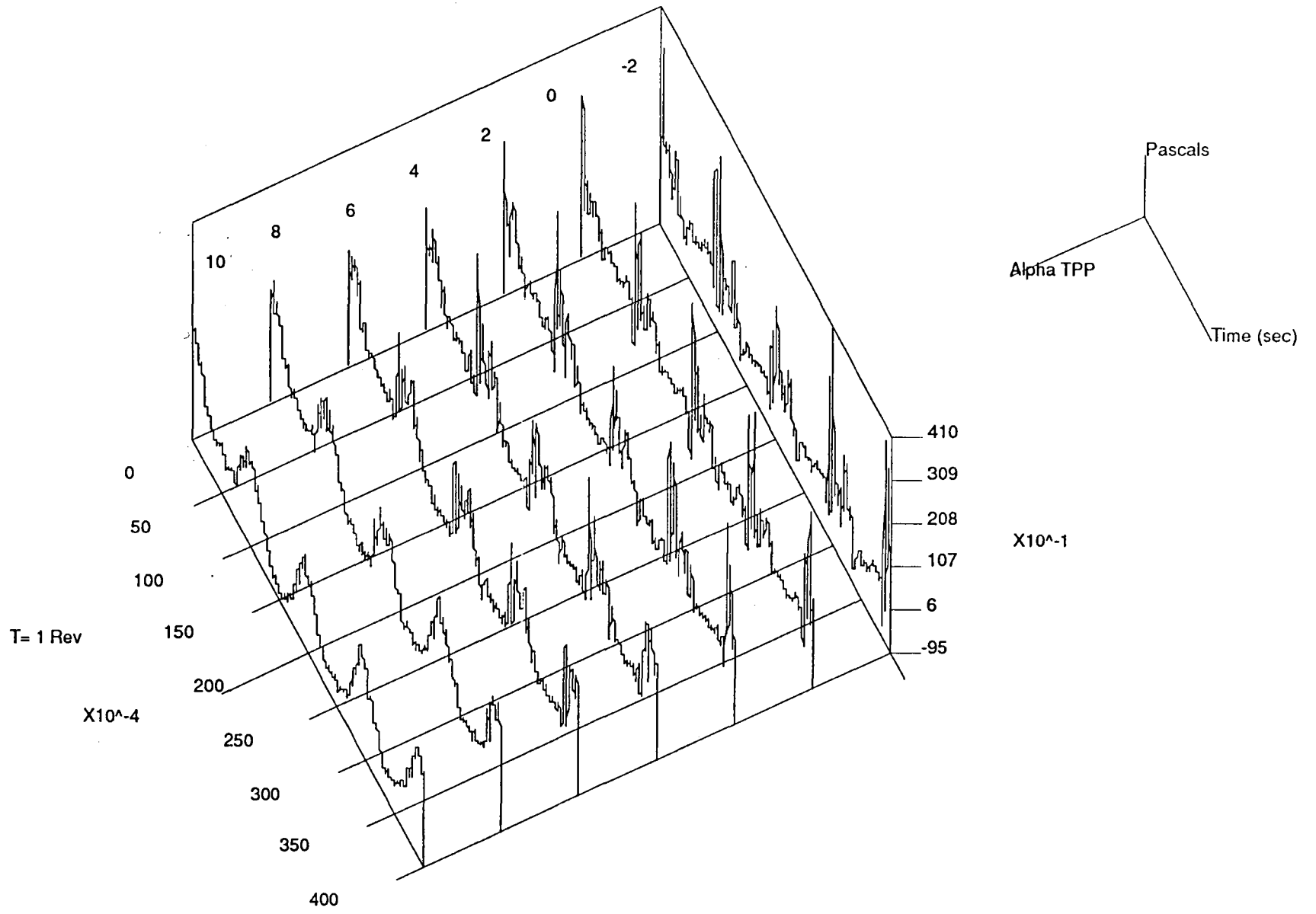

Figure 24. Averaged acoustic time histories for microphone 7 as a function of α_{tpp}, C_t=0.007, μ=0.178.

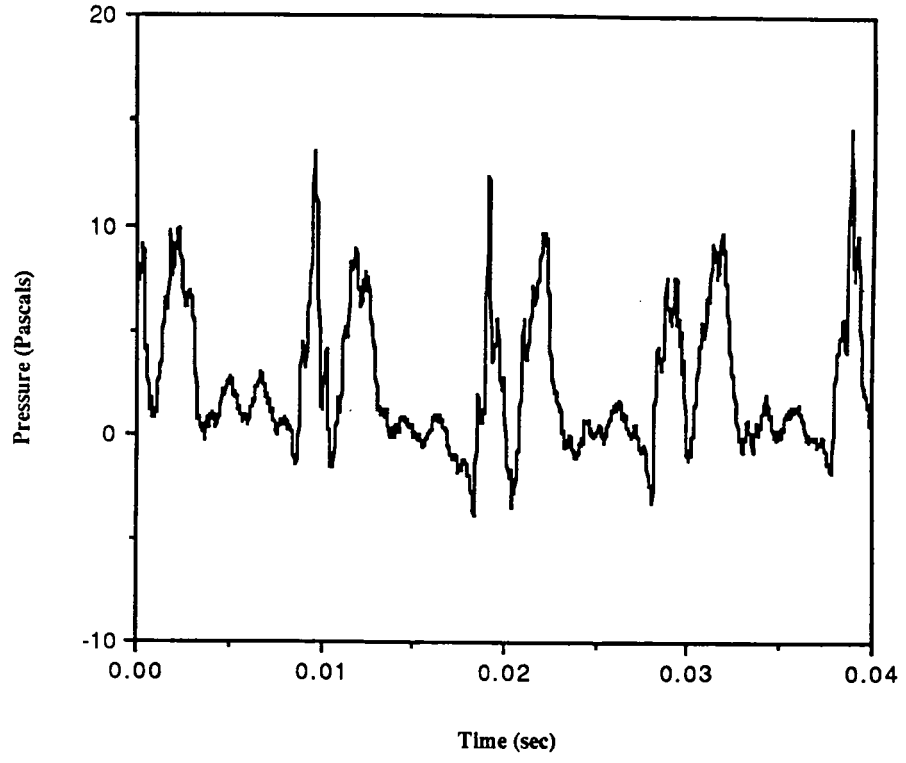

a) Alpha Shaft=4.5°, Alpha Tip-Path-Plane=5.1°, Run 114.1.

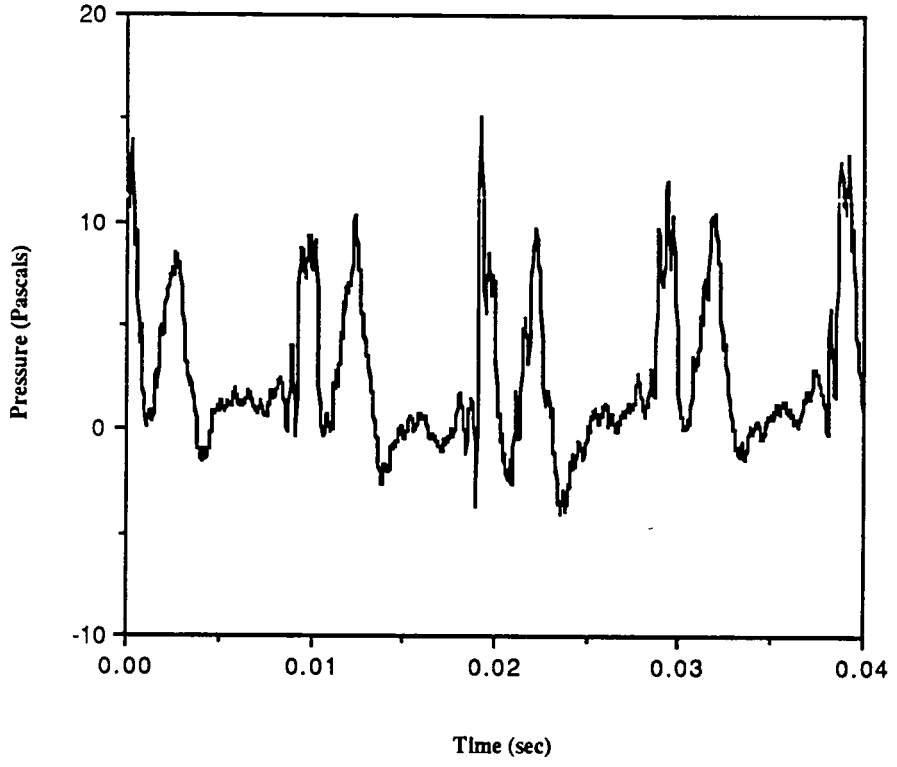

b) Alpha Shaft=8.6°, Alpha Tip-Path-Plane=5.1°, Run 114.2.

Figure 25. Effects of longitudinal flapping on the averaged MR acoustics, microphone 7, V=25.5 m/s, α_{tpp}=5.1°.

Figure 26. The effects of longitudinal flapping on the MR acoustics, microphone 7, V=25.5 m/s.

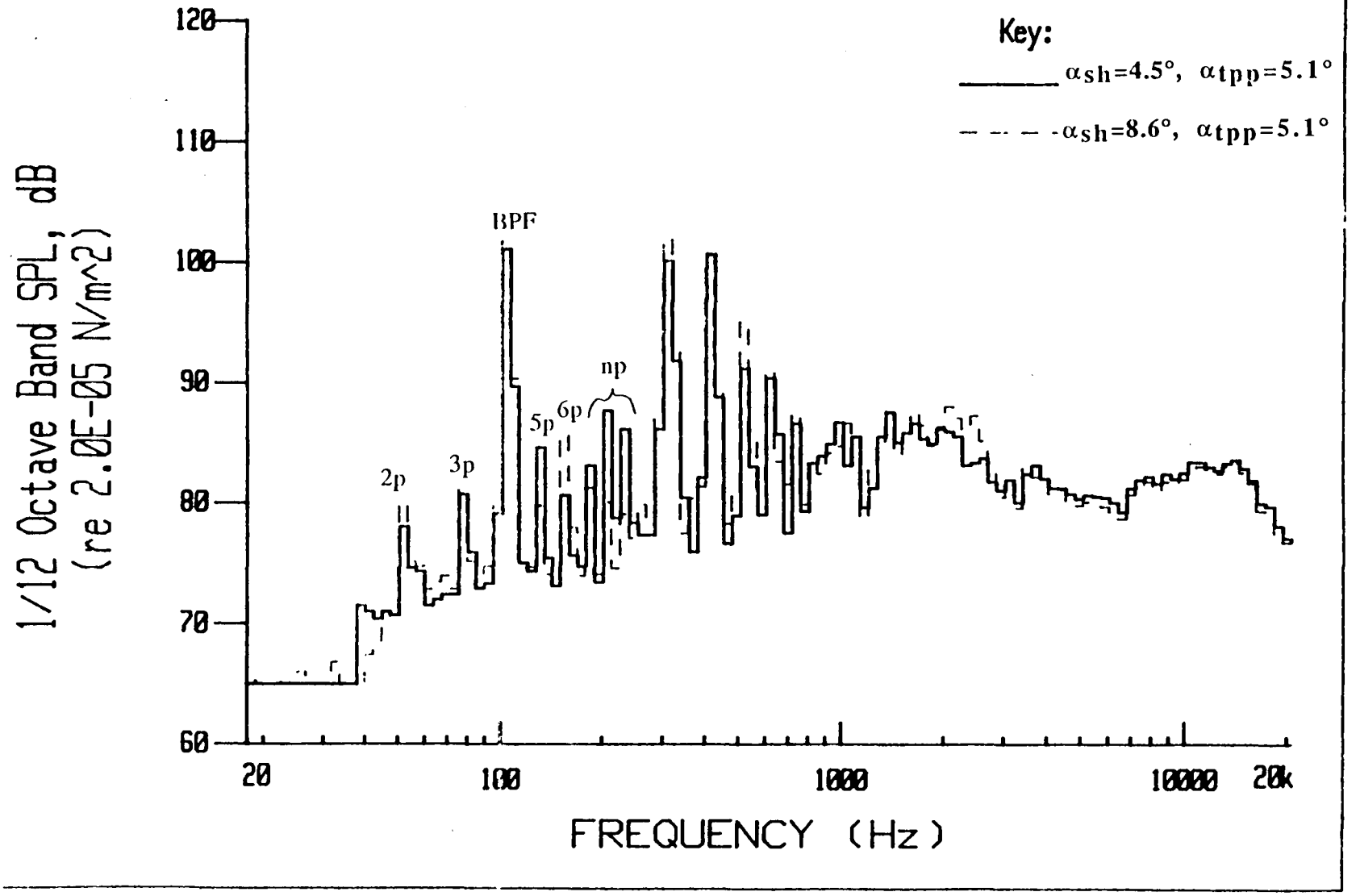

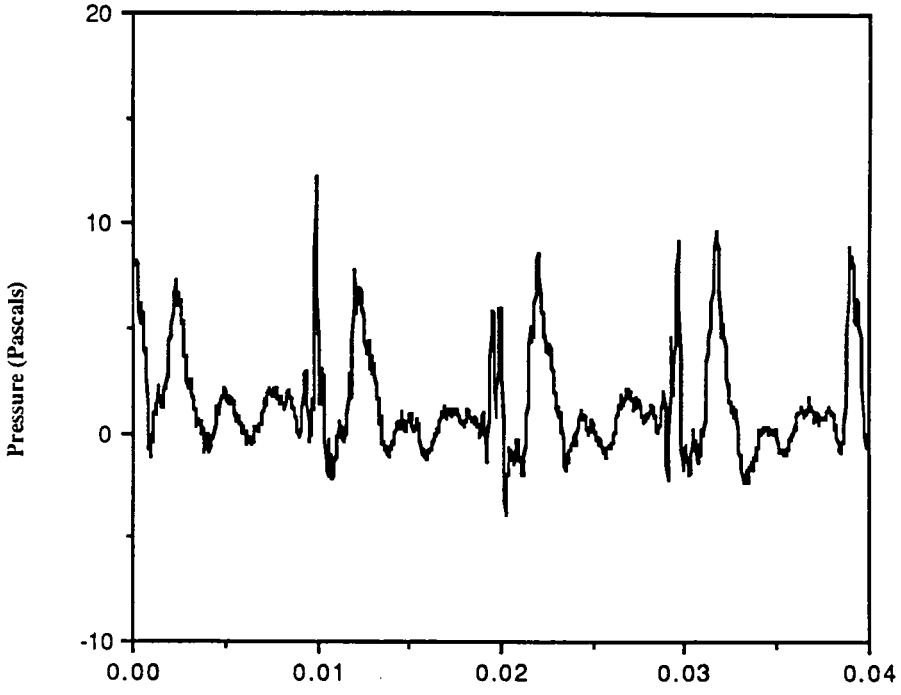

a) Alpha Shaft=-0.4°, Alpha Tip-Path-Plane=0°, Run 115.4.

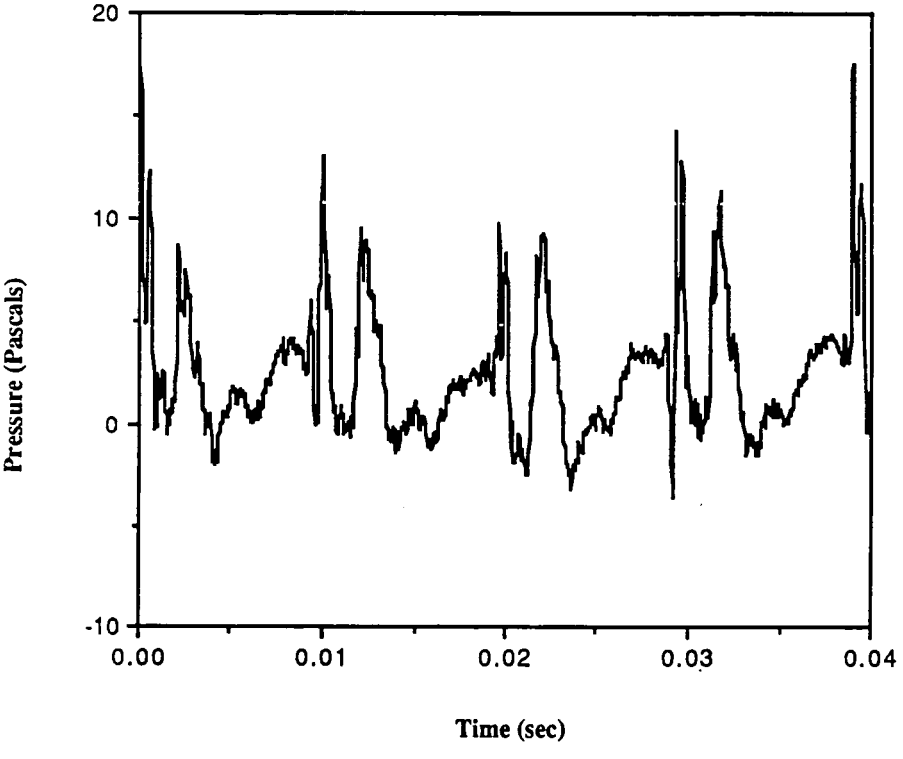

b) Alpha Shaft=3.1°, Alpha Tip-Path-Plane=0.1°, Run 115.6.

Figure 27. Effects of longitudinal flapping on the averaged MR acoustics, microphone 7, V=25.5 m/s, $\alpha_{tpp}=0°$.

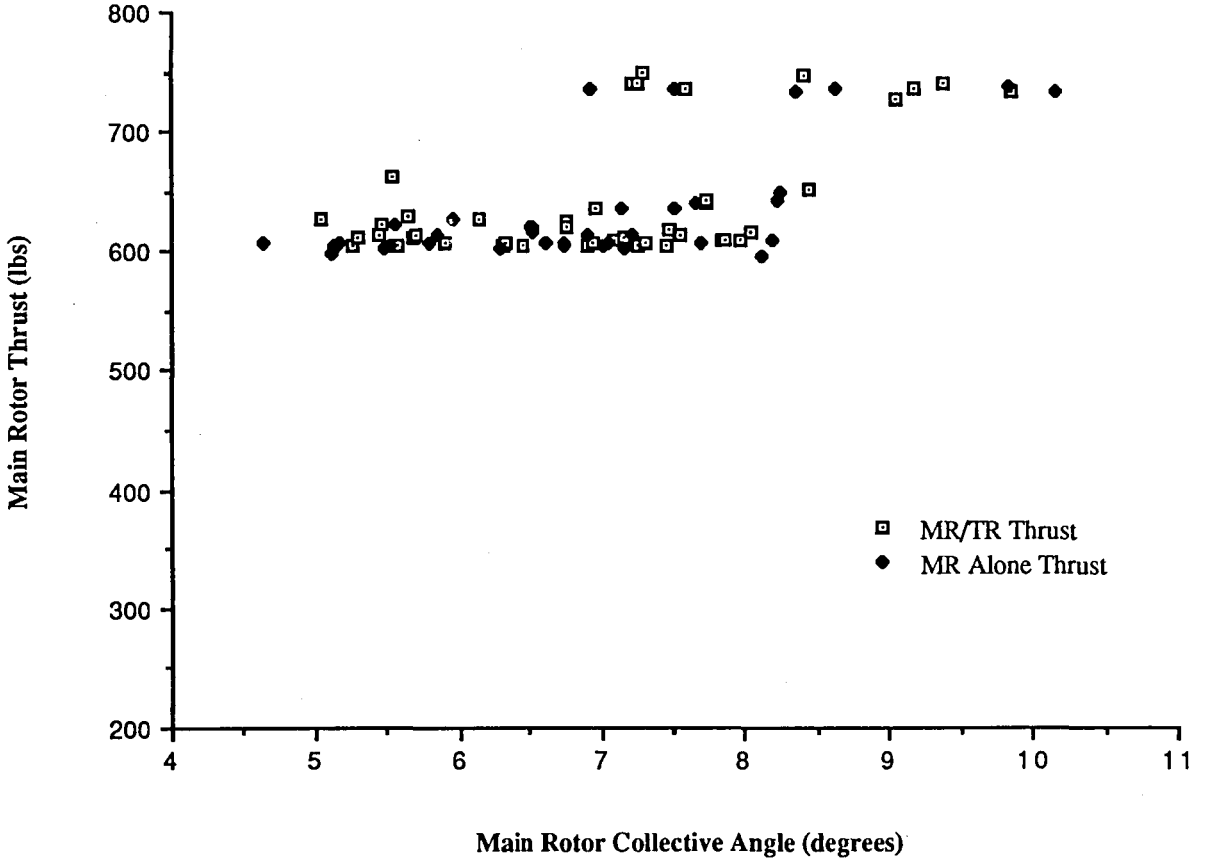

Figure 28. Main rotor thrust vs. collective performance.

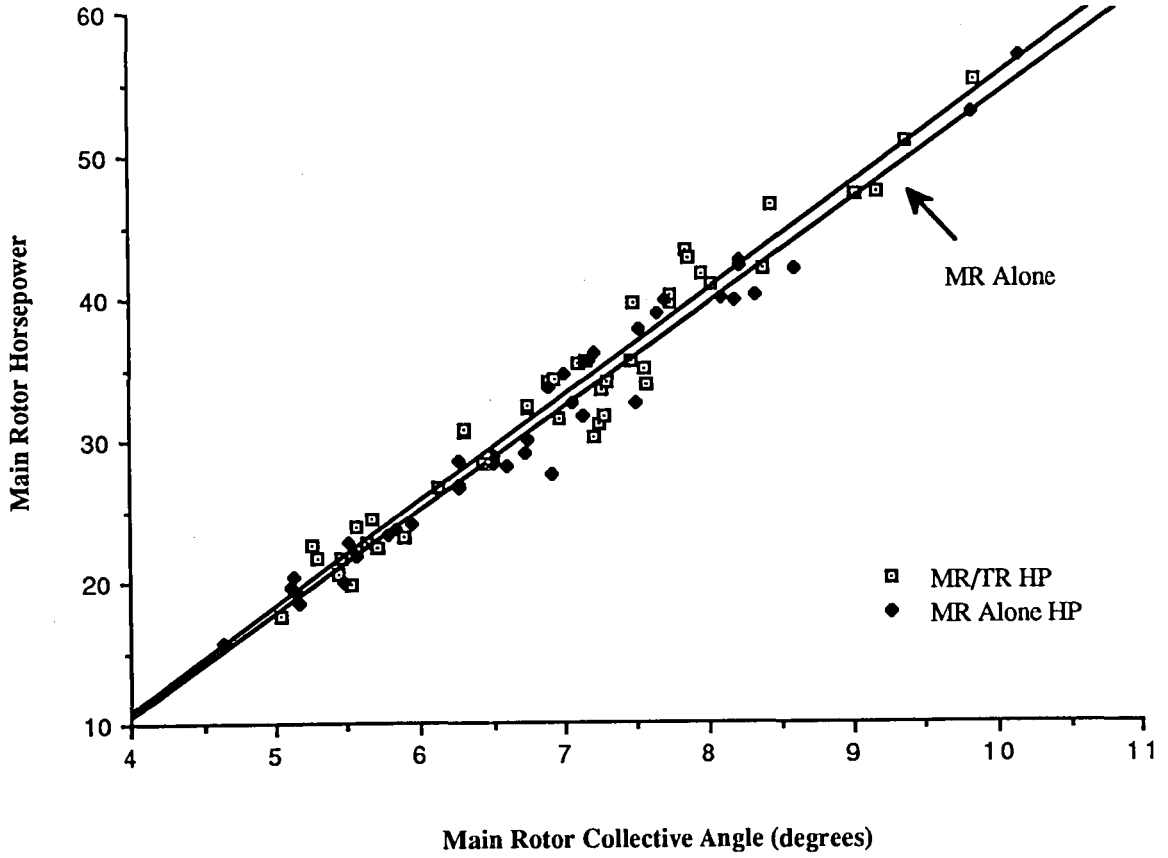

Figure 29. Main rotor horsepower vs. collective performance.

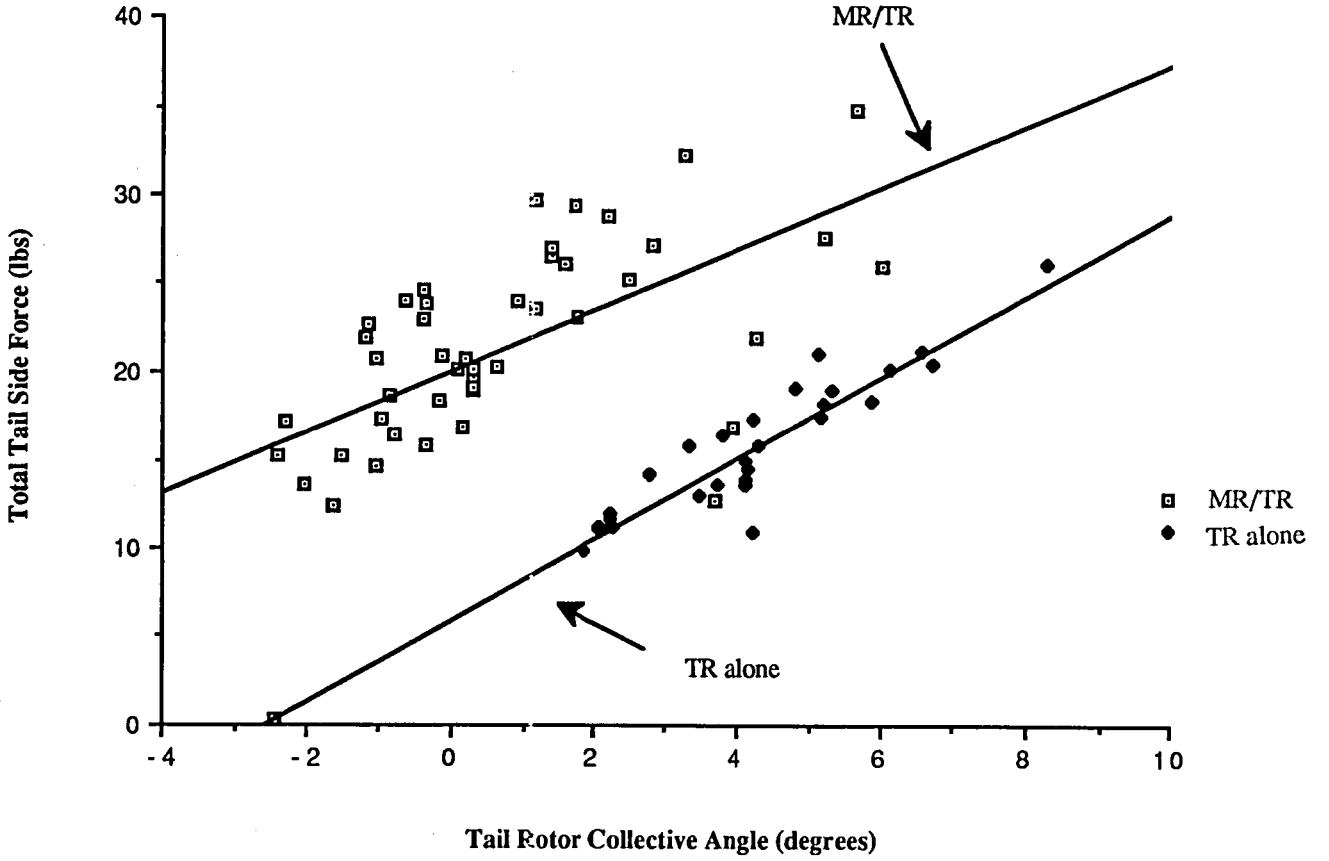

Figure 30. Indicated tail rotor thrust vs. collective angle.

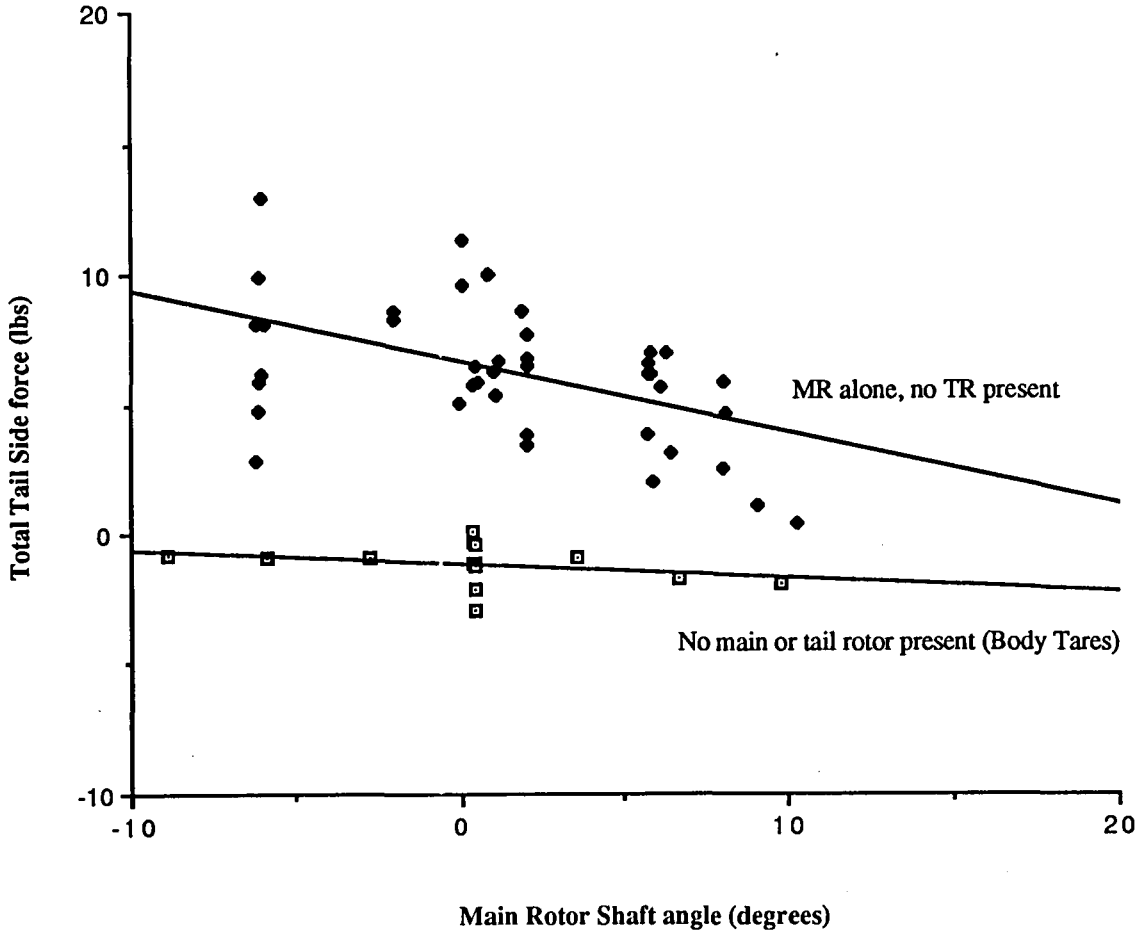

Figure 31. The effects of main rotor shaft angle on total tail side force.

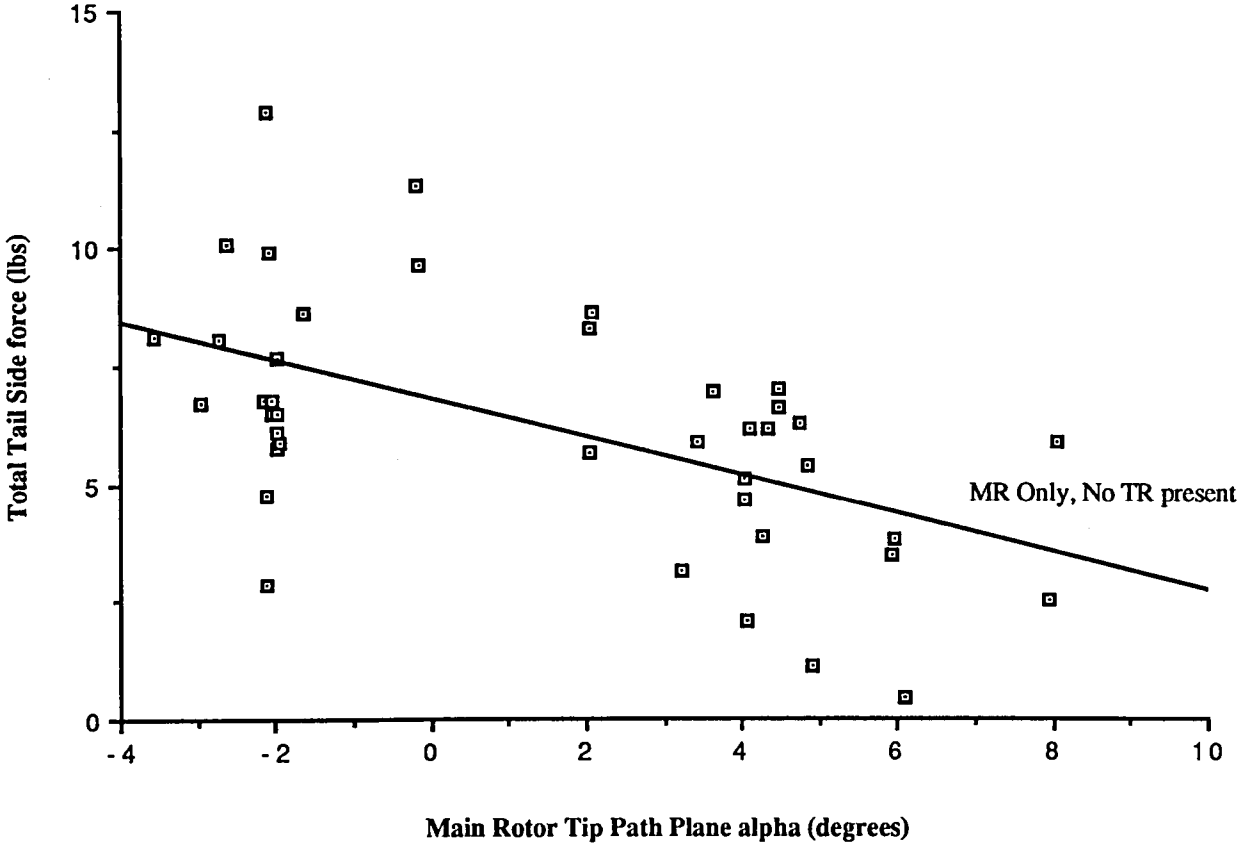

Figure 32. The effects of main rotor tip-path-plane angle on tail side force.

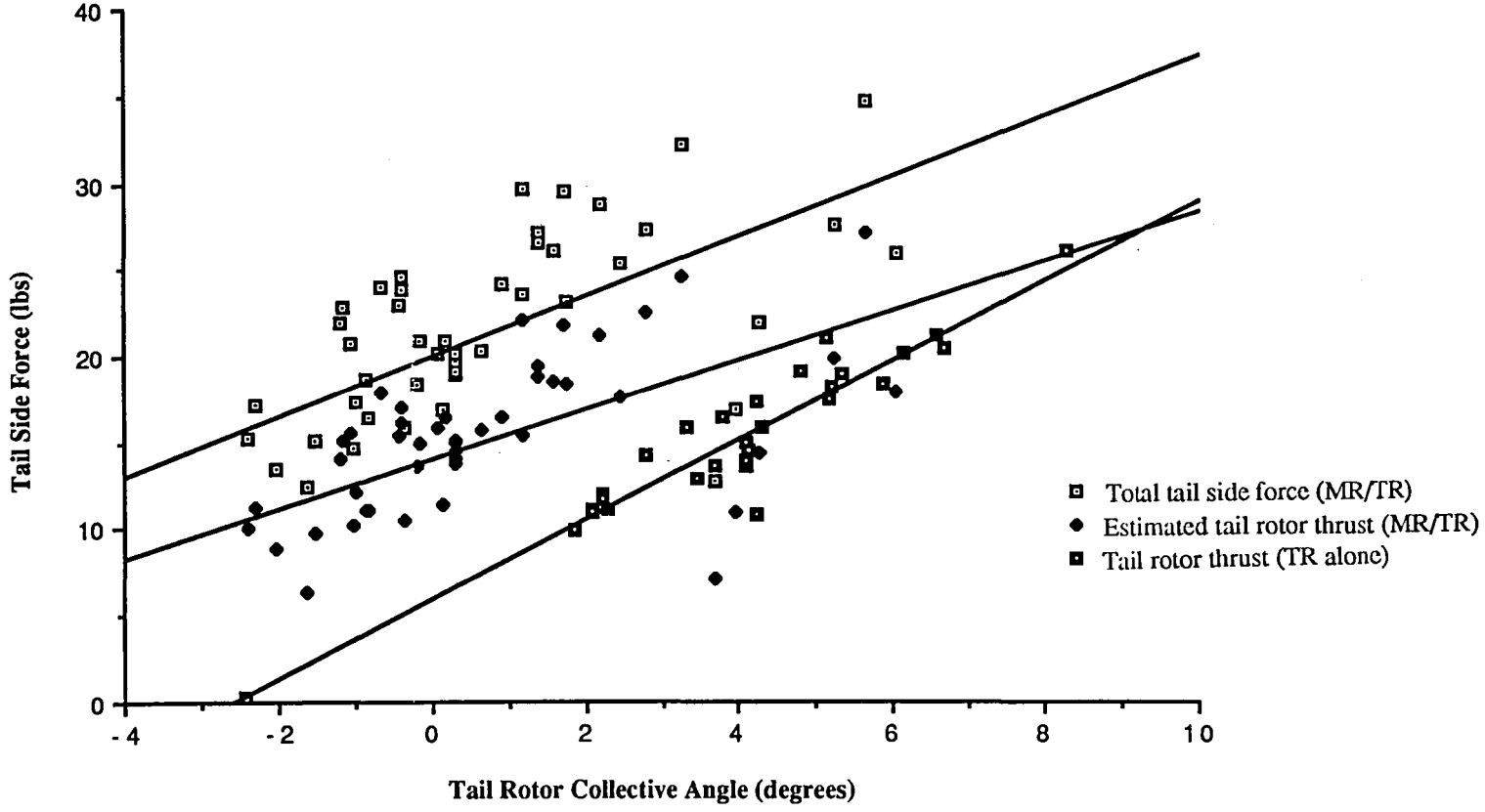

Figure 33. Tail side force vs. tail rotor collective angle.

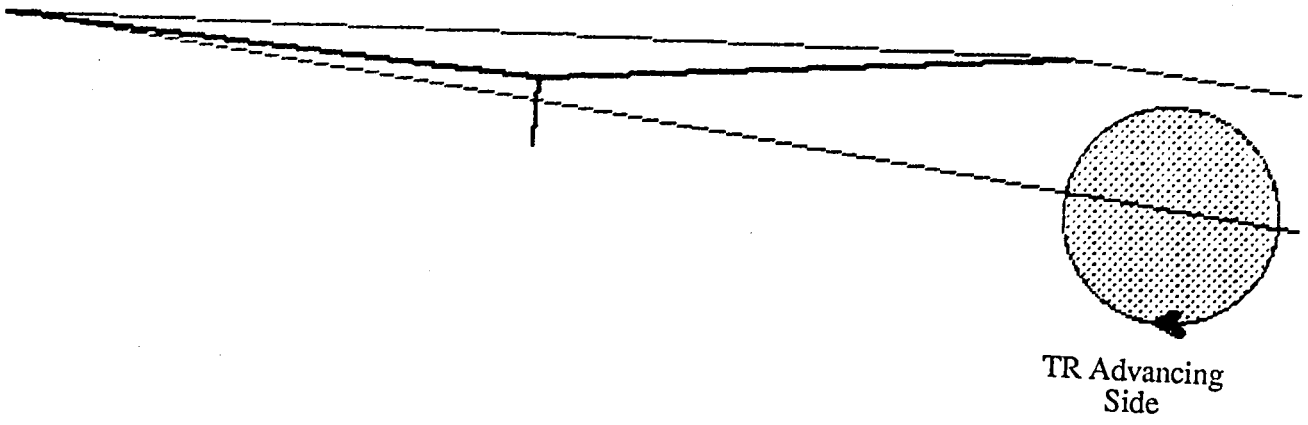

a) MR wake/TR intersection for α_{tpp}=2°, α_{sh}=6° (run 168.3).

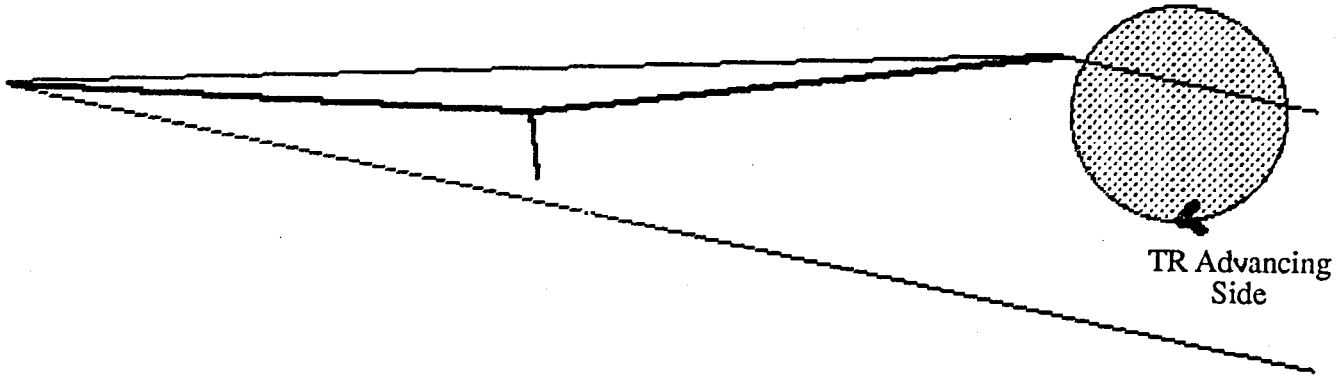

b) MR wake/TR intersection for α_{tpp}=-2°, α_{sh}=-6° (run 168.7).

Figure 34. Simple wake model results for MR/TR interaction (μ=0.186, C_t=0.007).

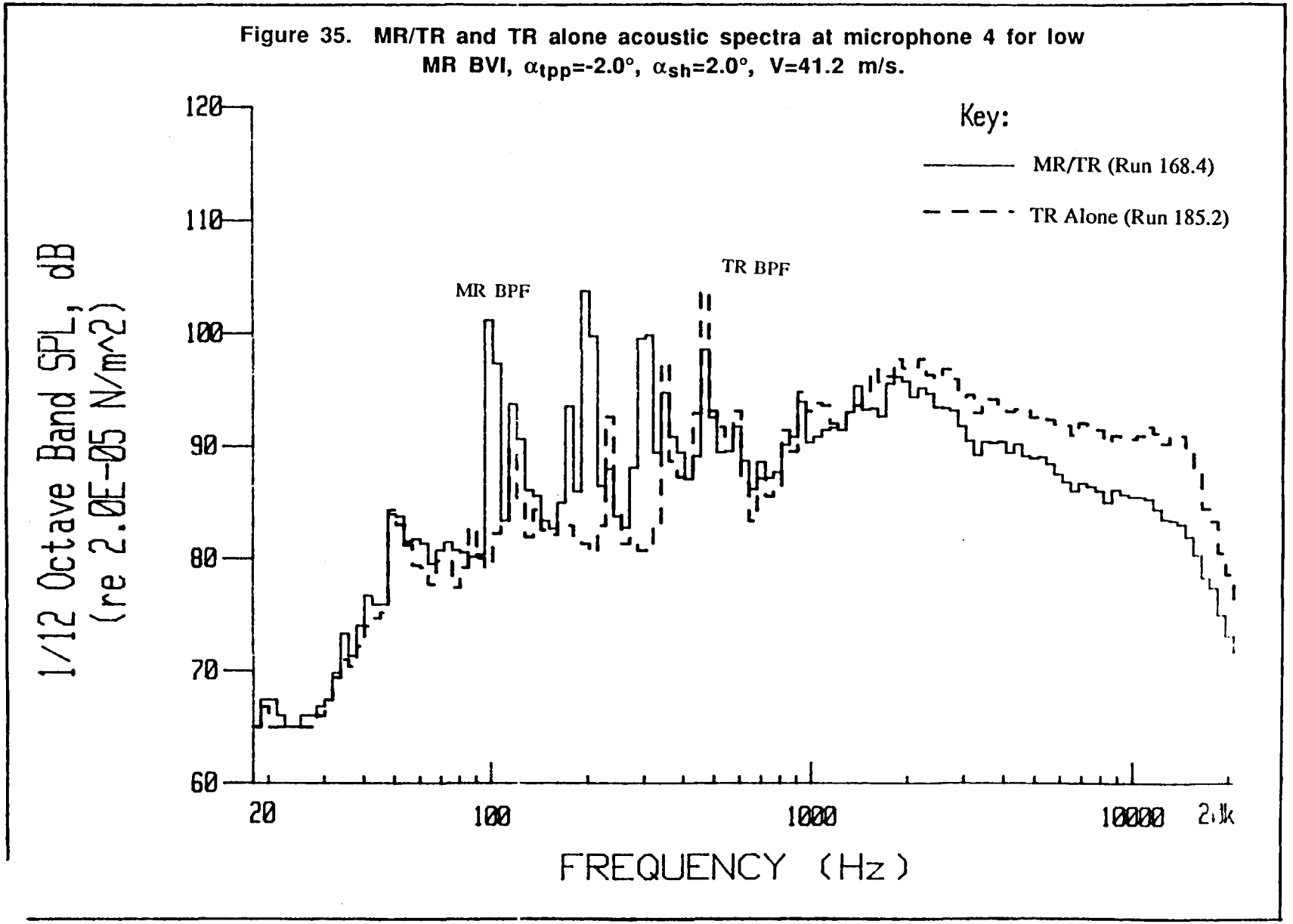

Figure 35. MR/TR and TR alone acoustic spectra at microphone 4 for low MR BVI, α_{tpp}=-2.0°, α_{sh}=2.0°, V=41.2 m/s.

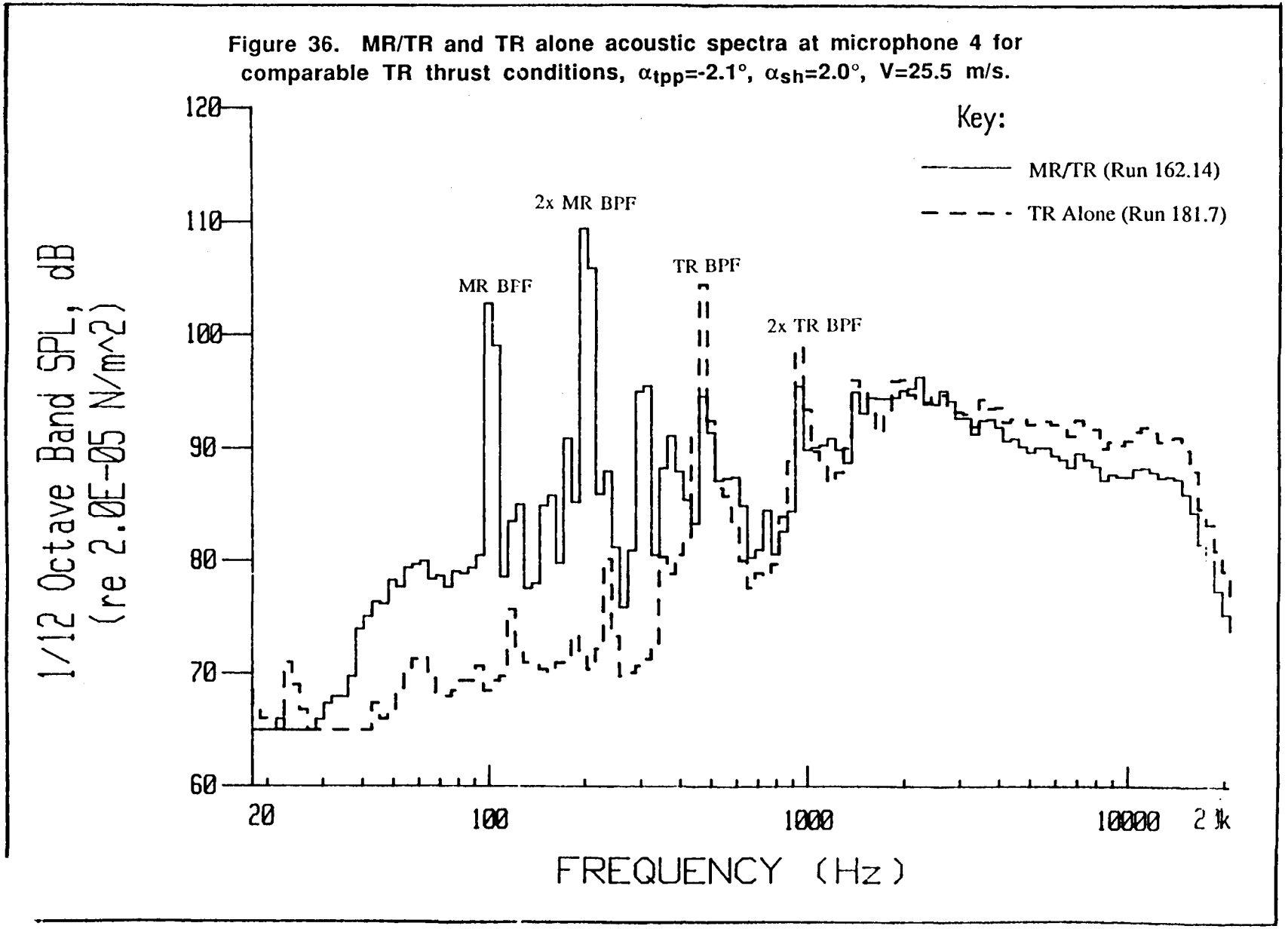

Figure 36. MR/TR and TR alone acoustic spectra at microphone 4 for comparable TR thrust conditions, α_{tpp}=-2.1°, α_{sh}=2.0°, V=25.5 m/s.

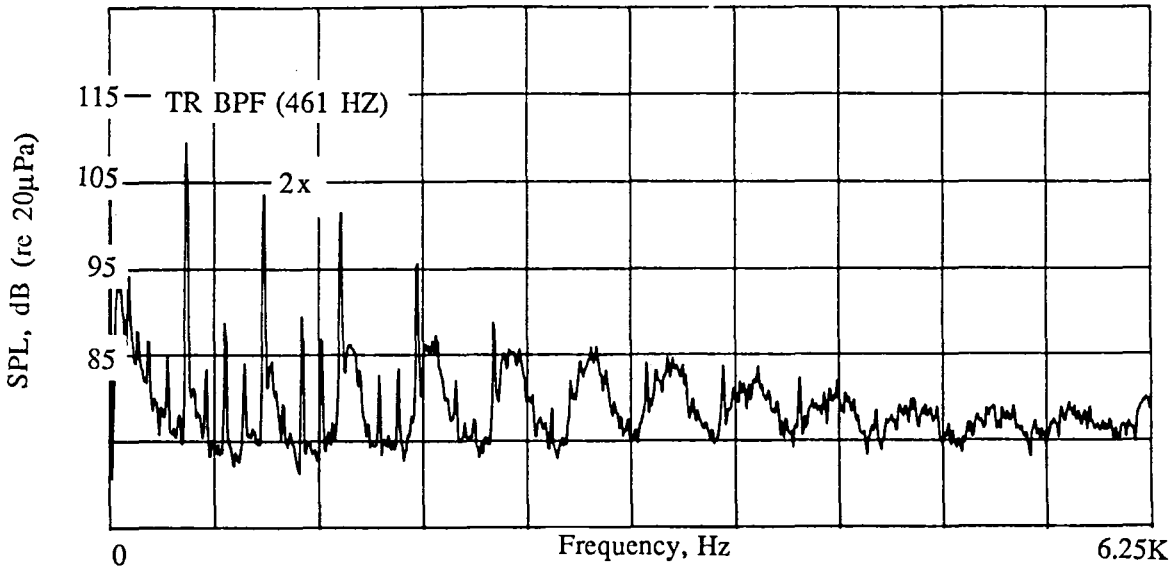

a) Baseband analysis (7.81 HZ resolution).

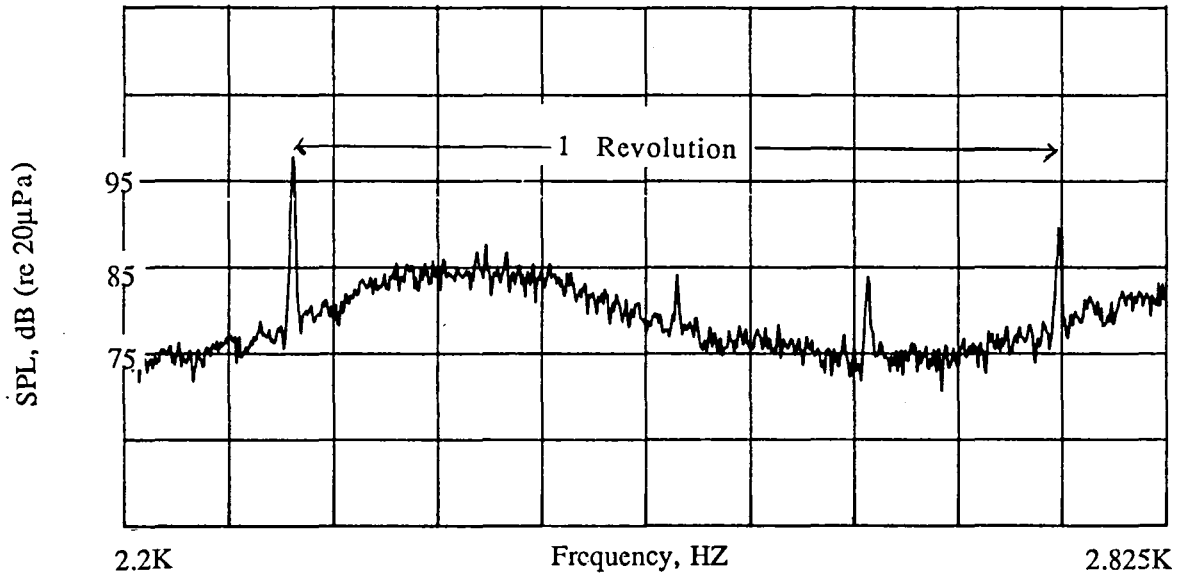

b) Zoom analysis (0.781 HZ resolution).

Figure 37. Narrow band and zoom spectral analysis of TR alone noise at microphone 1, α_{sh}=-6.0°, V=41.2 m/s (Run 185.5).

Figure 38. Model fuselage wake effects on the acoustic spectra for the TR alone at microphone 2, TR thrust ≈18 lbs., V=25.5 m/s .

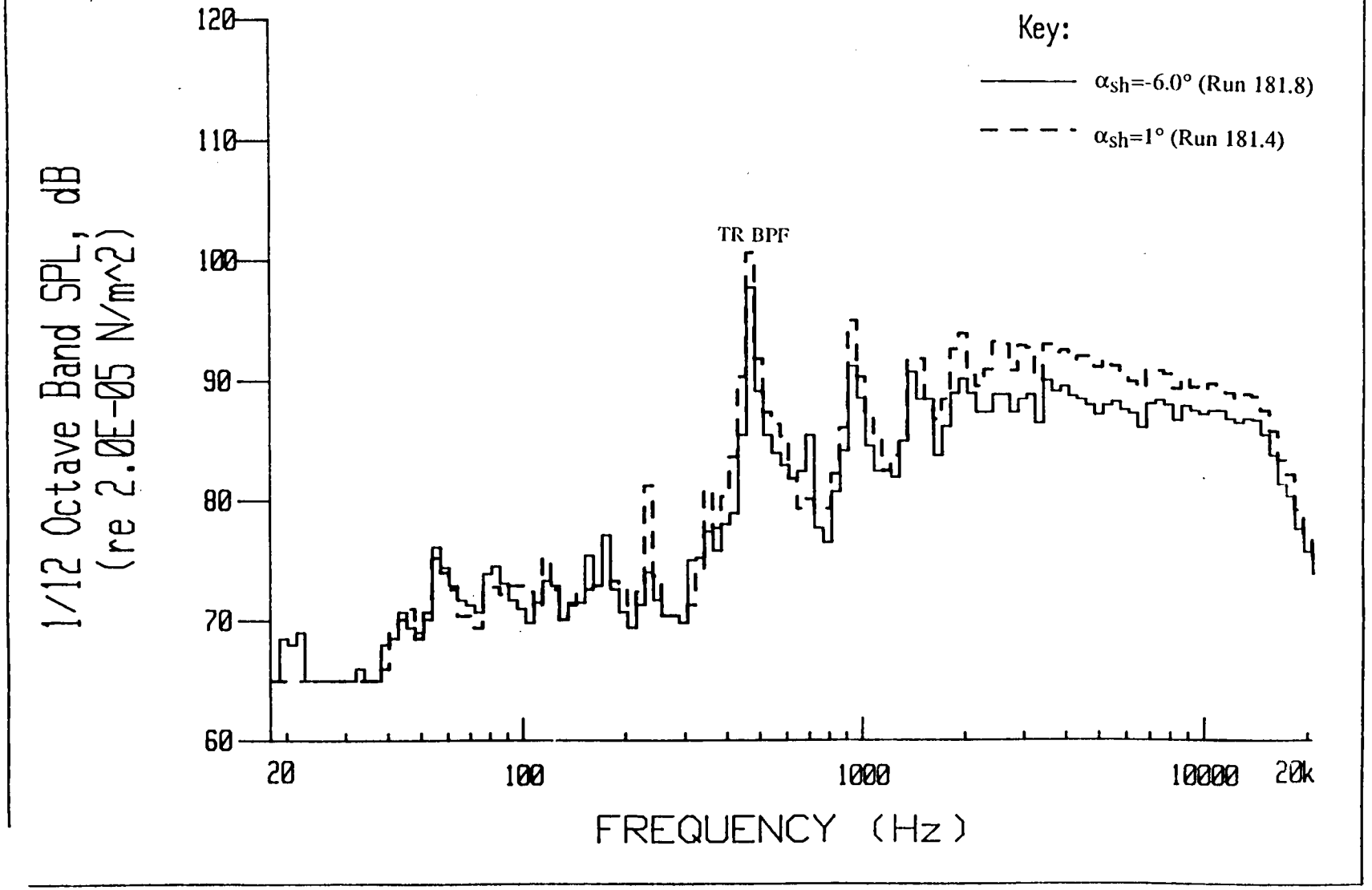

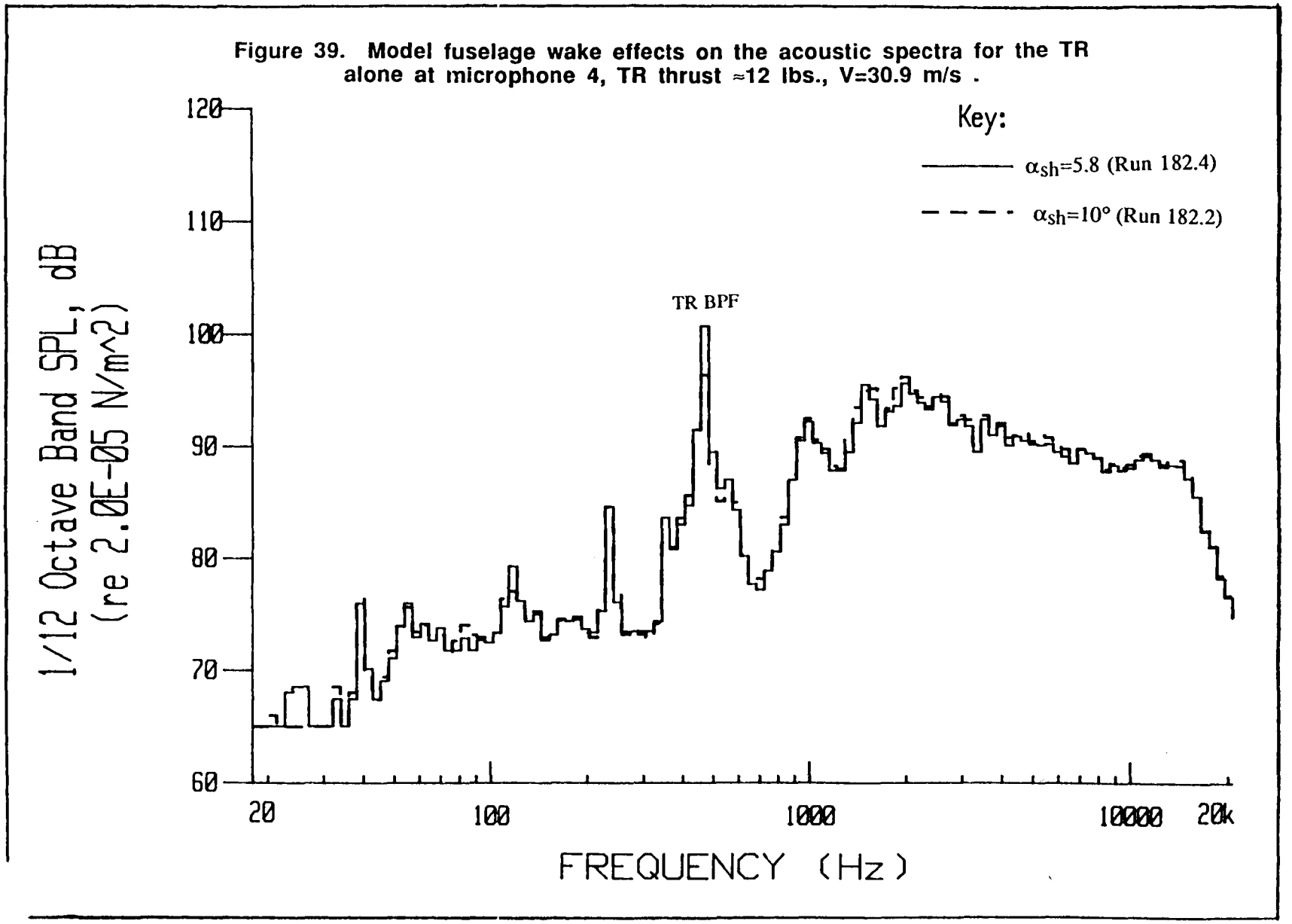

Figure 39. Model fuselage wake effects on the acoustic spectra for the TR alone at microphone 4, TR thrust ≈12 lbs., V=30.9 m/s .

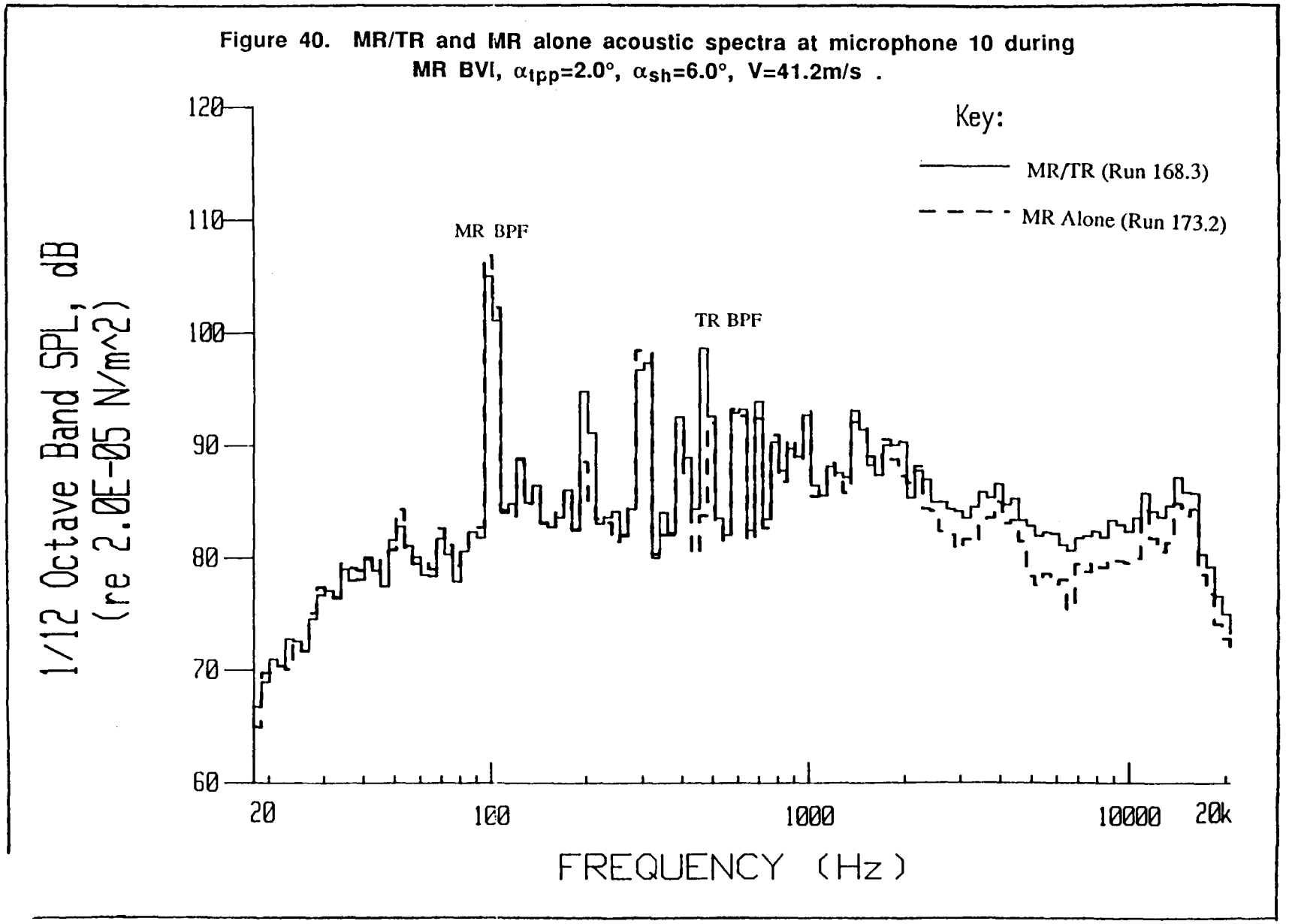

Figure 40. MR/TR and MR alone acoustic spectra at microphone 10 during MR BVI, α_{tpp}=2.0°, α_{sh}=6.0°, V=41.2m/s .

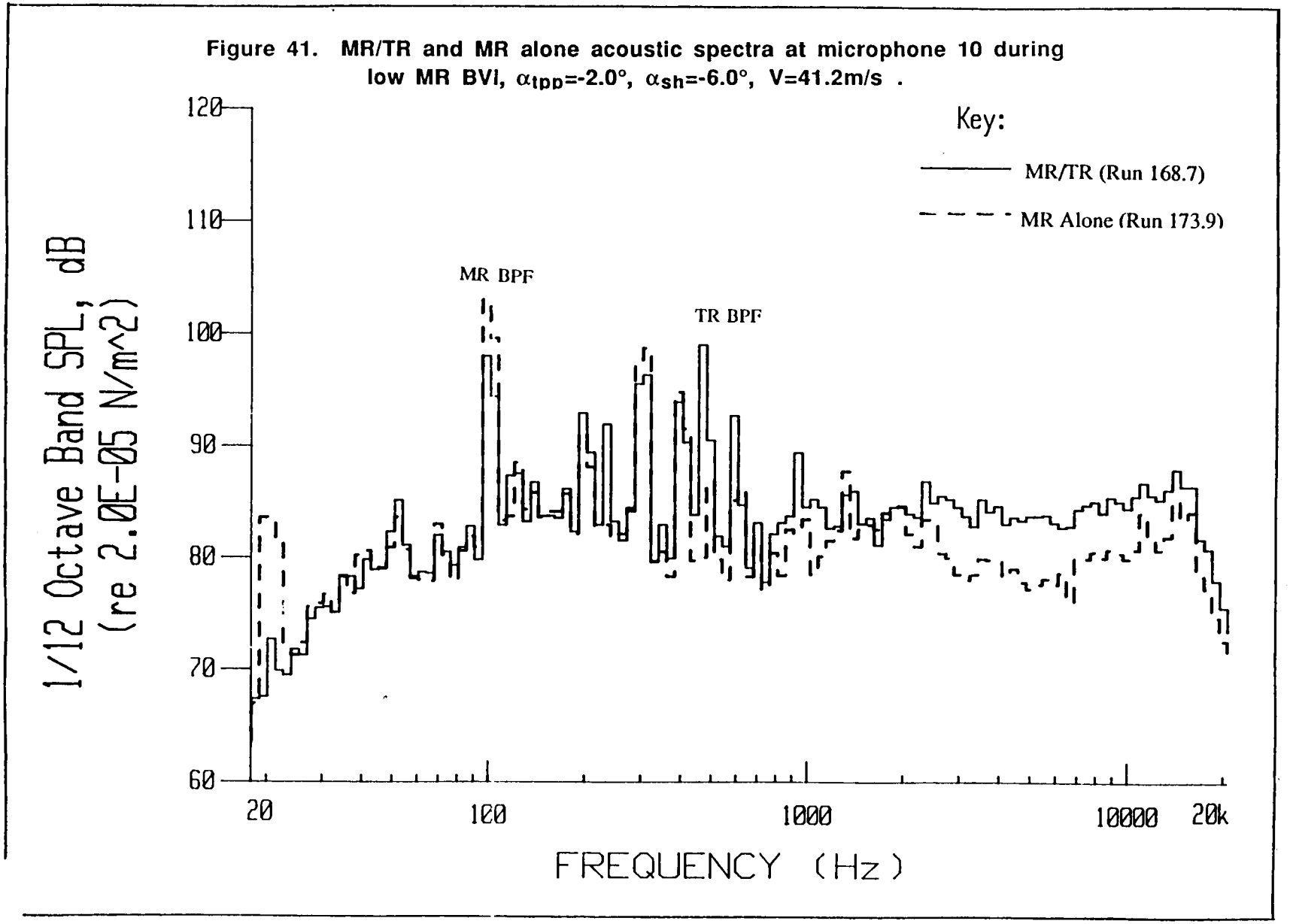

Figure 41. MR/TR and MR alone acoustic spectra at microphone 10 during low MR BVI, α_{tpp}=-2.0°, α_{sh}=-6.0°, V=41.2m/s .

Figure 42. MR/TR and MR alone acoustic spectra at microphone 7 during MR BVI, α_{tpp}=5.0°, α_{sh}=9.0°, V=25.5m/s .

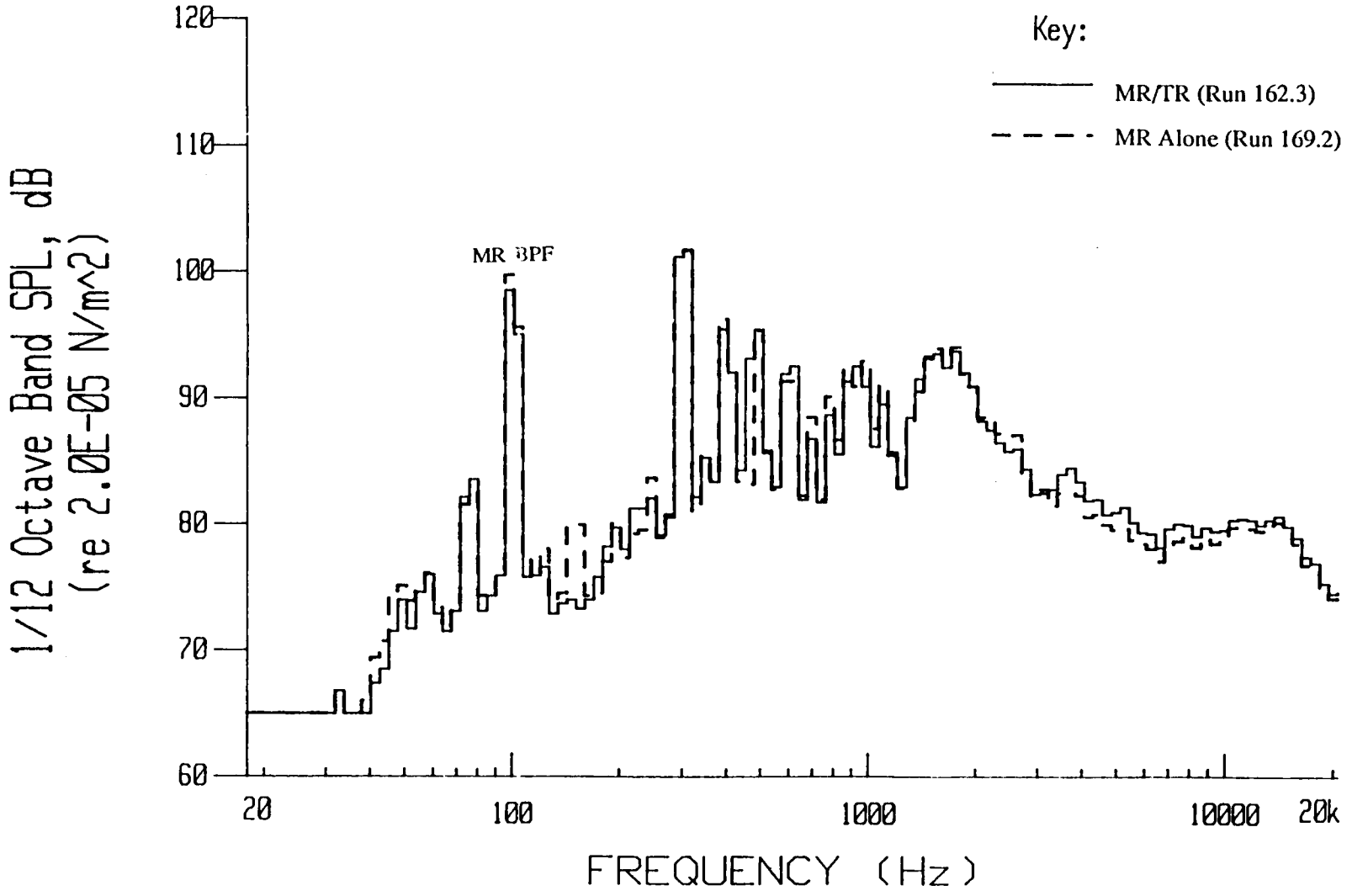

Figure 43. MR/TR and MR alone acoustic spectra at microphone 1 during MR BVI, α_{tpp}=5.0°, α_{sh}=9.0°, V=25.5m/s .

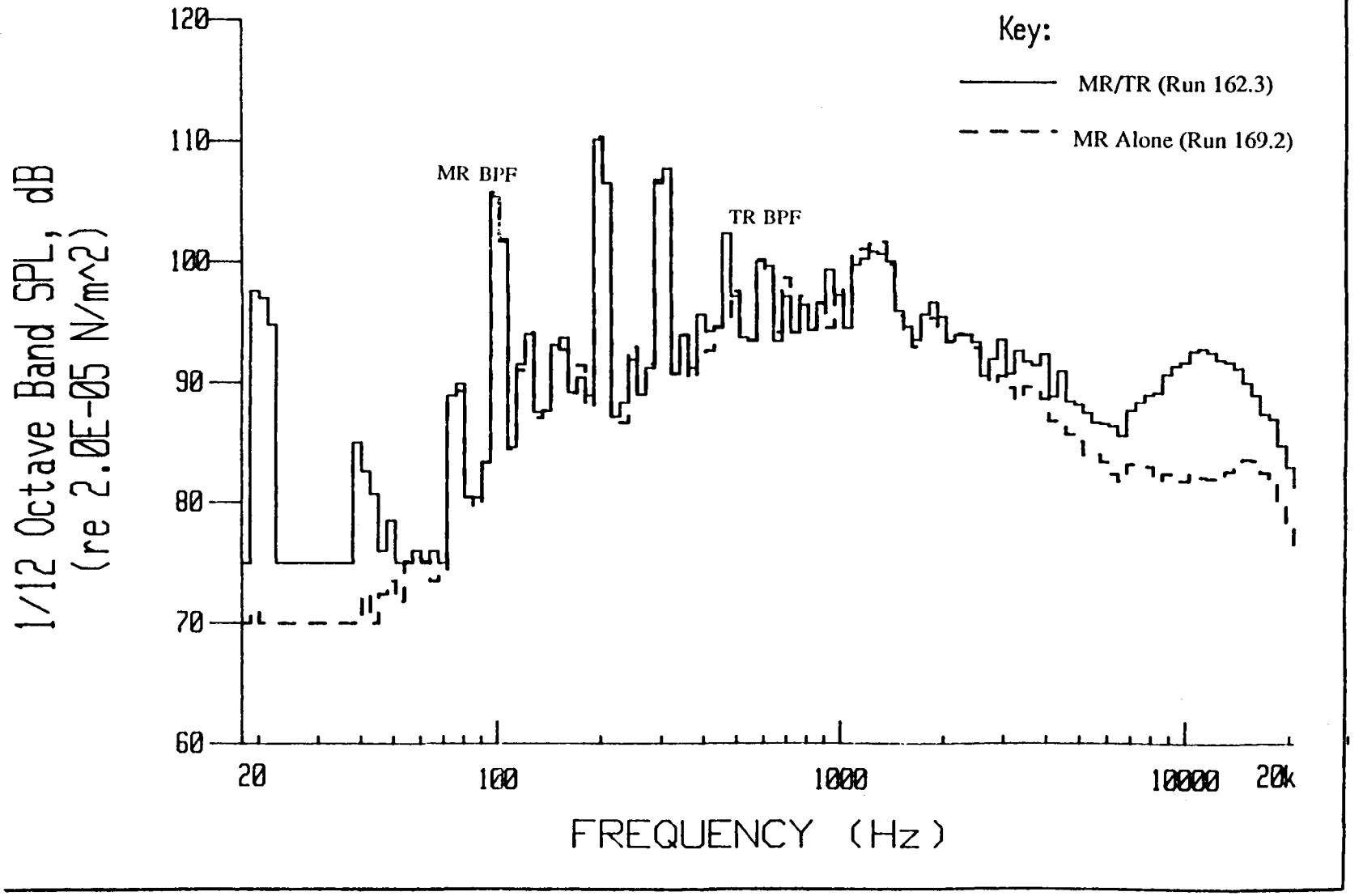

Figure 44. MR/TR and MR alone acoustic spectra at microphone 3 during MR BVI, α_{tpp}=5.0°, α_{sh}=9.0°, V=25.5m/s .

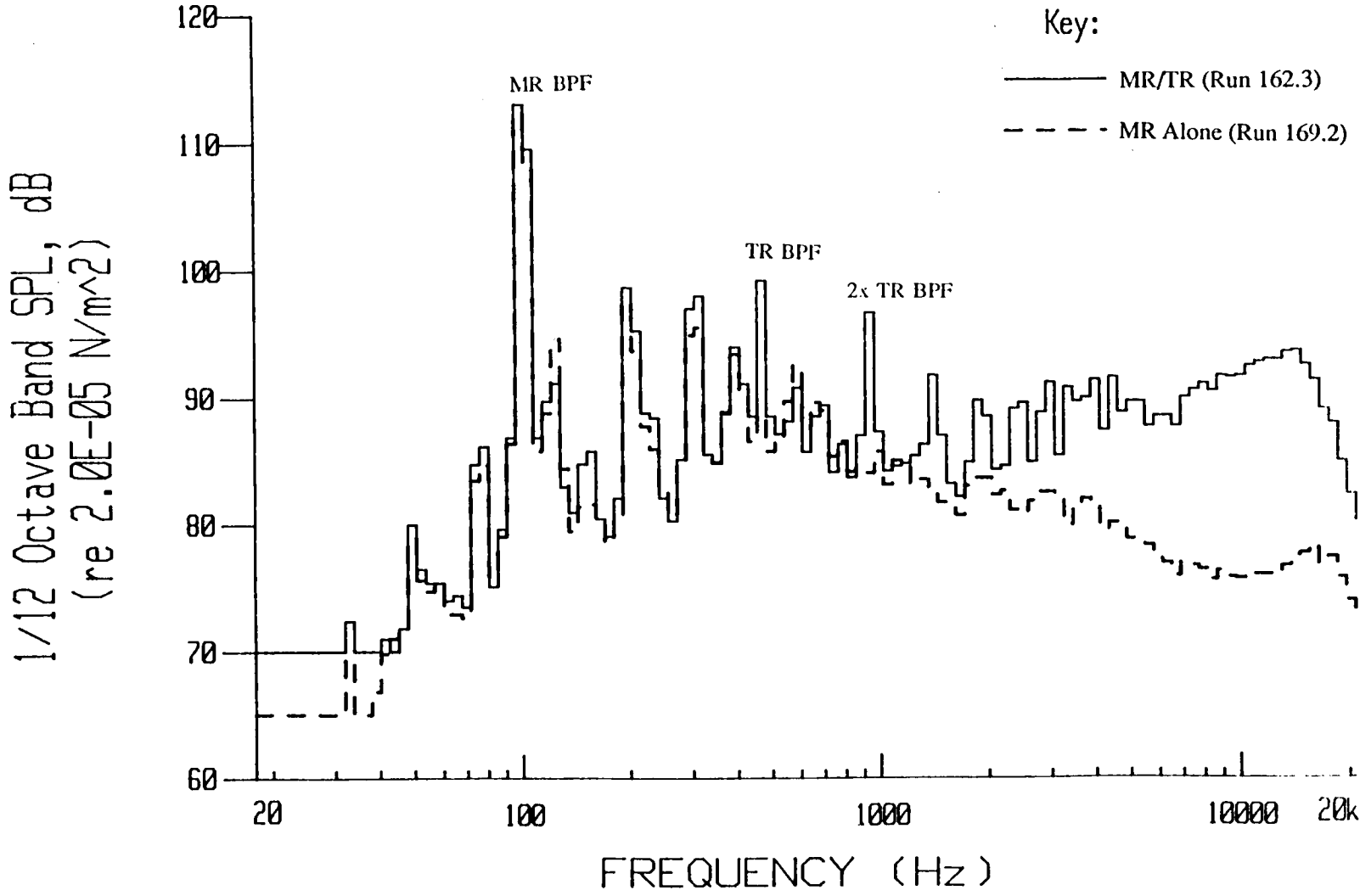

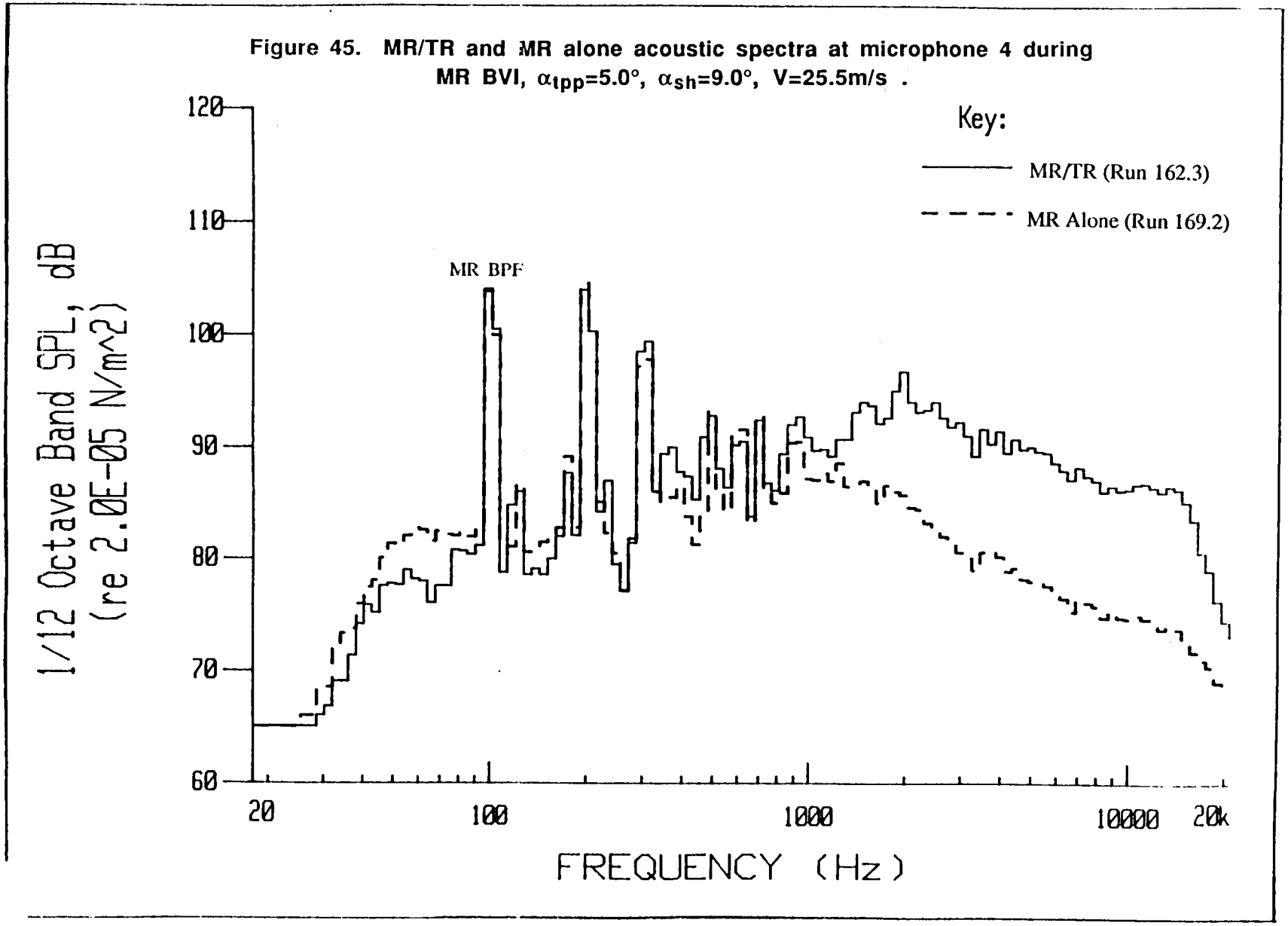

Figure 45. MR/TR and MR alone acoustic spectra at microphone 4 during MR BVI, α_{tpp}=5.0°, α_{sh}=9.0°, V=25.5m/s .

Figure 46. The effects of TR position inside the MR wake on the acoustic spectra at microphone 4, α_{tpp}=5.0°, V=25.5m/s .

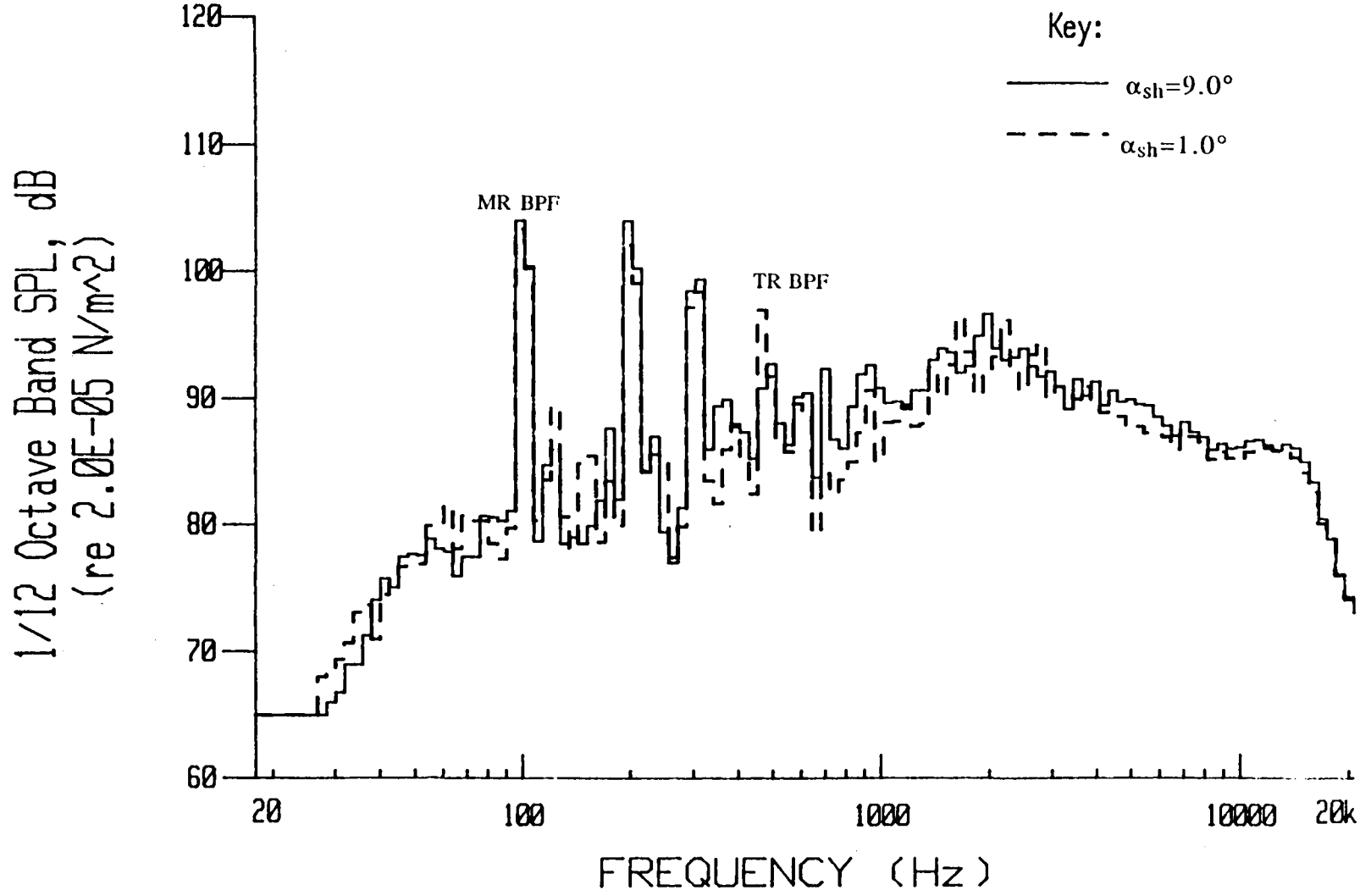

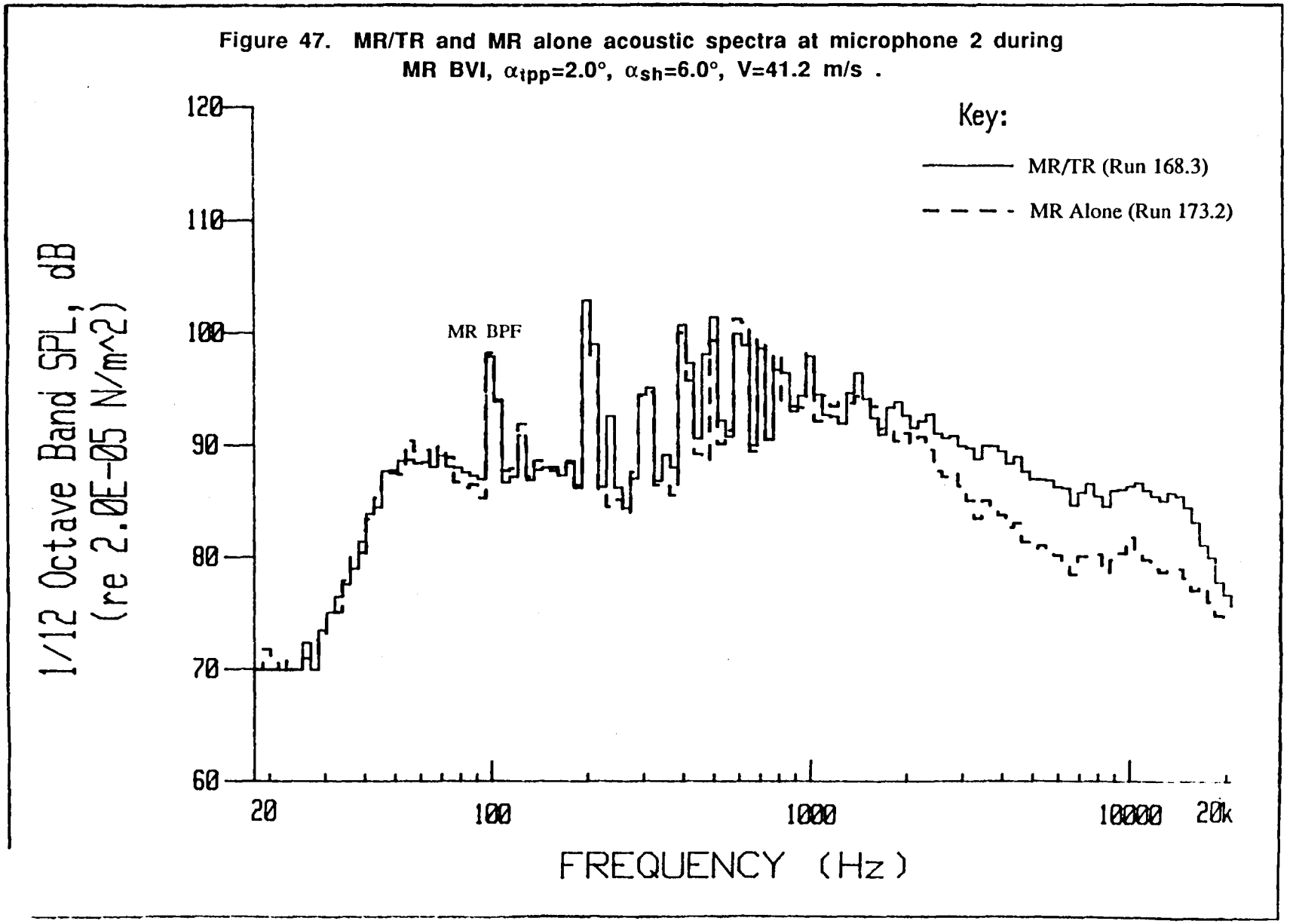

Figure 47. MR/TR and MR alone acoustic spectra at microphone 2 during MR BVI, α_{tpp}=2.0°, α_{sh}=6.0°, V=41.2 m/s .

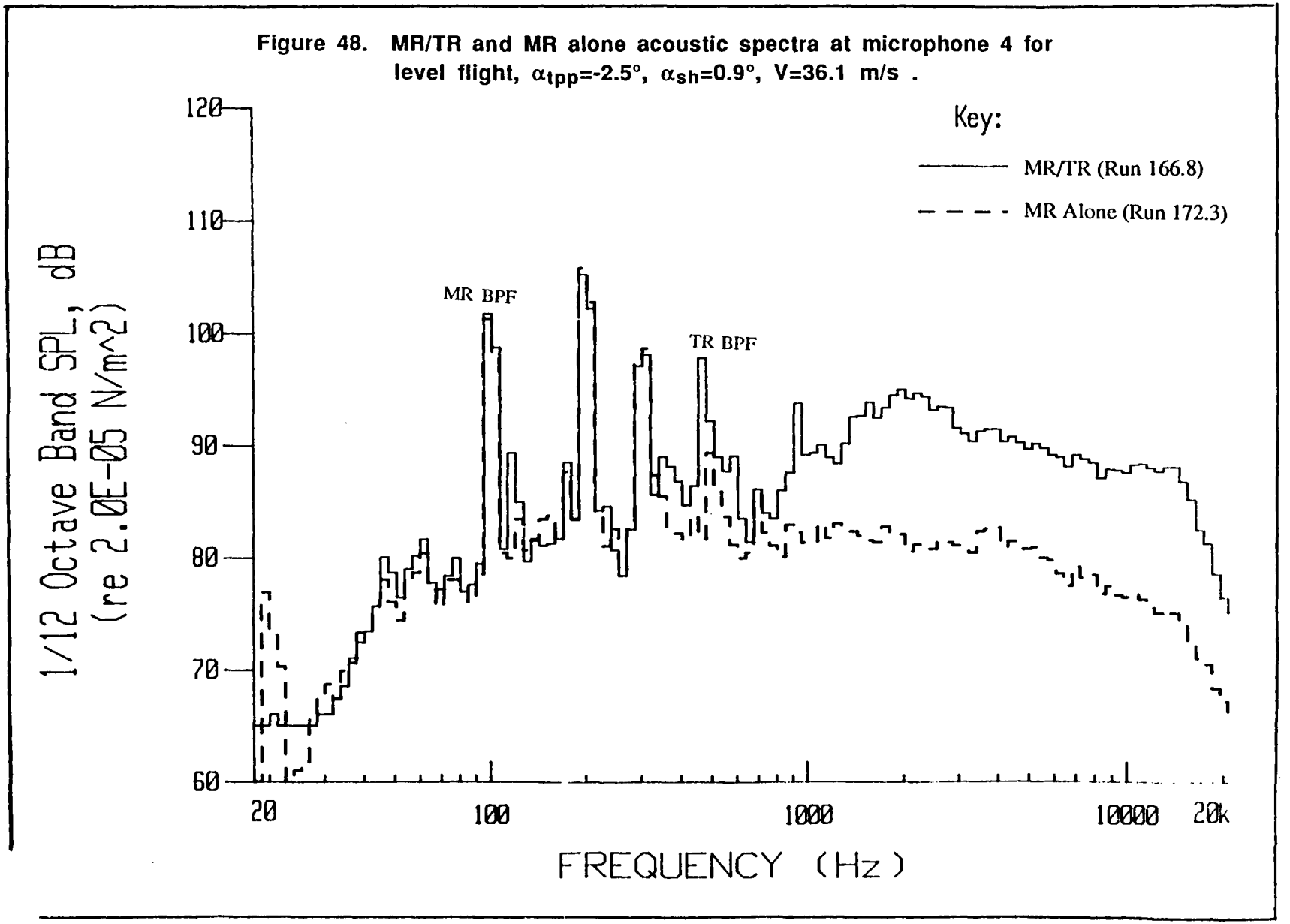

Figure 48. MR/TR and MR alone acoustic spectra at microphone 4 for level flight, α_{tpp}=-2.5°, α_{sh}=0.9°, V=36.1 m/s .

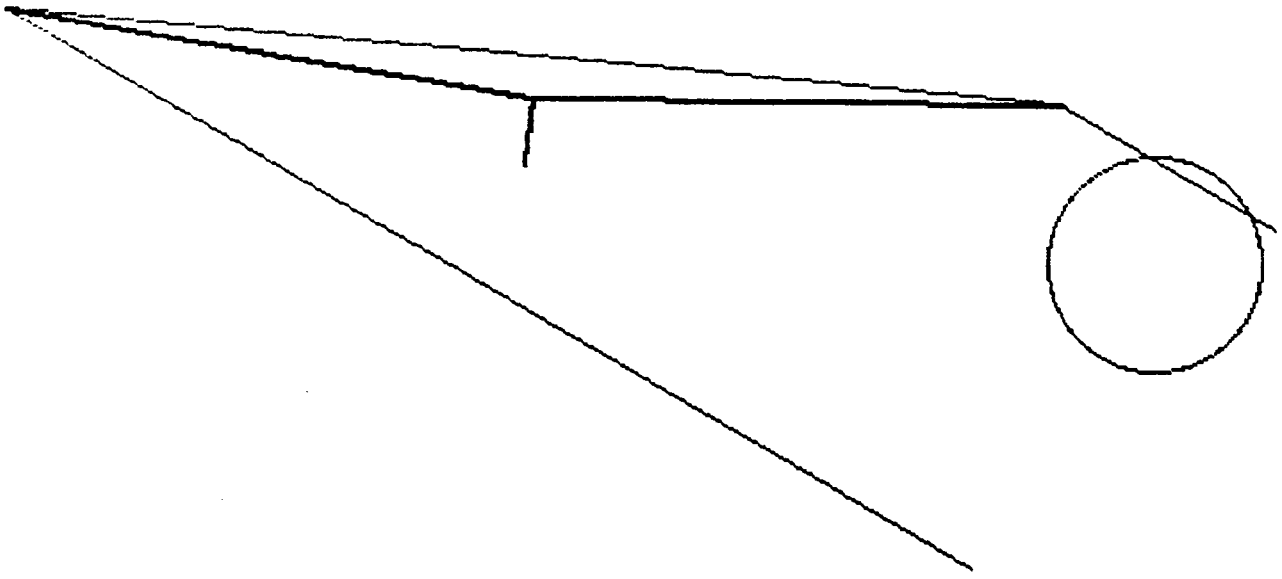

a) intersection at large shaft angle, $\alpha_{tpp}=5°$, $\alpha_{sh}=9°$.

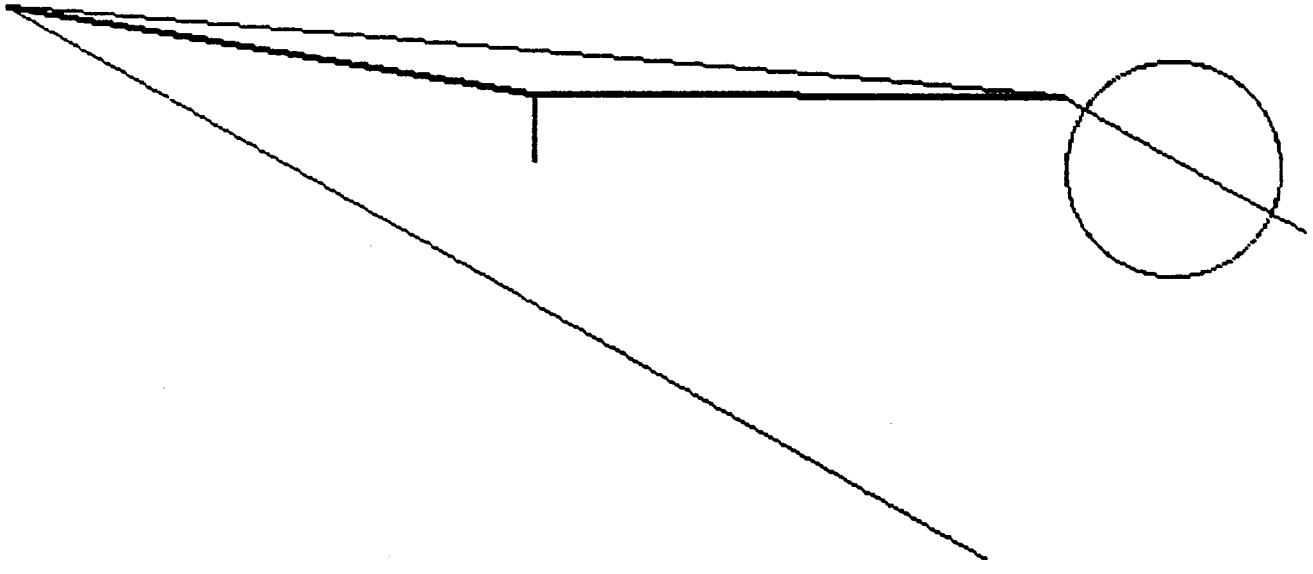

b) intersection at small shaft angle, $\alpha_{tpp}=5°$, $\alpha_{sh}=1°$.

Figure 49. MR wake/TR intersection in forward flight, V=25.5 m/s, μ=0.116, Ct=0.007.

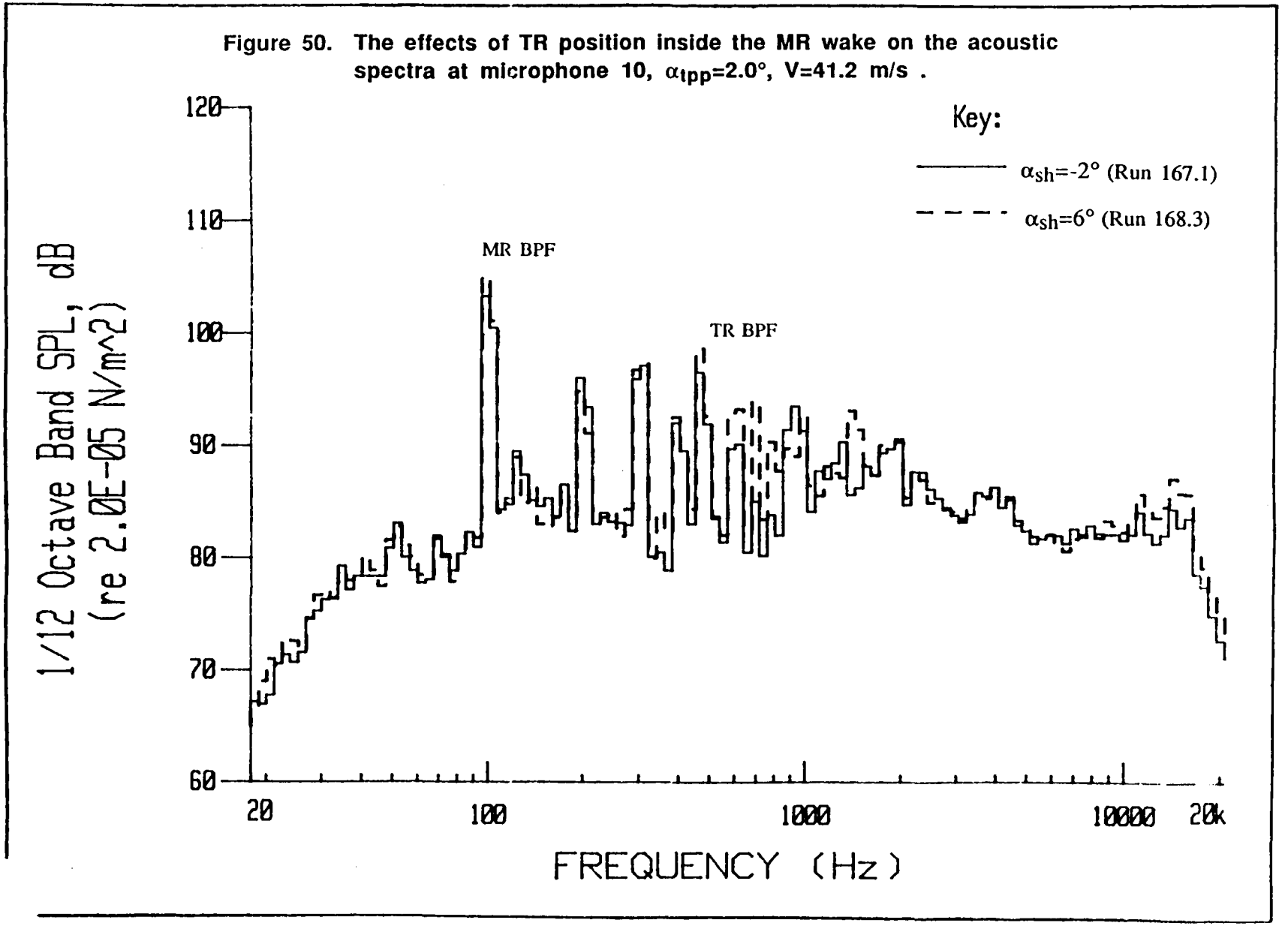

Figure 50. The effects of TR position inside the MR wake on the acoustic spectra at microphone 10, α_{tpp}=2.0°, V=41.2 m/s .

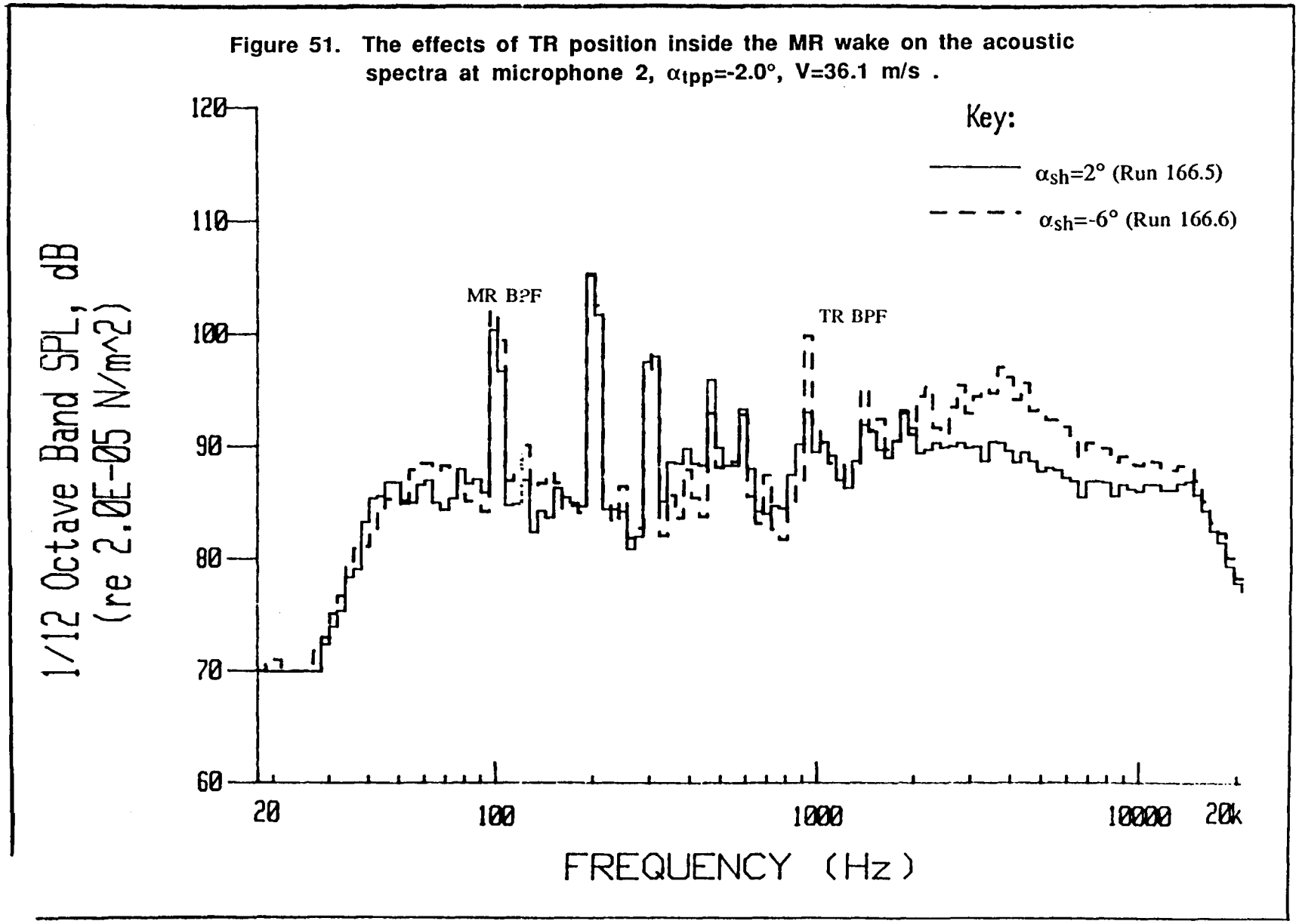

Figure 51. The effects of TR position inside the MR wake on the acoustic spectra at microphone 2, α_{tpp}=-2.0°, V=36.1 m/s .

NASA
National Aeronautics and Space Administration

Report Documentation Page

1. Report No.	2. Government Accession No.	3. Recipient's Catalog No.
NASA CR-4143		

4. Title and Subtitle	5. Report Date
Research Investigation of Helicopter Main Rotor/Tail Rotor Interaction Noise	May 1988
	6. Performing Organization Code

7. Author(s)	8. Performing Organization Report No.
J. Fitzgerald and F. Kohlhepp	
	10. Work Unit No.
	505-63-51

9. Performing Organization Name and Address	11. Contract or Grant No.
United Technologies Corporation Sikorsky Aircraft Division Stratford, CT 06601-1381	NAS1-17126
	13. Type of Report and Period Covered
12. Sponsoring Agency Name and Address	Contractor Report
National Aeronautics and Space Administration Langley Research Center Hampton, VA 23665-5225	14. Sponsoring Agency Code

15. Supplementary Notes

Langley Technical Monitor: Ruth M. Martin
Final Report

16. Abstract

Acoustic measurements were obtained in the NASA Langley 14 by 22 Foot Subsonic Wind Tunnel to study the aeroacoustic interaction of 1/5th-scale main rotor, tail rotor, and fuselage models. An extensive aeroacoustic data base was acquired for main rotor/tail rotor/fuselage aerodynamic interaction for moderate forward speed flight conditions. The details of the rotor models, experimental design and procedure, aerodynamic and acoustic data acquisition and reduction are presented. The model was initially operated in "trim" for selected fuselage angle of attack, main rotor tip-path-plane angle, and main rotor thrust combinations. The effects of repositioning the tail rotor in the main rotor wake and the corresponding tail rotor countertorque requirements were determined. Each rotor was subsequently tested in isolation at the thrust and angle of attack combinations for trim. The acoustic data indicated that the noise was primarily dominated by the main rotor, especially for moderate speed main rotor blade-vortex interaction conditions. The tail rotor noise increased when the main rotor was removed indicating that tail rotor inflow was improved with the main rotor present. The influence of tail rotor position within the main rotor wake on tail rotor noise could not be definitely established.

17. Key Words (Suggested by Author(s))	18. Distribution Statement
Helicopter Rotor Noise Main Rotor Tail Rotor Aeroacoustic Interaction	Unclassified-Unlimited Subject Category 71

19. Security Classif. (of this report)	20. Security Classif. (of this page)	21. No. of pages	22. Price
Unclassified	Unclassified	110	A06

NASA FORM 1626 OCT 86

NASA-Langley, 1988

For sale by the National Technical Information Service, Springfield, Virginia 22161-2171

End of Document